Growth of Two-Dimensional Materials at the Wafer Scale

Growth of Two-Dimensional Materials at the Wafer Scale

*Xiangming Xu, Tianchao Guo, Hyunho Kim, Mrinal K. Hota, Rajeh S. Alsaadi, Mario Lanza, Xixiang Zhang, Husam N. Alshareef**

Dr. X. Xu, T. Guo, Dr. H. Kim, Dr. M. K. Hota, R. S. Alsaadi, Prof. Mario Lanza, Prof. X. Zhang, Prof. H. N. Alshareef

Materials Science and Engineering, Physical Science and Engineering, King Abdullah University of Science and Technology (KAUST), Thuwal 23955-6900, Saudi Arabia

*Author to whom correspondence should be addressed.

E-mail: husam.alshareef@kaust.edu.sa

Keywords: van der Waal, 2D materials, wafer-scale, single crystalline, device integration.

Abstract

Wafer-scale growth has become a critical bottleneck for scaling up applications of van der Waal (vdW) layered two-dimensional (2D) materials in high-end electronics and optoelectronics. Most vdW 2D materials were initially obtained through top-down synthesis methods, such as exfoliation, which can only prepare small flakes on a micrometer scale. Bottom-up growth can enable 2D flake growth over a large area. However, seamless merging of these flakes to form large-area continuous films with well-controlled layer thickness and lattice orientation is still a significant challenge. In this review, we briefly introduce several vdW layered 2D materials covering their lattice structures,

This article has been accepted for publication and undergone full peer review but has not been through the copyediting, typesetting, pagination and proofreading process, which may lead to differences between this version and the Version of Record. Please cite this article as doi: 10.1002/adma.202108258.

representative physical properties, and potential roles in large-scale applications. Then, several methods used to grow vdW layered 2D materials at the wafer-scale are reviewed in depth. In particular, we summarize three strategies that enable 2D film growth with a single-crystalline structure over the whole wafer: growth of an isolated domain, growth of unidirectional domains, and conversion of oriented precursors. After that, we review the progress in using wafer-scale 2D materials in integrated devices and advanced epitaxy. Finally, future directions in the growth and scaling of vdW layered 2D materials are discussed.

1. Introduction

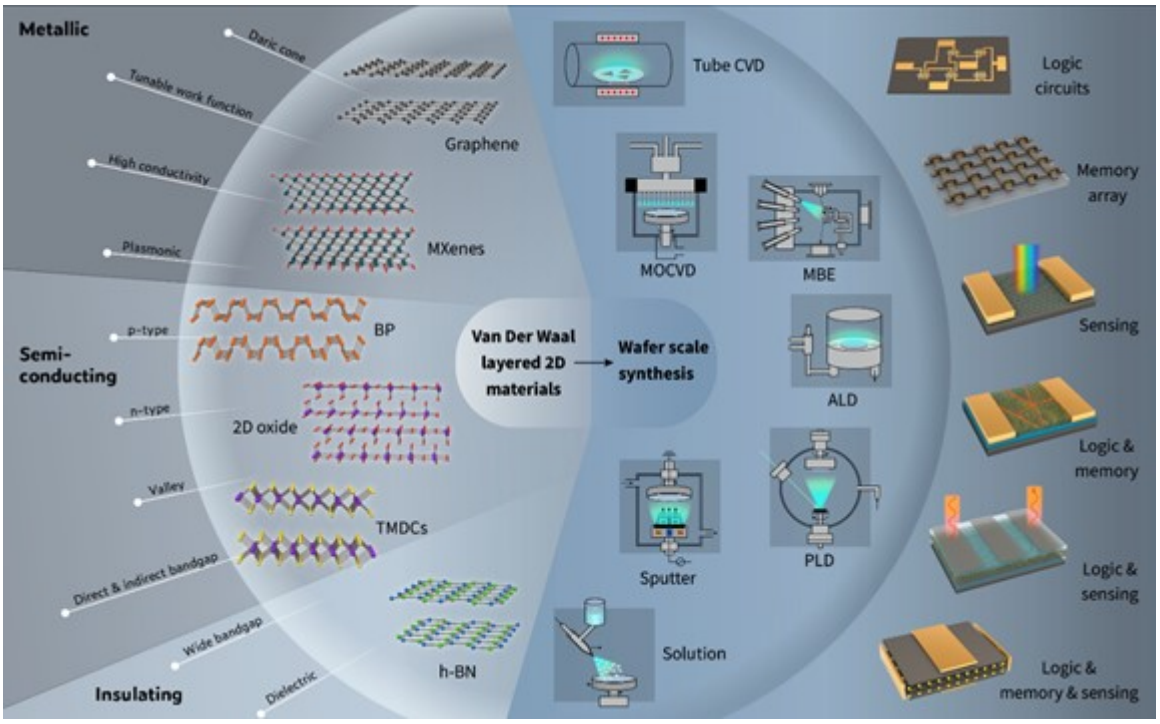

Figure 1 Schematic showing various layered 2D materials, the methods used to grow them at the *wafer-scale*, and their integrated device applications. The shown 2D materials all have van der Waals (vdW) bonds in their lattices, and include: metallic or semi-metallic, semiconducting, and insulating 2D materials. Wafer-scale growth methods include chemical and vacuum processes carried out using a wide range of temperatures. Various integrated devices that take advantage of 2D vdW films grown at wafer scale are also shown.

The rapid development of silicon-based integrated circuit (IC) technology has been strongly supporting the fourth industrial revolution for many years, significantly promoting the capacity and speed of information communications worldwide. In the era of big data, even more advanced electronic devices are needed to handle the massive amount of data at high speed. However, further scaling down of silicon transistor size to increase chip integration density has become prohibitively expensive, and in some cases, has encountered the limits of today's best semiconductor equipment. Especially from the device physics perspective, short channel effects dominate silicon transistor performance when the channel size is less than 5 nm, which degrades the transistor performance. Van der Waals (vdW) layered 2D materials are regarded as a very promising new material system to support post-silicon IC technologies because of their rich and excellent physical properties even with thickness at the atomic scale (< 1 nm).[1-3] It has been reported that monolayer MoS_2 as a transistor channel can be effectively controlled using one nm-length carbon nanotube gating. Electric field control on such a short channel can achieve MoS_2 transistors with excellent performance, including an on/off current ratio up to 10^6 and a subthreshold swing (*SS*) of 65 $mV \cdot s^{-1}$.[4] This indicates that 2D vdW semiconductors are promising candidates to replace silicon for continued downscaling.

Many vdW layered 2D materials have been synthesized and explored since the graphene discovery in 2004. They include highly-conductive graphene[1] and MXenes (atomic-thin transition metal carbides and nitrides)[5], transition metal chalcogenides (TMDCs, including both metallic[6] and

semiconducting[2]), 2D elemental semiconductors (black phosphorus (BP)[7], tellurium (Te)[8]), 2D insulators (*e.g.*, hexagonal boron nitride (h-BN)[9] and some oxides.[10] The large variety of vdW layered 2D materials provides a large potential for advanced 2D electronics.

However, for scalable applications, all vdW layered 2D materials face a common challenge: transitioning from micrometer-scale 2D flakes to wafer-scale.[1, 2, 11-13] This is necessary for scaling up 2D vdW materials application in the high-end semiconductor industry. The history of silicon wafer development and its significant impact on modern information technologies has already demonstrated the importance of a large wafer size for volume production at an acceptable cost. Some materials, such as graphene[14], h-BN[15], and TMDCs[16], have been heavily explored for wafer-scale growth, but the reality is that wafer-scale film quality still has enormous space to improve, especially when compared to chip-grade single-crystalline silicon. Other materials such as MXenes, BP, Te, and vdW oxides, have only a few reported papers focusing on their wafer-scale growth. Hence, we feel that this timely review focusing on wafer-scale growth methods of relevant 2D vdW layered materials is urgently needed.

The scope of this review is clarified in **Figure 1**, where the structures, properties, wafer-scale growth methods, and applications of representative vdW layered 2D materials. We begin by briefly introducing these 2D vdW layered materials and discuss their lattice structures and fundamental physical properties. Next, we discuss the status and recent developments of wafer-scale growth methods, including tube chemical vapor deposition (tube-CVD), metal-organic chemical vapor deposition (MOCVD), molecular beam epitaxy (MBE), atomic layer deposition (ALD), pulsed laser deposition (PLD), sputtering, solution process, and combination of these processes. We then discuss some strategies for the growth of high-quality single-crystalline films at a wafer-scale, including ①

growth of an isolated domain (GID), ② growth of unidirectional domains (GUD), and ③ conversion of oriented precursor (COP). After discussing these strategies, we provide some examples for relevant devices and functional integrated applications that have been enabled by 2D material growth. Finally, we give an outlook for future research directions for 2D vdW film growth at the wafer scale.

2. Classes of vdW 2D Materials

2.1. Graphene

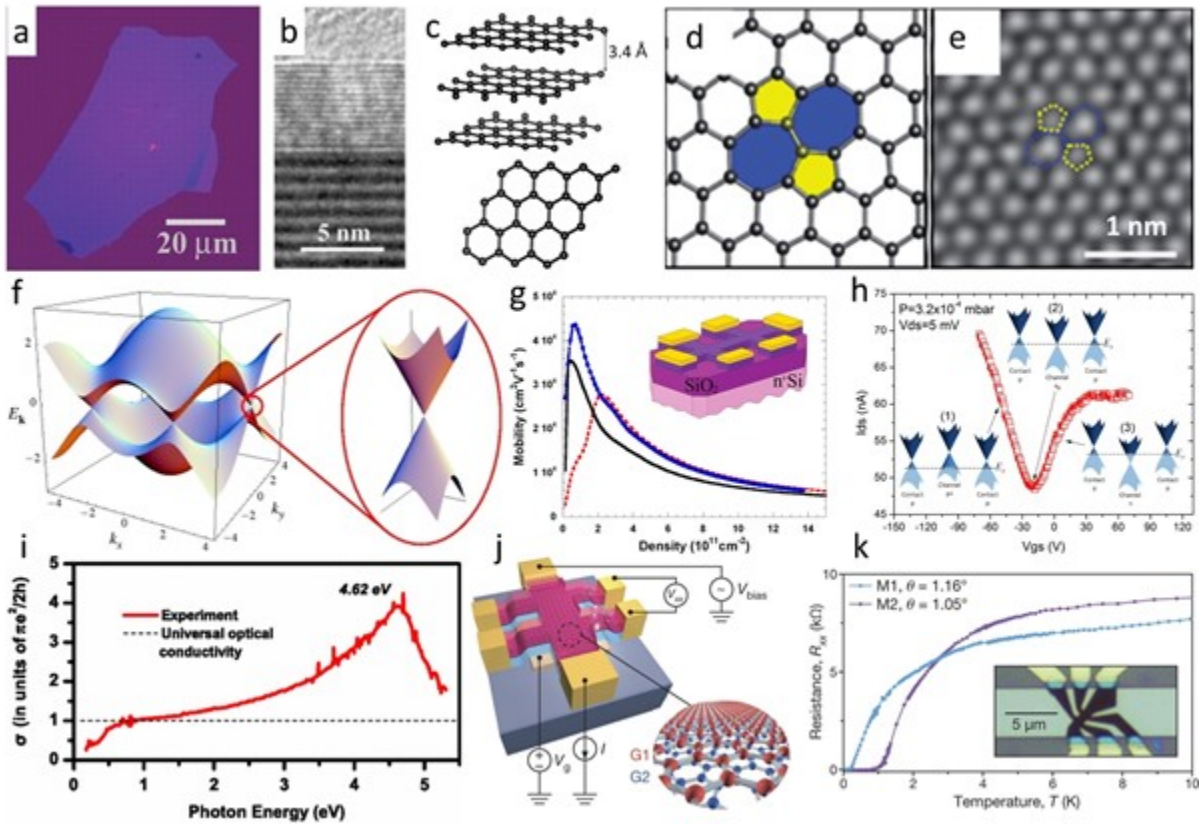

Figure 2 Characteristics of Graphene. (a) Photograph of the graphene flake. Reproduced with permission.[1] Copyright 2004, American Association for the Advancement of Science. (b) Cross-sectional TEM image of multilayer graphene layers. Reproduced with permission.[17] Copyright 2012, American Physical Society. (c) Lattice model of graphene in side and top views. (d) Atomistic model of graphene with certain defects. (e) The atomic-resolution STEM image of graphene with some defects. Reproduced with permission.[18] Copyright 2013, Royal Society of Chemistry. (f) The 3D

model of electronic dispersion in the graphene honeycomb lattice. (The zoom-in shows one Dirac point) Reproduced with permission.[19] Copyright 2009, American Physical Society. (g) The electronic mobility of graphene with different carrier densities under different dielectric environments. (The inset is the schematic of the graphene hall-bar device) Reproduced with permission.[20] Copyright 2009, IOP Publishing. (h) The I_{DS}-V_{GS} curve of graphene transistor, indicating the graphene Fermi level can be tuned by the electric field. Reproduced with permission.[21] Copyright 2015, IOP Publishing. (i) The optical conductivity of graphene. Reproduced with permission.[22] Copyright 2011, American Physical Society. (j) The schematic of a typical twisted bilayer graphene hall-bar device. (k) Resistance under different temperatures measured in two devices with twist angles 1.16° and 1.05°, respectively. (The inset is an optical image of the device) Reproduced with permission.[23] Copyright 2018, Nature Publishing Group.

In 2004, Novoselov and colleagues reported experimentally isolated atomically thin graphitic crystal, graphene.[1] The successful isolation of graphene has been achieved by mechanical exfoliation of highly oriented pyrolytic graphite. The morphology of the micrometer graphene flake is shown in **Figure 2a**. Each graphene layer interacts with the nearby layer by weak vdW bonds where carbon atoms share a solid covalent bond in the in-plane direction. The cross-sectional STEM image in Figure 2b clearly shows vdW gaps in few-layer graphene.[24] The lattice model of graphene is shown in Figure 2c, where a vdW gap of about 3.4 Å can be seen from the side view (top), and carbon atoms in honeycomb geometry can be seen from the top view (bottom). Experimentally observed graphene often includes point defects where benzene-ring structure consists of 5 or 7 atoms, as displayed in Figure 2d-e.[18] Graphene is electrically conductive, mechanically strong, and stable under ambient conditions.

Graphene has a unique electronic structure and properties. Figure 2f shows the 3D electronic dispersion of honeycomb graphene with unique Dirac cones.[19] A simulation study has predicted high electronic mobility up to 44,000 $cm^2\ V^{-1}\ s^{-1}$ for graphene, at low carrier density 10^{11} $cm^{-2,}$ as displayed in Figure 2g.[20] Due to the Dirac structure, graphene exhibits gate-tunable ambipolar behavior, as shown in Figure 2h.[21] The graphene channel shows a *p*-type behavior under

gate voltage lower than -30 V, and it shows the transition to the *n*-type once the gate voltage increases. Saturation of source to drain current at the *n*-type region is due to the *p*-doping effect of graphene at contact area using niobium electrodes. Experimental optical conductivity of monolayer graphene (Figure 2i) shows an asymmetric resonance peak at 4.62 eV due to their strong electron-hole interactions: saddle point excitons.[22] Twisted bilayer graphene (TBG) is overlapped two graphene layers with a certain angular mismatch, showing very promising superconducting properties with the magic twisting angle. Through characterizing TBG hall-bar device prepared as shown in Figure 2j, superconductivity has been discovered at a magic angle of 1.05° as shown in Figure 2k.[23]

Graphene, with a vdW layered, hexagonal honeycomb structure and its single-atomic thin state, exhibits many unique electrical, optical, and superconducting properties. It has received extensive focus from several groups to grow at the wafer scale.

2.2. Hexagonal boron nitride (h-BN)

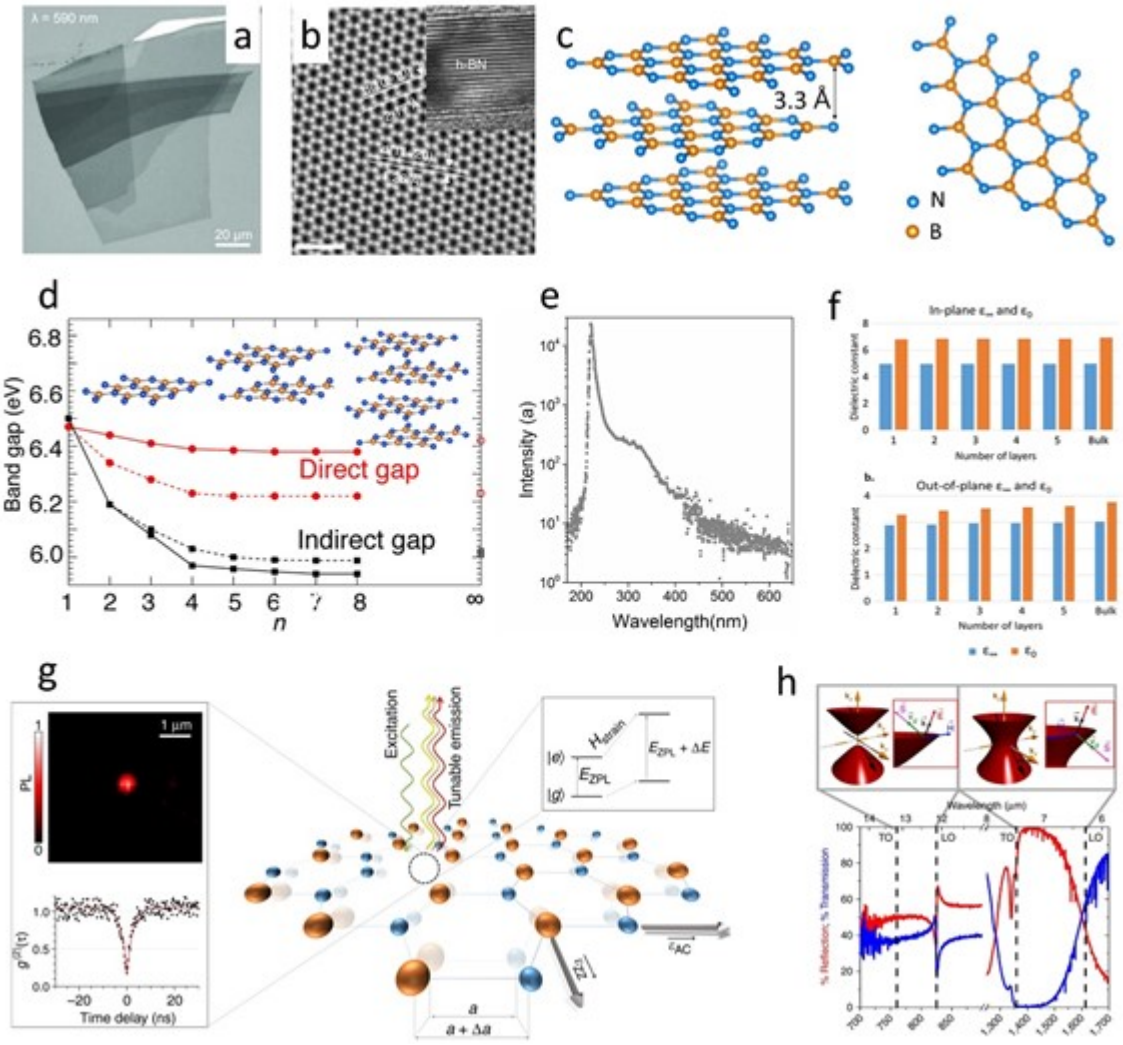

Figure 3 Characteristics of hexagonal boron nitride (h-BN). (a) The photograph of the h-BN flake. Reproduced with permission.[12] Copyright 2018, Nature Publishing Group. (b) The atomic-resolution h-BN high-angle annular dark-field STEM image. (The inset is a cross-sectional TEM image) Reproduced with permission.[25] Copyright 2015, Nature Publishing Group. (c) Lattice model of h-BN with both top and side views. (d) Evolution of the K_v–K_c direct gaps and the K_v–M_c indirect band gaps as a function of the number of layers n. Reproduced with permission.[9] Copyright 2018, American Chemical Society. (e) Cathodoluminescence spectrum at room temperature with indirect free exciton luminescence of pure diamond as a reference. Reproduced with permission.[26] Copyright 2004, Nature Publishing Group. (f) The layer-dependent macroscopic dielectric constant. Reproduced with permission.[27] Copyright 2018, Nature Publishing Group. (g) The single-photon emission of atom-like defects in h-BN at room temperature. Reproduced with permission.[28] Copyright 2017, Nature Publishing Group. (h) The schematic of isofrequency surfaces for a Type I (left) and II (right) hyperbolic media and the FTIR reflection (red curve) and transmission (blue curve)

spectra of a 900-nm thick h-BN flake exfoliated onto a 500-mm thick BaF_2 substrate. Reproduced with permission.[29] Copyright 2014, Nature Publishing Group.

Two-dimensional hexagonal boron nitride (2D h-BN), often called "white graphene", is analogous to graphene. Due to the weak interaction between nanosheet layers, few-layer h-BN could be mechanically exfoliated (**Figure 3a**).[12] Boron atoms and nitrogen atoms are alternately arranged in a honeycomb structure, and their vdW gaps can be observed by the STEM image in Figure 3b.[25] The h-BN lattice structure can be visualized in Figure 3c, where the side view on the left shows vdW gap of about 3.3 Å, while the top view on the right shows honeycomb structure. 2D h-BN is a large bandgap insulator with a wider indirect bandgap compared to the bulk counterpart, and both the direct and indirect bandgap values are changing with different number of layers, as shown in Figure 3d.[9] A cathodoluminescence spectrum in Figure 3e for the h-BN crystal reveals an intense ultraviolet luminescence at 5.765 eV,[26] indicating the optical bandgap value of more than 5 eV. Thus, h-BN is insulating due to its wide bandgap. However, h-BN flakes with 5 and 11 layers have shown high in-plane thermal conductivity of 250 and 360 W m^{-1} K^{-1} at room temperature, respectively.[30] These values are two orders of magnitude higher than widely used SiO_2 dielectric, suggesting a great potential for future electronic applications where heat dissipation is desired. Figure 3f summarizes the in-plane and out-of-plane dielectric constant of h-BN with weak layer number dependency.[27] The out-of-plane static dielectric constant of h-BN (3.29 eV for monolayer; 3.76 eV for bulk) is comparable to that of SiO_2 (3.8 eV). By introducing point defects into the hexagonal lattice, h-BN could show a unique stable single photon emission property at room temperature, and it can be engineered by introducing lateral strains, as schematically illustrated in Figure 3g.[28] Besides, the multilayer h-BN has been demonstrated as an excellent natural hyperbolic

material with unique sub-diffractional volume-confined polaritons, as illustrated in Figure 3h, embodying its potential in nanophotonics.[29]

The insulating h-BN with excellent thermal conductivity, low dielectric constant, ultrahigh wide bandgap, and excellent photonic properties indicates the essential role it can play in 2D electronics. Thus, realizing h-BN film growth at the wafer scale will be a big step forward in the field of 2D electronics.

2.3. 2D transition metal dichalcogenides (TMDCs)

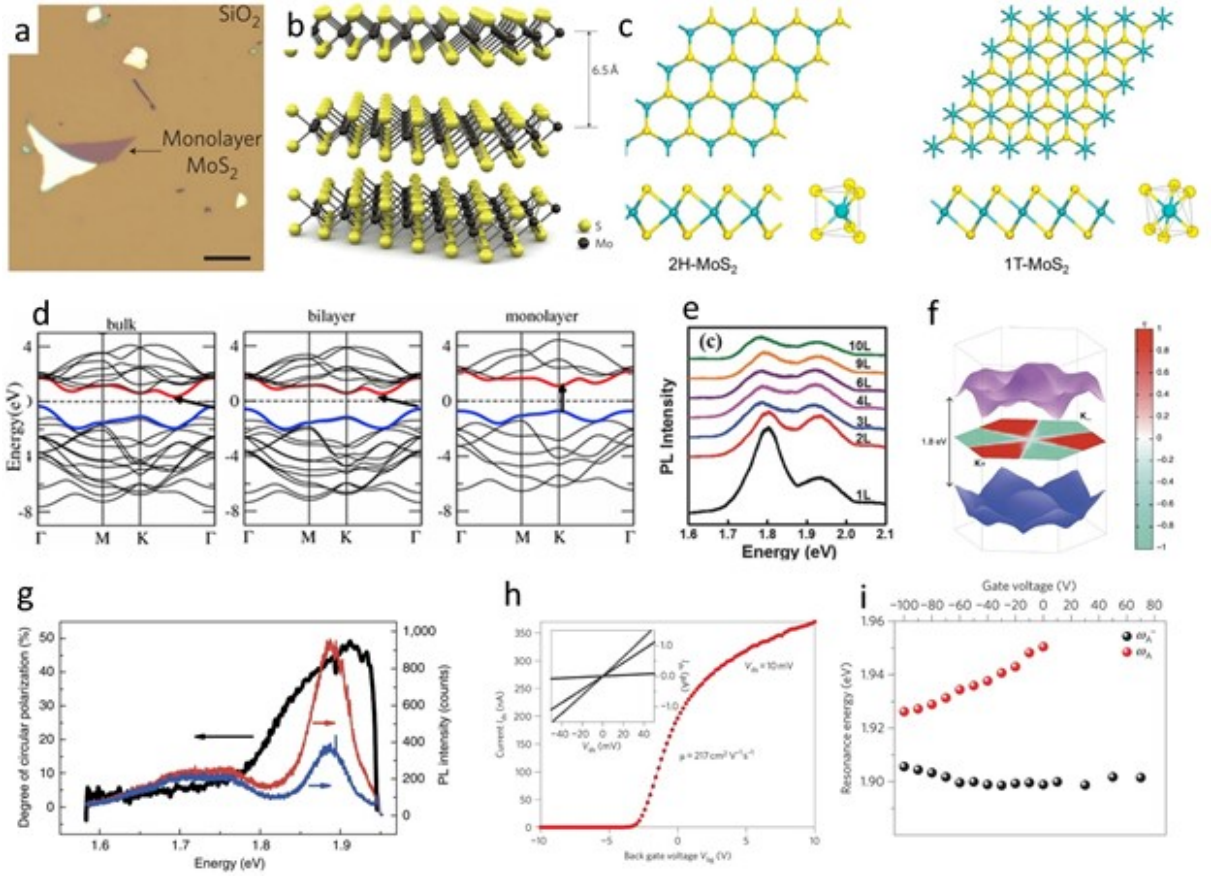

Figure 4 Characteristics of transition metal dichalcogenides (TMDCs). (a) The photograph of the MoS_2 microsized flake. (b) The layered structure atomic model of the MoS_2 lattice. Reproduced with permission. [2] Copyright 2011, Nature Publishing Group. (c) Multiphase of MoS_2. Reproduced with permission.[6] Copyright 2015, American Chemical Society. (d) Energy band structures of bulk, bilayer, and monolayer MoS_2. Reproduced with permission.[31] Copyright 2014, Springer International Publishing. (e) The photoluminescence (PL) measurement of MoS_2 films with different layers. Reproduced with permission.[32] Copyright 2017, Wiley-VCH. (f) Top valence band (blue) and bottom conduction band (pink). The central hexagon is the Brillouin zone color-coded by the degree of circular polarization. Reproduced with permission. Copyright 2012, Nature Publishing Group. (g) Circularly polarized micro-PL of the monolayer MoS_2 at 83 K, along with the degree of circular polarization of the PL spectra. Red and blue curves correspond to intensities of σ^+ and σ^- polarizations, respectively, in the luminescence spectrum. The black curve is the net degree of polarization. Reproduced with permission.[33] Copyright 2012, Nature Publishing Group.The I_{DS}-V_{GS} linear transfer curve of MoS_2 transistor (inset is the output I_{DS}-V_{DS} curve) Reproduced with permission.[2] Copyright 2011, Nature Publishing Group. (h) The I_{DS}-V_{GS} linear transfer curve of MoS_2

transistor (inset is the output I_{DS}-V_{DS} curve). Reproduced with permission.[2] Copyright 2011, Nature Publishing Group. (i) Threshold energies of the trion ω_A^- (black symbols) and the neutral exciton ω_A (red symbols) as a function of the gate voltage. Reproduced with permission.[34] Copyright 2013, Nature Publishing Group.

Transition metal dichalcogenides (TMDCs) are a large family of 2D vdW layered materials that can exhibit metallic or semiconducting phases. In general, their chemical formula is MX_2, where M is transition metal (Ti, Zr, Hf, V, Nb, Ta, Mo, W, Re, Pd or Pt) and X represents chalcogen (S, Se, or Te). Some of them have several phases: 2H, 1T, and 1T'. TMDCs combined with different transition metal elements and chalcogen elements may have different thermodynamically stable phases.[35] MoS_2 is one of the most representative TMDCs obtained from nature because its 2H phase is chemically and mechanically stable in the natural environment.[36] The first robust 2D transistor is made using monolayer 2H MoS_2 flakes as the semiconducting channel.[2] Besides, research on MoS_2 wafer-scale growth and device integration is relatively more mature than the other 2D TMDCs. Therefore, we will give the basic introduction of TMDCs, taking MoS_2 as the representative introduction object.

Similar to graphene research, the monolayer MoS_2 micro flake (**Figure 4a**) could be obtained by mechanical exfoliation because of weak vdW gaps in their layered structure, as illustrated in Figure 4b. [2] MoS_2 has both trigonal prismatic phase (semiconducting 2H phase) and octahedral phase (metallic 1T phase). Their phase structure schematics are shown in Figure 4c. [6] In semiconducting 2H MoS_2 (including 2H phases of $MoSe_2$, WS_2, and WSe_2), the bandgap increases from bulk to monolayer, as shown in band structure diagrams for monolayer, bilayer, and bulk 2H MoS_2 in Figure 4d.[32] Moreover, monolayer semiconducting TMDCs have a direct bandgap that allows strong photoluminescence (PL). Representative PL spectra of 2H MoS_2 flakes with different layers are shown in Figure 4e, in which the monolayer flake shows much stronger PL intensity.[32]

Also, the monolayer MoS_2 possesses near-perfect valley-selective circular dichroism, which was confirmed theoretically (Figure 4f) and experimentally (Figure 4g).[33] Many reports have demonstrated MoS_2 as an excellent *n*-type semiconducting channel in field-effect transistors with robust field-effect electron mobility of 217 $cm^2 V^{-1} s^{-1}$, even after reducing the MoS_2 layer thickness to less than 0.7 nm. The first demonstrated single-layer MoS_2 transistor I_{DS}-V_{GS} transfer curve is shown in Figure 4h. [2] However, other TMDCs such as 2H WSe_2 and 2H $MoTe_2$ also show excellent *p*-type behavior in transistors.[37, 38] Not only electron, but also exciton (electron-hole pair) or charged exciton (trion: electron-hole pair combined with another free electron) has been observed in monolayer MoS_2 and can be tuned by gate electric field (Figure 4i). The exciton resonance becomes dominant under negative gate bias with significant peak center shift, while trion resonance is not significantly affected by gate modulated Fermi level.[34]

The huge TMDCs family, together with their rich and unique physical properties (such as monolayer PL, valleytronics, high-mobility carrier in *p*-type and *n*-type, electric field tunable excitons, *et al*), indicate that their significant roles in 2D electronics would be boosted if wafer-scale growth methods are developed.

2.4. Layered transition metal carbides and nitrides (MXenes)

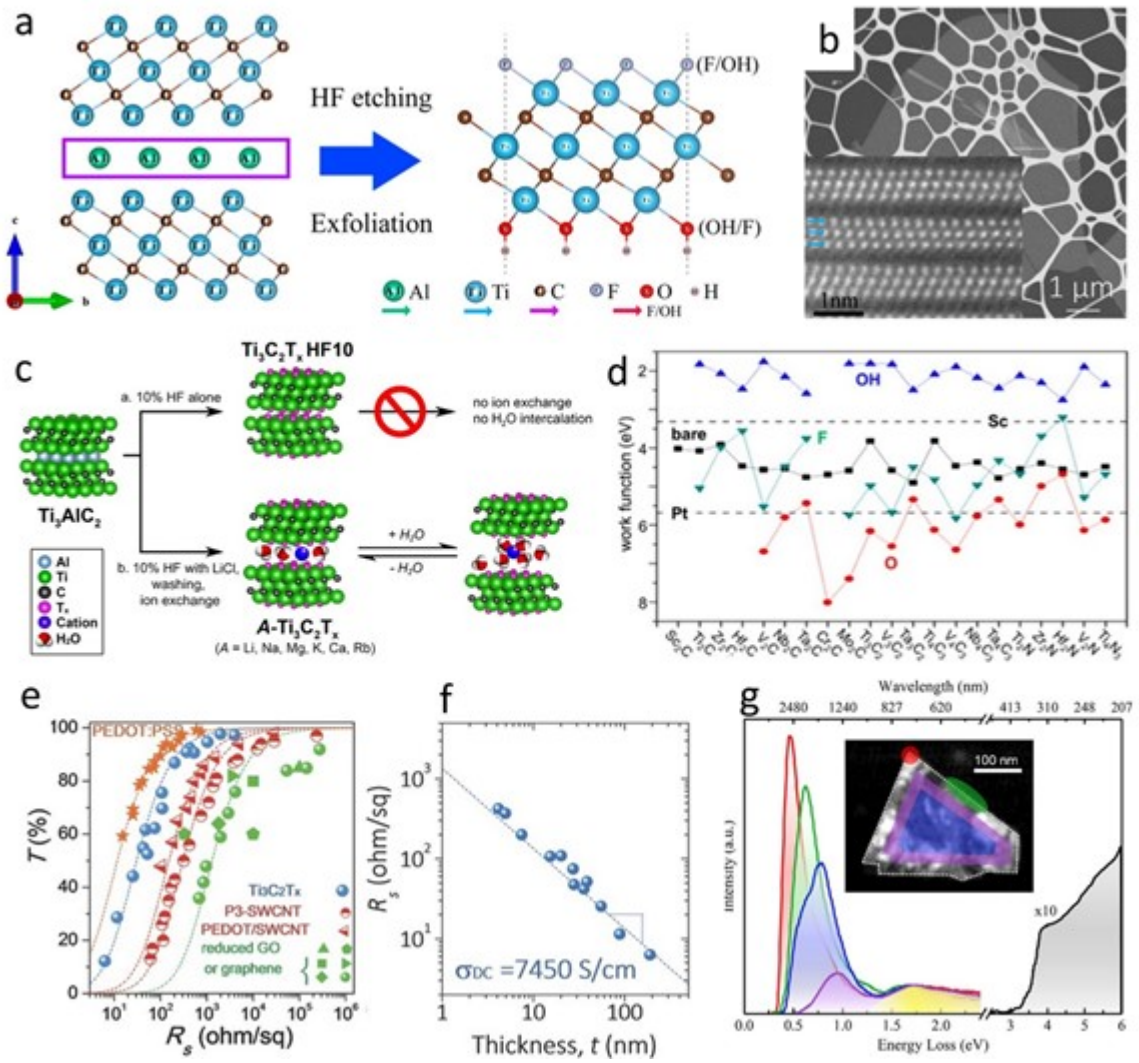

Figure 5 Characteristics of MXenes. (a) The schematic of MXene synthesis from the HF etching of the MAX phase. Reproduced with permission.[39] Copyright 2015, American Chemical Society. (b) The TEM morphology of the MXene flake. Reproduced with permission.[40] Copyright 2017, Wiley-VCH. (Inset is the cross-sectional TEM image) Reproduced with permission.[39] Copyright 2015, American Chemical Society. (c) Surface functional group engineering based on the different acid etching of MAX phase. Reproduced with permission.[41] Copyright 2016, American Chemical Society. (d) Work functions of different MXenes with different surface groups. Reproduced with permission.[42] Copyright 2016, American Chemical Society. (e) The transmittance as a function of resistance for $Ti_3C_2T_x$ compared to the other representative materials. Reproduced with permission.[40] Copyright 2017, Wiley-VCH. (f) The resistance as a function of the MXene film thickness. Reproduced with permission.[40] Copyright 2017, Wiley-VCH. (g) Zero-energy loss peak (ZLP)-subtracted EEL spectra

acquired on a truncated triangular flake of $Ti_3C_2T_x$ (Inset: STEM-HAADF micrograph). Reproduced with permission.[43] Copyright 2018, American Chemical Society.

MXenes (atomic thin transition metal carbides and nitrides with some surface groups), a family of 2D materials derived from ternary layered precursors MAX phase, had been first reported in 2011.[5] Their interlayer vdW gaps are introduced by selective chemical etching of the MAX phase using F-containing acidic solutions. The schematic in **Figure 5a** shows the representative $Ti_3C_2T_x$ (T_x including =O, -F, -OH) MXene through the selective chemical etching Ti_3AlC_2 MAX phase:[39] Al layer is removed by chemical reaction, and remaining $Ti_3C_2T_x$ MXene layer with surface groups can be isolated. The presence of surface termination allows MXenes to exhibit hydrophilic surface, which is a distinct advantage over other 2D materials. The lateral size of MXene can be up to 10 μm (Figure 5b).[40] MXene layered flakes with large vdW gaps are visible in the TEM image as shown in the inset in Figure 5b. [40] The $Ti_3C_2T_x$ MXene shows unique interlayer spacing and intercalation properties because of its tunable surface groups. For example, as discussed in Figure 5c, MXene etched by 10% HF does not show ion exchange capability or intercalation of water, while additional LiCl in 10% HF enables these capabilities.[41] Spontaneous intercalation of Li^+ cation between the MXene layer allows co-intercalation of water molecules. The interlayer spacing can be much wider so ex-situ ion exchange can be done.

Surface groups of MXenes play an essential role also in their electronic properties. A theoretical study has predicted a wide-range coverage of various MXenes with different surface groups.[42] Oxygen surface groups result in high work function while hydroxyl-terminated MXenes are with very low work functions (Figure 5d). Conductive material with such low work function is highly desired for electronic applications. It is believed that the ultralow work function is due to the strong surface dipole of the hydroxyl group.[44] $Ti_3C_2T_x$ MXene is a very conductive 2D metal, which

shows even higher conductance and better transparency than graphene, single-wall carbon nanotube (SWCNT), or SWCNT/polymer thin films and is comparable to PEDOT: PSS (Figure 5e).[40] The high conductivity of different thick MXene films is illustrated in Figure 5f.[40] $Ti_3C_2T_x$ MXene thin films have shown high electrical conductivity that is based on the high free-carrier density of MXene. Figure 5e shows zero-loss peak subtracted electron energy loss spectroscopy (EELS) of $Ti_3C_2T_x$ MXene flake.[43] Minor changes in incident electron beam energy indicate different surface plasmonic energy modes in the MXene flake at different positions.

MXene is a large 2D material family with weak vdW gaps introduced by chemical etching. They have many unique properties, such as high conductivity, various surface groups, and tunable work-function over a large range. These charatceristics promote MXenes for various applications in next-generation electronics, including excellent contact material. Thus, growth of large-scale MXenes is crucial to realize its potential.

WILEY-VCH

2.5. 2D elemental semiconductors

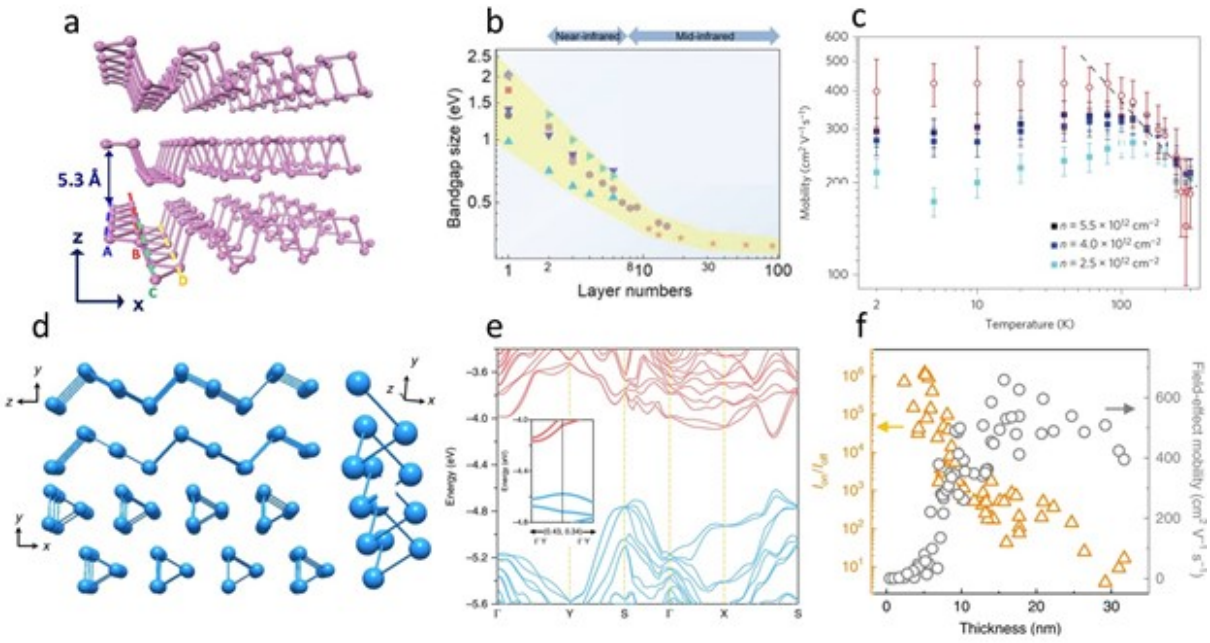

Figure 6 Characteristics of 2D elemental semiconductors. (a) Lattice model of layered black phosphorus (BP). Reproduced with permission.[7] Copyright 2015, National Academy of Sciences. (b) Bandgap size as the function of BP layer number. Reproduced with permission. [45] Copyright 2020, Wiley-VCH. (c) The carrier mobility of BP as the function of temperature under the different carrier densities. Reproduced with permission.[11] Copyright 2014, Nature Publishing Group. (d) The lattice model of Tellurium (Te) structure. Reproduced with permission.[46] Copyright 2020, Nature Publishing Group. (e) The energy band structure of Te. Reproduced with permission.[47] Copyright 2018, Nature Publishing Group. (f) I_{on}/I_{off} ratio and field-effect mobility as a function of Te thickness. Reproduced with permission. [47] Copyright 2018, Nature Publishing Group.

Similar to graphene, numerous efforts have been exerted for the discovery of other mono-elemental 2D materials. Borophene and silicene are other kinds of 2D materials with strong

interlayer interaction [48, 49] will not be discussed here. They would have a much different synthesis mechanism to the vdW layered 2D materials in question. Phosphorene (black phosphorus, BP) and Tellurene have been confirmed with a weak vdW gap and will be included in our discussion. Besides, both of them are very promising 2D semiconductors; discussion of their large-scale growth could be very meaningful for 2D device integration. **Figure 6a** shows the crystal structure of 2D BP. Each layer of semiconducting BP has a puckered orthorhombic geometry.[7] Like semiconducting 2D TMDCs, the BP bandgap depends on the number of layers, with a range between 2.5 and 0.1 eV, covering the middle and near-infrared regions, as shown in Figure 6b.[45] BP has excellent carrier transport (mainly *p*-type) properties, hall mobility and field-effect mobility of 8 nm thick BP shows temperature dependence in a range of several hundred $cm^2\ V^{-1}\ s^{-1}$ as shown in Figure 6c.[11] Tellurene is another promising mono-elemental 2D semiconductor. The crystal structure in Figure 6d can be described as aligned Te molecular chains.[46] Figure 6e shows the electronic band structure of 4-layered Te simulated by conventional Perdew-Burke-Ernzerhof (PBE) functional, where a slight mismatch of conduction band minimum (CBM) and valence band maximum (VBM) points results in an indirect bandgap. According to the Heyd–Scuseria–Ernzerhof (HSE) functional, the bandgap of the 2D Te increases from 0.38 eV (bulk) to 0.83eV (4-layer) and 1.28 eV (2-layer). [47] Figure 6f summarizes the current modulation ratio and field-effect mobility of 2D tellurene transistors. From the thinner 2D Te flakes, the higher I_{on}/I_{off} ratio was found, but with smaller mobility. [47] The peak mobility was ~700 $cm^2\ V^{-1}\ s^{-1}$ at room temperature for a thickness of 16 nm. Thus, 2D BP and Te are auspicious high-performance *p*-type semiconducting layered materials. Their large-scale growth and integration are absolutely important research topics.

WILEY-VCH

2.6. 2D vdWs oxides

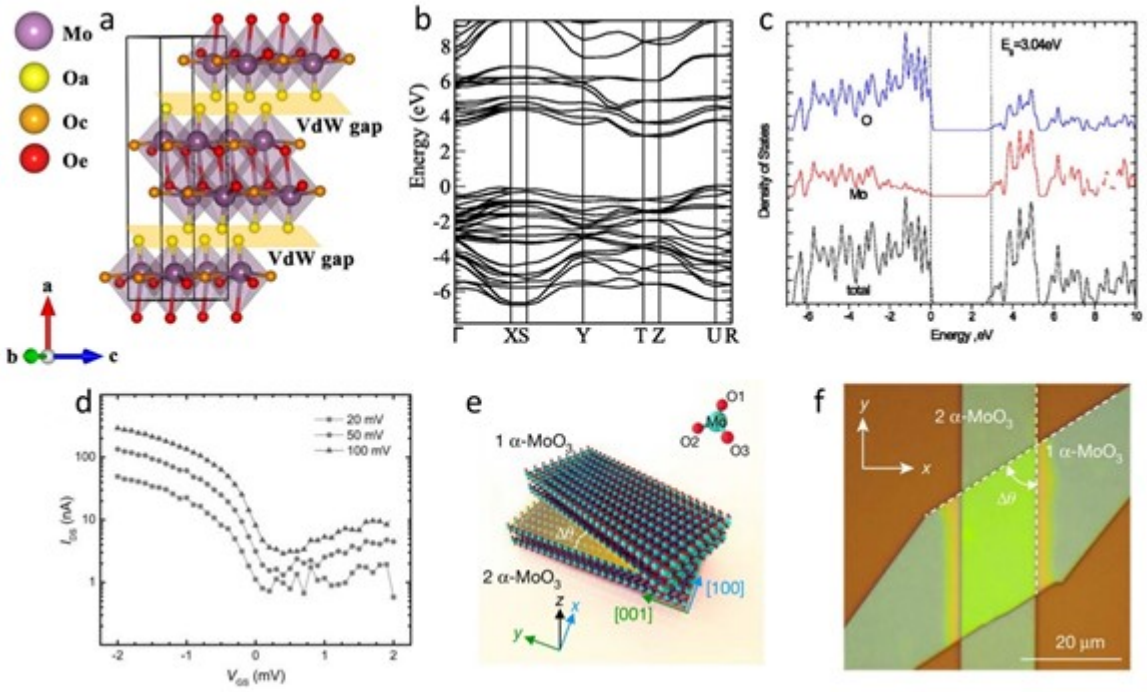

Figure 7. Characteristics of 2D oxides. (a) The schematic lattice model of vdW layered MoO_3. Reproduced with permission.[50] Copyright 2017, Elsevier. (b) The band structure and (c) partial density of states of MoO_3 as calculated by the s-X hybrid functional. Reproduced with permission. [51] Copyright 2014, American Physical Society. d) The I_{DS}-V_{GS} linear transfer curve of *p*-type MoO_3 transistor. Reproduced with permission.[52] Copyright 2016, Wiley-VCH. (e) The schematic of twisted bilayer α-MoO_3. f) Optical image of a twisted bilayer α-MoO_3 flake ($\Delta\vartheta$ = −57°, d_1 = d_2 = 150 nm). The white dashed lines denote the [001] crystal directions of the two layers. Reproduced with permission. [10] Copyright 2020, Nature Publishing Group.

The interest in 2D materials includes the oxide family. Some binary oxides materials (MoO_3, WO_3, V_2O_5, etc) have weak vdW layered atomic structures, which allow them to be exfoliated into 2D nanosheets. The vdW gap of representative orthorhombic MoO_3 (α-MoO_3) consists of alternatively arranged MoO_6 octahedrons as shown in **Figure 7a**,[50] making their exfoliation energy slightly higher than that of 2D TMDCs. The bandgap energy of α-MoO_3 is predicted as 3.04 eV where CBM and VBM

are modulated by Mo-d orbital and O-p orbital, respectively. The polar Mo-O bands result in large bandgap energy and a large work function of 6.25 eV, as the theoretical simulation analysis in Figure 7b-c.[51] The bandgap energy of α-MoO_3 can be tuned to smaller by ionic intercalation (proton or alkali metal ions), resulting in the substoichiometric $MoO_{(3-x)}$. Experimental $MoO_{(3-x)}$ field-effect transistors have been reported, and $MoO_{(3-x)}$ was used as a *p*-type semiconducting channel, as shown in Figure 7d.[52] Interestingly, it has been discovered that photonic dispersion of phonon polaritons can be precisely controlled in the twisted bilayer α-MoO_3. The "magic angle" determines the topological transition between hyperbolic and elliptical dispersion at the given frequency. The schematic and optical images of the reported twisted bilayer α-MoO_3 stacking heterojunction are shown in Figure 7e-f, respectively.[10] The unique electrical and optical properties of the vdW oxides make them also a non-negligible part for further 2D device application and integration.

The vdW layered 2D materials discussed above, including graphene, h-BN, TMDCs, MXene, elemental semiconductors Te and BP, and layered oxides, cover most physical properties (metallic, semiconducting, insulating, superconducting, and photo-sensing), which dramatically broaden the types of device application based on 2D materials. Most works on these materials have focused on small flakes with sizes at the micrometer scale. Growing these materials at the wafer-scale has been challenging. Thus, the next part of this review will discuss the status and prospects of wafer-scale growth methods of 2D materials.

3. Wafer-scale growth methods

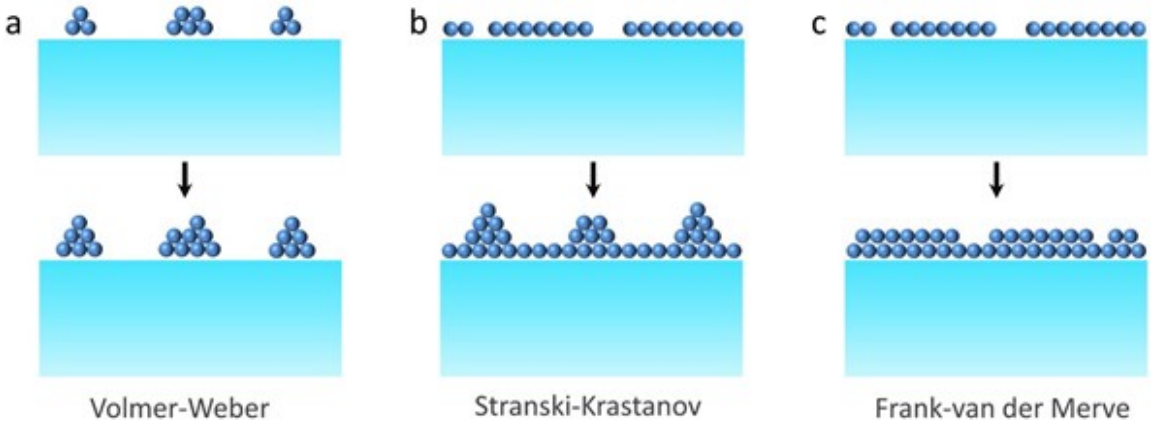

Figure 8. Schematics of three kinds of thin-film growth modes. (a) Volmer-Weber mode (3D island growth). (b) Stranski-Krastanov mode (layer plus island growth). (c) Frank-van der Merve mode (layer-by-layer growth).

The growth of atomically thin 2D vdW materials at the wafer-scale requires understanding the basics of thin-film growth, as shown in **Figure 8**. There are three thin-film growth modes, which include: Vollmer-Weber (island, Figure 8a), Stranski-Krastanov (layer-plus-island, Figure 8b), and Frank-van der Merve (layer by layer, Figure 8c).[53, 54] Their determinant factors are mainly the binding energy ($E_{fa\text{-}sa}$) between film atom (fa) and substrate surface atom (sa), the binding energy ($E_{fa\text{-}fa}$) in-between film atoms, the strain between film and substrate lattice, and growth conditions. If $E_{fa\text{-}fa} > E_{fa\text{-}sa}$, then three-dimensional island growth mode is preferred. If $E_{fa\text{-}sa} > E_{fa\text{-}fa}$, the layer-by-layer growth mode is preferred. However, in the case of layer-plus-island growth mode, thin films grow initially through layer-by-layer growth mode until a thickness of several monolayers has been achieved, followed by island growth mode. Besides these basics of thin-film growth, the unique week vdW bonds in the 2D materials lattice need to be seriously considered when developing their wafer-scale film growth methods.

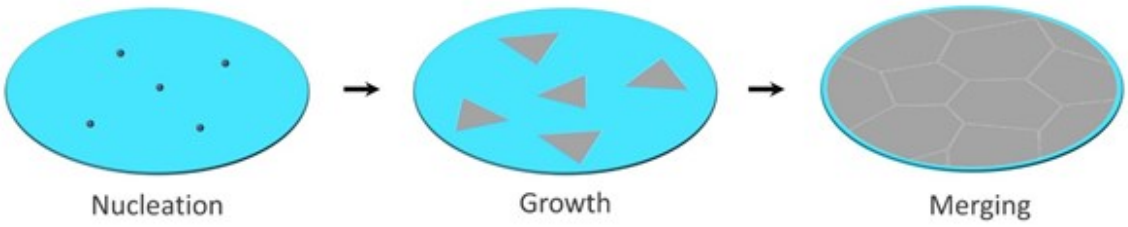

Figure 9. Schematic of the wafer-scale 2D film growth process: firstly, the nucleation is formed as the growth center of grain domains; Secondly, the growth of the 2D grain domains; thirdly, the merging of 2D domains into a continuous film at the wafer scale.

Explorations of wafer-scale 2D film growth started more than 12 years ago when the large-scale graphene growth was first demonstrated in 2009.[55] Most of the 2D vdW films that have been successfully grown at the wafer scale share a similar growth process: (1) nucleation of 2D flake center, (2) growth of 2D domains, and (3) merging of 2D domains into a continuous film, as illustrated in **Figure 9**. Since 2D vdW materials have a unique vdW gap, the 2D adatoms have much weaker binding energy on both substrate and 2D domain surfaces than on the domain edges.[56, 57] Thus, the 2D vdW film growth usually proceeds through layer-by-layer growth rather than by island growth mode.[58] This characteristic has imposed fewer constraints on the substrate surface structures (lattice type and orientation) and has led to the development of several growth methods for 2D material growth at the wafer scale.

WILEY-VCH

3.1. Co-vapor tube CVD Growth Process

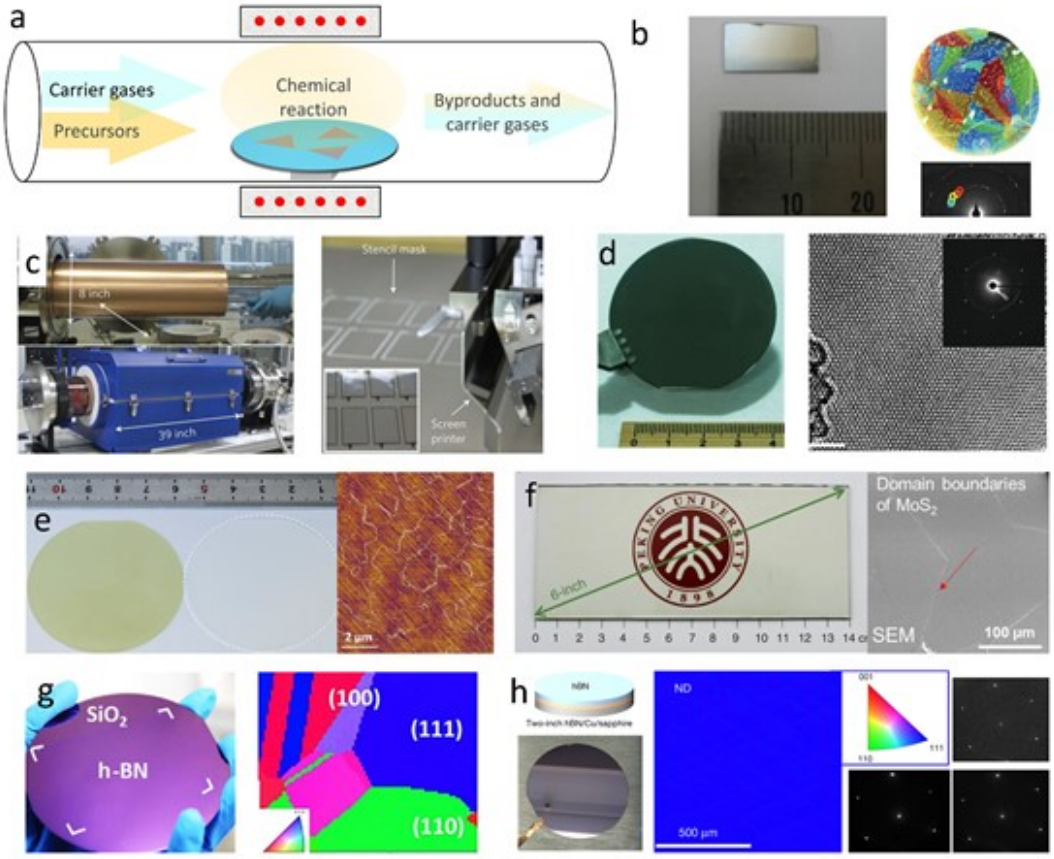

Figure 10. Growth of wafer-scale 2D films based on tube CVD System. (a) The schematic of a tube CVD system. (b) The graphene film is grown on a Ni (300 nm)/SiO_2 (300 nm)/Si substrate. Reproduced with permission.[55] Copyright 2009, Nature Publishing Group. Figures on the Left side show the polycrystalline graphene domain size by DF-TEM and SAEDs. Reproduced with permission.[59] Copyright 2011, Nature Publishing Group. (c) Photographs of the roll-based production of graphene films and transferred on a PET substrate. Reproduced with permission.[60] Copyright 2010, Nature Publishing Group. (d) Single-crystalline Graphene film grown in the Germanium substrate. Reproduced with permission.[14] Copyright 2014, American Association for the Advancement of Science. (e) Highly orientated MoS_2 film grown on a sapphire substrate. Reproduced with permission.[16] Copyright 2017, American Chemical Society. (f) Polycrystalline MoS_2 film grown on a 6-inch glass. Reproduced with permission.[61] Copyright 2018, Nature Publishing Group. (g) Polycrystalline BN grown on a Cu and transferred on a SiO_2/Si substrate. Reproduced with permission.[62] Copyright 2015, Springer Nature. (h) Single-crystalline h-BN grown on

Cu(111)/sapphire substrate. Reproduced with permission.[63] Copyright 2020, Nature Publishing Group.

The co-vapor tube CVD is the most popular process used to grow 2D vdW flakes. Recently, it has been demonstrated to be an effective method to also grow wafer-scale 2D films. Graphene, TMDCs (MoS_2, $MoSe_2$, WS_2, $TaSe_2$, *etc*) and h-BN films have been successfully grown through well-designed CVD systems at the wafer scale. These materials were first grown as polycrystalline film and later were improved where the single-crystalline structure at the wafer-scale was achieved. Most tube CVD systems used in this process share several common features: ①precursor vapor(s) are transported inside the growth chamber by special carrier gases at a certain pressure; ② the growth substrate is placed in the hot zone; ③the precursor vapors start the chemical reaction to deposit 2D flakes on the substrate surface, the byproducts are exhausted by the carrier gases; ④the initial growth stage is forming randomly distributed 2D flakes, then the flakes enlarge and merge over time to form a continuous film on the wafer. This co-vapor CVD process is shown schematically in **Figure10a**.

Graphene was the first 2D material to be grown at the large-scale using the tube CVD system (on Ni film surface in 2009).[55] Figure 10b displays one graphene/Ni sample and its polycrystalline structure was also pointed out. It is difficult to grow a uniform graphene film on a Ni surface because of significant C solubility in Ni. However, Cu arises as an excellent candidate for growing large-area graphene films with uniform thickness due to the low solubility of C in Cu.[64] Several reports verified wafer-scale or even 30 inch-scale graphene films on the Cu foil surface.[60, 65] Figure 10c shows the roll-to-roll tube CVD process for preparing 30 inch-long graphene films, which can be transferred onto the flexible PET substrate.[60] However, initial graphene films were grown with a polycrystalline

structure, containing many grain boundaries, which are not favorable for device applications. The first single-crystalline wafer-scale graphene film with monolayer thickness was grown on a germanium (110) surface in 2014 (Figure 10d).[14] In the following years, single-crystalline *AB*-stacking bilayer graphene films were also reported on both the Cu(111)/sapphire in 2016 [66] and liquid Pt_3Si/solid Pt surfaces in 2019.[67] In 2020, single-crystalline graphene films were grown on polycrystalline metal surfaces with the help of mono-oriented seed arrays.[68] More details of graphene single-crystalline CVD growth could be found in another recent review.[69]

Besides graphene, several 2D TMDCs films have been grown at the wafer scale using a co-vapor CVD system. In 2017, highly oriented continuous MoS_2 monolayer films (Figure 10e) were successfully grown on 2-inch sapphire substrates.[16] In the following years, larger wafer-scale MoS_2 films were grown on 6-inch glass (Figure 10f)[61] and 4-inch sapphire substrate.[70] Other TMDCs such as $MoSe_2$, [71] WS_2, [72] and $TaSe_2$ [73] were also successfully grown over a wafer through a co-vapor tube CVD system. Most of these wafer-scale films are polycrystalline with micrometer-scale domain sizes. However, single-crystalline MoS_2 films have been recently reported on Au (111) surface using a CVD system.[74] Another reported single-crystalline MoS_2 film was successfully grown on the insulating sapphire substrate through an epitaxial phase conversion method,[75] which will be discussed later.

Growth of insulating h-BN films at the wafer-scale was first demonstrated in 2012 using the tube CVD.[15] Both polycrystalline and single-crystalline films were achieved. Similar to graphene, h-BN CVD growth occurs preferentially on metal substrates, especially Cu and Ni.[57, 62, 76-78] The polycrystalline h-BN film was obtained in the tube CVD process when using a randomly oriented Cu foil as the substrate, and the h-BN film can be transferred on other substrates for device fabrication,

see Figure 10g. [62] Single-crystalline monolayer h-BN films growth at wafer-scale were also reported on liquid Au metal,[79] Cu(110) [80] and Cu (111).[63] Figure 10f displays one example of a single-crystalline h-BN film on Cu(111)/Sapphire.[63] To avoid metal ion contamination after transferring the 2D film away from the metal substrate, wafer-scale h-BN films were explored to be grown on insulating substrates such as sapphire. [81] However, the growth of single-crystalline (or, at least, low defect density) multilayer h-BN remains a challenge ;[82, 83] this is especially important for the fabrication of electronic devices because h-BN is the only 2D material employed as dielectric, and the leakage current across monolayers is prohibitive (>10 A/cm^2 at 0.1 V), even if they are of perfect quality (i.e., single-crystalline).[84] There are currently no reports on using a tube CVD system to grow MXene, 2D BP, Te and vdW oxides at the wafer scale.

3.2. MOCVD growth process

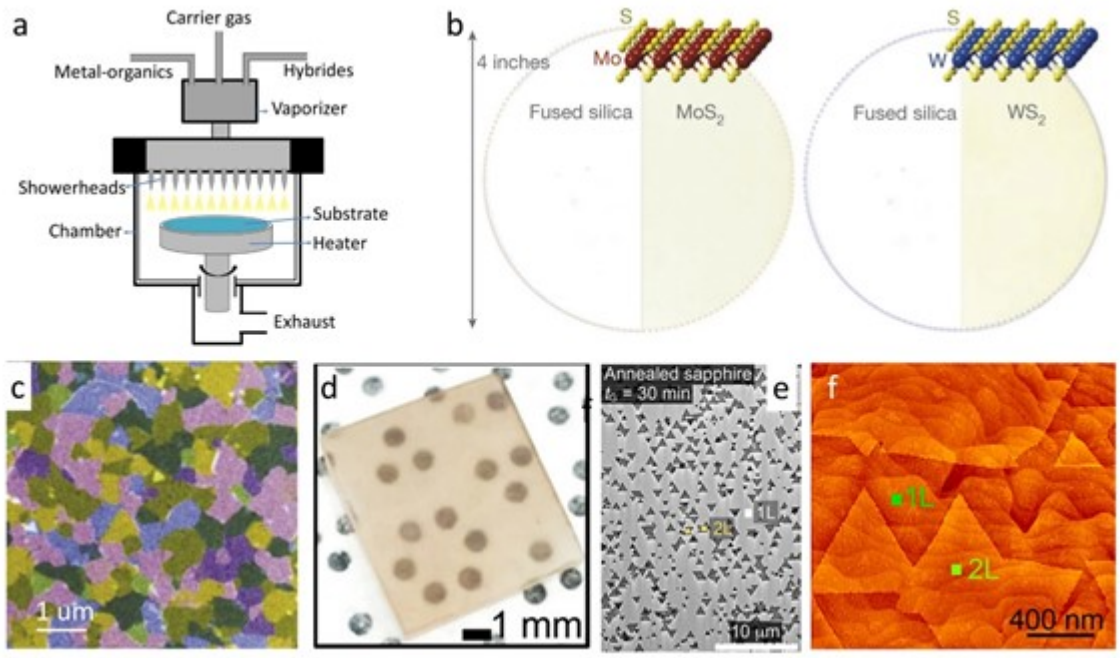

Figure 11. Growth of wafer-scale 2D films by MOCVD. (a) The schematic of the MOCVD system. (b) MoS_2/WS_2 film grown on a 4-inch fused silica substrate. Reproduced with permission. [85] Copyright 2015, Nature Publishing Group. (c) Polycrystalline MoS_2 domains characterized by TEM. Reproduced with permission.[85] Copyright 2015, Nature Publishing Group. (d) The WSe_2 film grown in the sapphire substrate. Reproduced with permission.[86] Copyright 2018, American Chemical Society. WSe_2 triangle domains with highly orientated growth direction displayed by (e) SEM image and (f) AFM height image on the sapphire substrate. Reproduced with permission.[86] Copyright 2018, American Chemical Society.

MOCVD is another type of chemical vapor deposition system which uses a pulsed precursor gas vapor source. **Figure 11a** illustrates a schematic of a simplified MOCVD system. This approach has been most commonly used to grow 2D films TMDCs at the wafer scale. The reason is the growth of TMDC films by the tube CVD process is very challenging because of the difficulty in precisely controlling the precursor vapor concentration and stable distribution, which leads to poor repeatability and uniformity of the 2D film over large wafers. However, MOCVD can more precisely control the supply of precursors using pulse time, pressure, and precursor concentration. It is very

promising in 2D film stable growth at a larger wafer, overcoming the challenges faced by the tube CVD. However, some precursors may cause possible carbon residuals contamination in the grown 2D film.[58, 87] In contrast to TMDCs, few studies were reported on the growth of graphene and h-BN by the MOCVD process.[88-90] Examples of MOCVD processes used to grow TMDCs are illustrated in Figure 11b-f. The first paper in 2015 reported MOCVD growth of MoS_2 and WS_2 monolayer continuous films on 4-inch SiO_2/Si wafers, as shown in Figure 11b. Their polycrystalline feature can be visualized in the TEM image (Figure 11c). The Mo, W, and S precursors used in this report are $Mo(CO)_6$, $W(CO)_6$, and $(C_2H_5)_2S$. However, this process takes a relatively long time (about 26 hrs) for the whole growth process. [85] Another recent study in 2017 reported MoS_2 film MOCVD growth on 6-inch SiO_2/Si wafers using H_2S and $Mo(CO)_6$ as the S and Mo precursors, respectively. The growth temperature was relatively low (400 ^oC) with a growth time of about 9 hrs.[91] The MoS_2 growth on sapphire substrates was explored in 2019 using Na_2MoO_4 and $(C_2H_5)_2S$ precursors with a short growth time of about 20 mins. However, controlling the TMDCs film crystal orientation began to be reported recently through carefully-controlled growth parameters on single-crystalline substrates. Both highly-oriented WSe_2 film[86] and mono-oriented WS_2 films[92] were reported by MOCVD growth on the c-cut sapphire substrate. This large-area film sample is displayed in Figure 11d, and near unidirectional nucleation is displayed in the SEM image in Figure 11e. However, few-layer islands on top of the continuous monolayer film could be detected through the AFM analysis, as shown in Figure 11f. [86]

TMDCs MOCVD film growth has achieved noticeable progress and is regarded as one of the most industrially favorable growth methods. However, reproducibility, large-area uniformity, and island-free monolayer film growth with single-crystalline features over the whole wafer still need further

improvement. Also, the precursor sources and some gaseous by-products (e.g., CO) are toxic, thus precautions need to be implemented to deal with the toxic gases in the MOCVD growth of TMDCs.[87] The growth of other 2D vdW materials (MXene, BP and Te, MoO_3) has not been reported by MOCVD yet.

3.3. MBE growth process

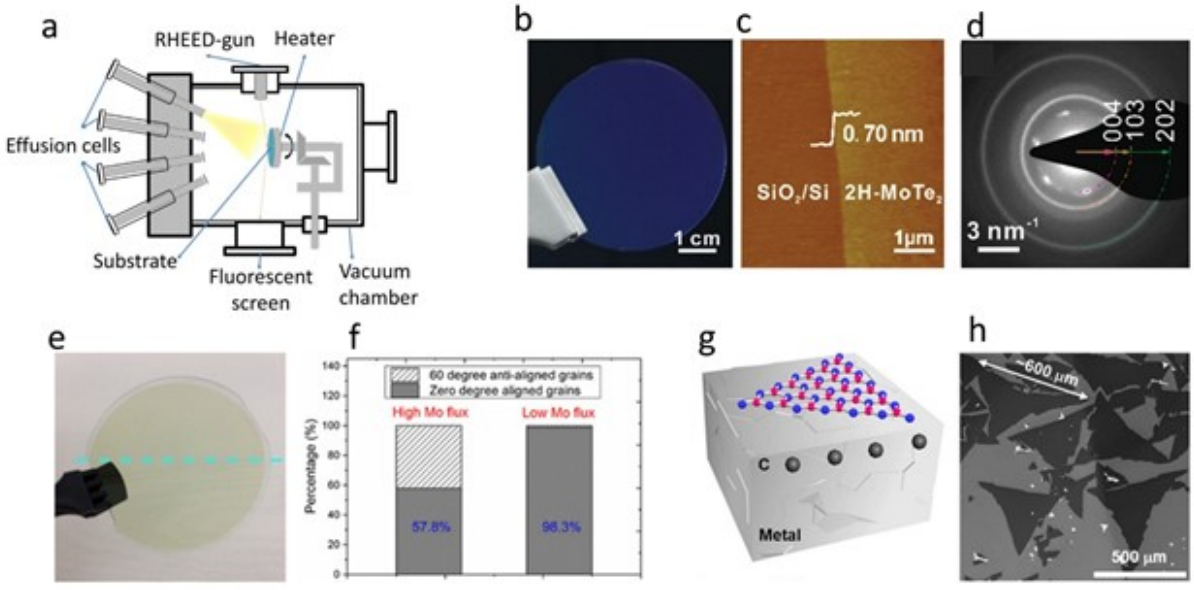

Figure 12. Growth of wafer-scale 2D films by MBE. (a) The schematic of the MBE system. (b) The $MoTe_2$ film grown on a 2-inch SiO_2/Si substrate. (c) Monolayer thickness of the film confirmed by AFM height image. (d) Polycrystalline feature of $MoTe_2$ confirmed by TEM SAEDs. Reproduced with permission.[38] Copyright 2018, Wiley-VCH. (e) The MoS_2 film grown in the h-BN/sapphire substrate. (f) High-orientation of MoS_2 film growth can be achieved by tuning Mo precursor flux. Reproduced with permission.[93] Copyright 2017, American Chemical Society. (g) large-size h-BN grown on Ni(001) substrate. (h) SEM image of large-size h-BN domains. Reproduced with permission.[94] Copyright 2019, Wiley-VCH.

MBE is another growth method that has been used to grow 2D films at the wafer scale. A schematic of a typical MBE system is shown in **Figure 12a**. The substrate is placed inside an ultra-high vacuum (UHV) chamber on a stage held at the desired growth temperature. Precursors are placed in effusion cells and are pulse-evaporated inside the UHVchamber where they react at the substrate surface. The MBE growth holds several advantages: ①the UHV environment could minimize impurities during the growth; ②the UHV environment enables in-*situ* electron diffraction monitoring the film growth process; ③high-purity precursor elements could be used in the effusion cell, which is very important to minimize film defects; ④the very slow deposition rate (typically less than 5 Å/min) could enable precise layer-by-layer growth.[95] For these reasons, the wafer-scale growth of 2D vdW films by MBE has been investigated by several groups.

For example, the 2H $MoTe_2$ film growth on 2-inch SiO_2/Si wafer (Figure 12b) by MBE with 100% monolayer (Figure 12c) coverage has been successfully developed by the Yao group. However, the film was polycrystalline with random domain orientations, as confirmed by the SAED pattern in Figure 12d. The Loh group successfully grew highly-oriented monolayer MoS_2 films by MBE on 2-inch h-BN/sapphire substrates (Figure 12e). They could achieve 96.3% zero aligned domain orientation with the help of low Mo precursor flux during the growth, as shown in Figure 12f. Other TMDCs, such as ferroelectric In_2Se_3[96] and ferromagnetic Fe_3GeTe_2[97] films, were also grown at the wafer

scale using the MBE. Also, one study reported the possibility of using an MBE system to grow a large-area h-BN on a Ni metal surface (Figure 12g). However, the film was not continuous and consisted of semi-isolated flakes, as shown in Figure 12e.

The growth of TMDCs films by MBE at the wafer scale is effective at controlling the domain orientation and the number of atomic layers. But the required UHV systems are complex and the processes are quite sensitive to the growth environment, which limits its industrial application. Thus, MBE-grown 2D vdW films are mainly serving as an important research and development tool. Similar to the other methods, there are still no reports involving MBE growth of MXene, BP, Te, and MoO_3.

3.4. ALD Growth Process

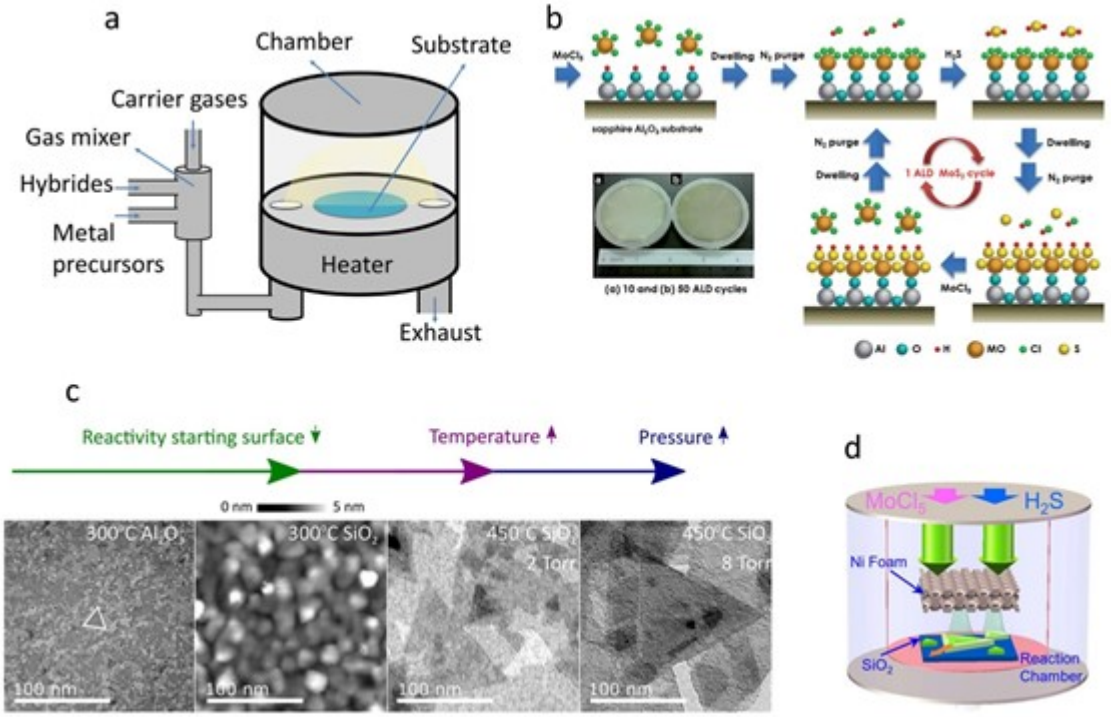

Figure 13. Growth of wafer-scale 2D films by ALD. (a) The schematic of the ALD system. (b) The ALD process flow schematic of the MoS_2 film grown on a 2-inch sapphire substrate. Reproduced with permission.[98] Copyright 2014, Royal Society of Chemistry. (c) Domains are influenced by substrate surface, temperature, and pressure. Reproduced with permission.[99] Copyright 2018, American Chemical Society. (d) The Schematic of Ni foam assistant ALD growth of uniform and high-quality MoS_2 film. Reproduced with permission.[100] Copyright 2019, American Chemical Society.

The semiconductor industry, which has funded vdW layered film growth research over the past five years, is particularly interested in the possibility of inserting TMDCs into the back-end-of-line (BEOL) to enable Si CMOS compatible integration. This limits the growth temperatures for 2D vdW films to ~450 °C and lower.[95] ALD appears to be the proper technique to synthesize 2D materials at low temperatures because of its simplicity, versatility, and control of the thickness at the angstrom level. Based on self-terminated surface reactions, the precursors are kept separated and react only with surface species in a self-limiting process, forming at most one single atomic layer

per cycle, as shown in **Figure 13a**. The reaction is well confined on the substrate surface with few reactions happening in the vapor phase, differentiating the ALD from CVD. Each surface reaction is separated by a purge step to remove the unreacted precursor and the by-product. The sequence of reactant surface reactions and purges constitutes a cycle. Due to the self-limiting character of the ALD reactions, the thickness of the as-deposited film is simply controlled by the number of cycles with precision at the angstrom level.[101] In 2014, Loh et al. first reported the ALD of a MoS_2 film on a 2-inch sapphire substrate via employing $MoCl_5$ and H_2S as reactants and an exposure mode at 300 ^oC (Figure 13b).[98] Owing to the self-limiting reactions of the vapors, this ALD process could control the film thickness precisely, thus leading to wafer-scale monolayer and multilayer MoS_2 film. Meanwhile, after annealing at 800 °C in saturated sulfur vapor, the crystallization improved effectively. The effect of growth parameters on films has also been investigated. Delabie et al. utilized plasma-enhanced ALD (PEALD) to grow WS_2 film at low deposition temperature (≤450 ^oC). [99] The results showed that the substrate and deposition conditions had a significant impact on the nucleation and growth of the films, as shown in Figure 13c. By using amorphous Al_2O_3 as the substrate, the nucleation rate was very rapid, resulting in a small grain size. In order to increase the grain size, SiO_2 substrate with an inherently lower reactivity was used. The enhanced deposition temperature and reactor pressure could further expand the grain size up to ~200 nm. Additionally, Liu et al. reported the influence of precursor flow on the grain size of MoS_2 (Figure 13d). [100] After placing one Ni foam on top of the substrate, a trickle-fluidization source flow was obtained, giving rise to the larger MoS_2 grain sizes up to ~400 nm. Although the ALD technique has been employed to grow various 2D materials, the growth of high-quality wafer-scale films is still challenging. Another recent review paper gives more details on the 2D layered materials ALD growth. [102]

3.5. Two-step precursor conversion growth processes

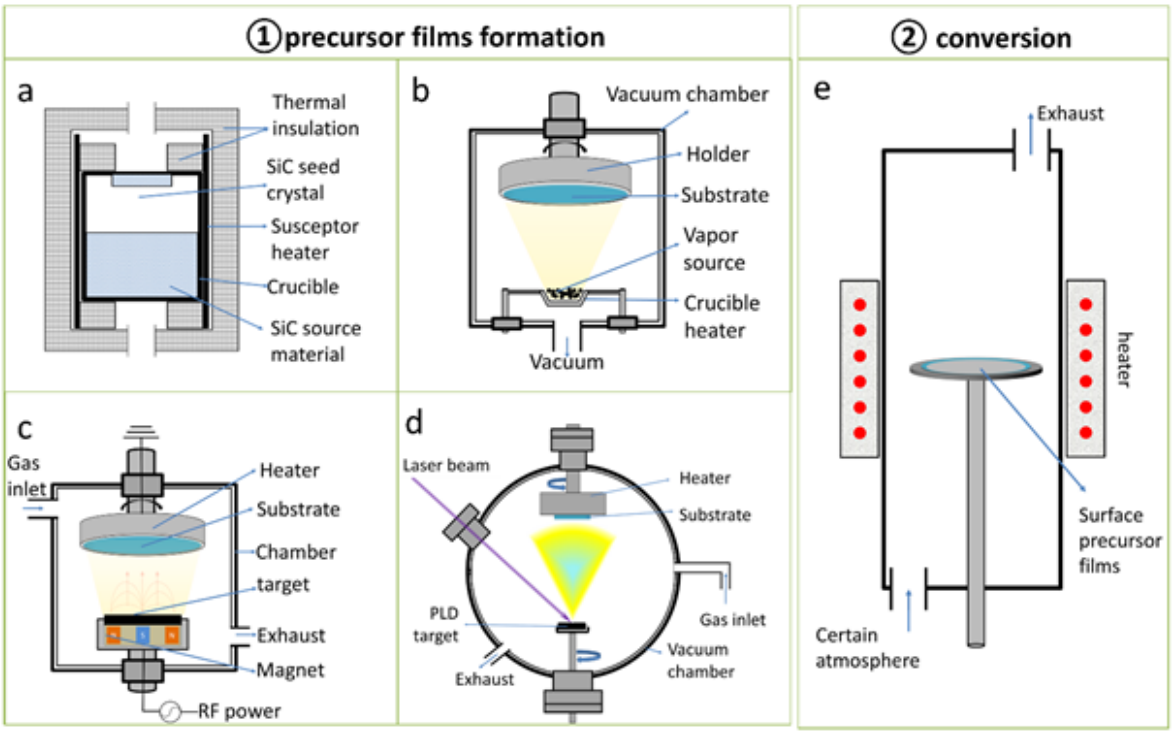

Figure 14. Growth of wafer-scale 2D films by precursor conversion:①precursor films formation through several possible PVD systems ②chemical or physical conversion in the particular high-temperature atmosphere. Schematic of (a) SiC seeded sublimation growth system. (b) Thermal evaporation system (c) Sputtering system (d) PLD system (e) Chemical conversion system.

The two-step process is another method that has been used to grow wafer-scale 2D films by chemical or physical transformation of precursor films or wafer surfaces. The two-step growth process includes (1) precursor film formation, and (2) precursor film conversion, as illustrated in **Figure 14**. The precursor formation process can be achieved by several methods including: seeded sublimation growth (Figure 14a),[103] thermal & E-beam evaporation (Figure 14b),[104-108] sputtering (Figure 14c),[109] pulsed laser deposition (Figure 14d),[75, 110, 111] and spin or bar coating.[112-115] The conversion step could include: decomposition, [115-117] chemical [75, 105, 107, 118, 119] or physical [120, 121] conversion. This process has been successfully demonstrated for growth of wafer-scale graphene,[116, 117] 2D TMDCs (MoS_2, [75, 109-115] $MoTe_2$,[120] 1T-WS_2,[107] In_2S_3,[118] SnS,[122] $PtTe_2$,[119] $PtSe_2$,[123] *etc*) and BP films.[121]

There are two types of two-step film conversion processes: one is the chemical conversion of precursor films, the other is the physical conversion of precursor films. Many 2D vdW films have been obtained by chemical conversion of their precursor films or wafer surface. Graphene was converted from the surface of the SiC wafer. Many TMDC films were grown by chemically converting their metal-based precursor films, which will be discussed in detail in **Figure 15**. There are also several reports about the physical conversion of their allotrope films, as in the case with $MoTe_2$ and BP film formation as will be discussed in Figure 16.

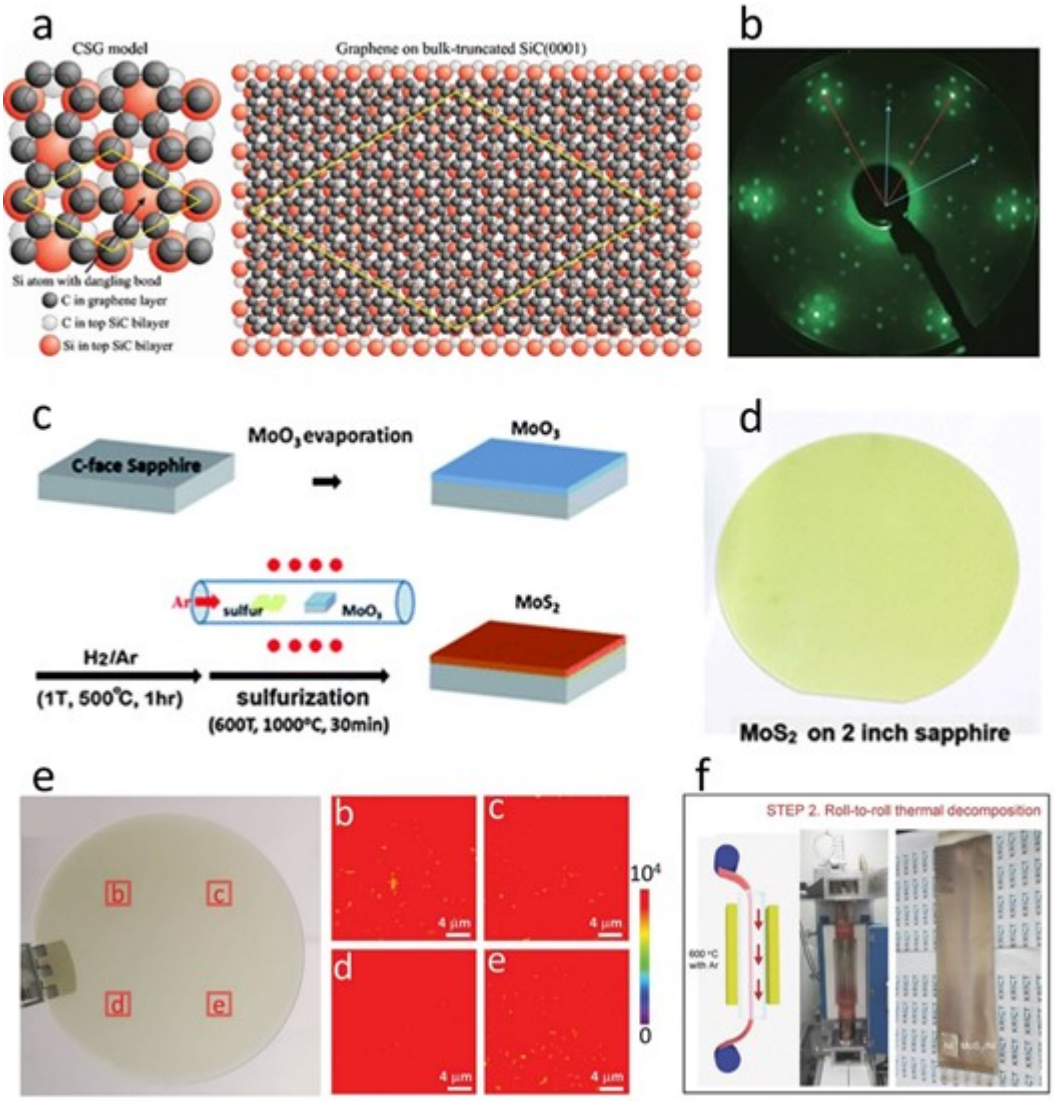

Figure 15. Wafer-scale growth of 2D graphene and MoS_2 films by a two-step chemical conversion process. The schematic of (a) Left: Top view of the covalently bound stretched graphene (CSG) model on (001) SiC. Right: a monolayer graphene epitaxial placed on the bulk-truncated (001) SiC surface. Reproduced with permission.[116] Copyright 2008, American Physical Society. (b) The LEED pattern of epitaxial monolayer graphene obtained from the graphitization of (001) SiC. Reproduced with permission.[117] Copyright 2009, Nature Publishing Group. (c) The sulfurization process of the thermal evaporated MoO_3 film. (d) A 2-inch few-layer MoS_2 film on the sapphire substrate. Reproduced with permission.[108] Copyright 2012, Royal Society of Chemistry. (e) A 2-inch monolayer MoS_2 film obtained through epitaxial phase conversion process, uniformity confirmed by PL mapping at four different locations. Reproduced with permission.[110] Copyright 2019, Wiley-VCH. (f) The roll-

to-roll production of MoS_2 film through chemical conversion of $(NH_4)_2MoS_4$/Ni film. Reproduced with permission.[115] Copyright 2018, Wiley-VCH.

The two-step chemical conversion process chemically transforms the as-prepared precursor films or wafer surfaces to obtain wafer-scale 2D films, as shown in **Figure 15**. The chemical conversion could be thermal decomposition or chemical cation exchange or intercalation. Monolayer graphene has been successfully obtained through the thermal decomposition of the (0001) SiC wafer surface.[117] This film has been confirmed theoretically (Figure 15a) and experimentally (Figure 15b) to have a mono-oriented epitaxial feature. [116, 117] Two-step processes used to grow TMDCs films usually include oxygen-chalcogen cation chemical exchange in the ultrathin transition metal oxide films or chalcogen cation intercalation inside the ultrathin transition metal films. Wafer-scale MoS_2, WS_2, In_2S_3 and SnS_2 films were successfully grown through high-temperature O-S exchange in the MoO_3 [108, 109, 124] (Figure 15c, d) or MoO_2[110] (Figure 15e), WO_3,[125] In_2O_3[118] and SnO_2[126] films. The chemical O-Se exchange process in WO_3[127] and MoO_3[128] films results in WSe_2 and $MoSe_2$ films. The process of S, Se and Te [129] intercalation inside ultrathin metal Mo,[105, 112] W[105] and Pt[119, 123, 130] films can also produce wafer-scale MoS_2, WS_2, PtS_2, $PtSe_2$ and $PtTe_2$ films. These two-step cation exchange or interaction processes have been usually performed at high temperatures above 600 ^oC, which limits their use in low-temperature electronic applications. Thermal decomposition of precursor films is also one type of two-step growth of 2D TMDC films at relatively low temperatures. As we can see from Figure 15f, bar-coated $(NH_4)_2MoS_4$ film on Ni foils could be decomposed at 400 ^oC to realize industrial-scale MoS_2 film production by a roll-to-roll method.[115] $(NH_4)_2MoS_4$[112, 114] or Mo-containing polymer-precursor[113] films could be coated on rigid silicon or flexible substrates as precursors then decomposed into MoS_2 films at low temperature.

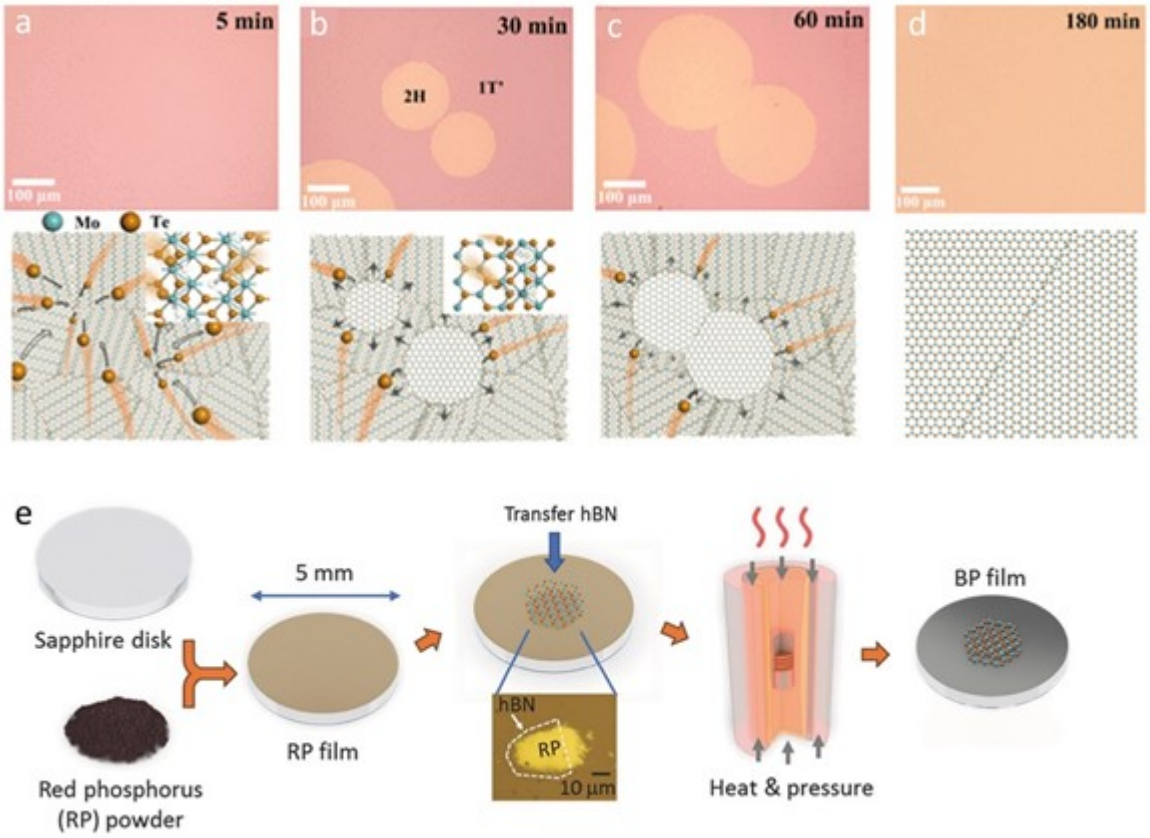

Figure 16. The growth of $MoTe_2$ and BP films through a two-step physical conversion process. (a-d) the optical morphology variation and schematic of the 1T' to 2H $MoTe_2$ film physical phase transformation. Reproduced with permission.[120] Copyright 2019, American Chemical Society. (e) The schematic of BP film growth through the red phosphorus (RP) phase change process. Reproduced with permission.[121] Copyright 2018, Wiley-VCH.

Another reported two-step process is to grow large-area 2D semiconductors through the physical conversion of their allotrope precursor films. It is a rare method for large-scale 2D film growth. To our knowledge, only semiconducting 2H $MoTe_2$[120] and BP[121] films have been achieved through the physical conversion process, as displayed in **Figure 16**. Figure 16a-d illustrates the

process used for conversion from 1T' $MoTe_2$ to 2H $MoTe_2$. The Te vacancies in the 1T' $MoTe_2$ film were regarded as the phase transformation center (Figure 16a). Under certain high-temperature and reducing atmospheres, the 2H domain size increased with time (Figure 16b-c) until a much larger 2H $MoTe_2$ domain could be obtained after 180 mins (Figure 16d).[120] The wafer-scale 2H $MoTe_2$ film was also achieved by the same group, but the physical conversion needs almost 126 hrs for one 1-inch sample fabrication.[131] The BP film could also be obtained through the physical transformation of red phosphorus (RP) film, as shown schematically in Figure 16e. The RP film was firstly grown through thermal evaporation on the sapphire substrate. A BN film was coated as a protection layer on the RP film surface. Then, the BN-capped RP film was treated in a high-temperature/pressure furnace until a BP film was successfully achieved. [121] Another study also demonstrated a two-step process to obtain BP film from RP film.[132]

Compared to the popular MOCVD or CVD processes (taking the well-studied MoS_2 growth as an example), two-step processes have some advantages: the large-scale area and thickness of the 2D films could be predefined by the precursor films. However, 2D semiconducting films obtained through most of the two-step processes have inferior lattice and electronic properties. Another issue is that it is very challenging to grow continuous monolayer films. Our group has performed several studies to improve MoS_2 film quality in two-step processes.[75] [110] Unlike amorphous precursors used in the traditional two-step growth, we used single-crystalline epitaxial precursors that were converted into the MoS_2 film, which resulted in a single-crystalline structure with much better electronic performance.[75, 110]Our group also achieved uniform and continuous monolayer MoS_2 films by minimizing the gas flow fluctuation in the two-step process, as shown in Figure 15e. [110]

3.6. PVD growth process

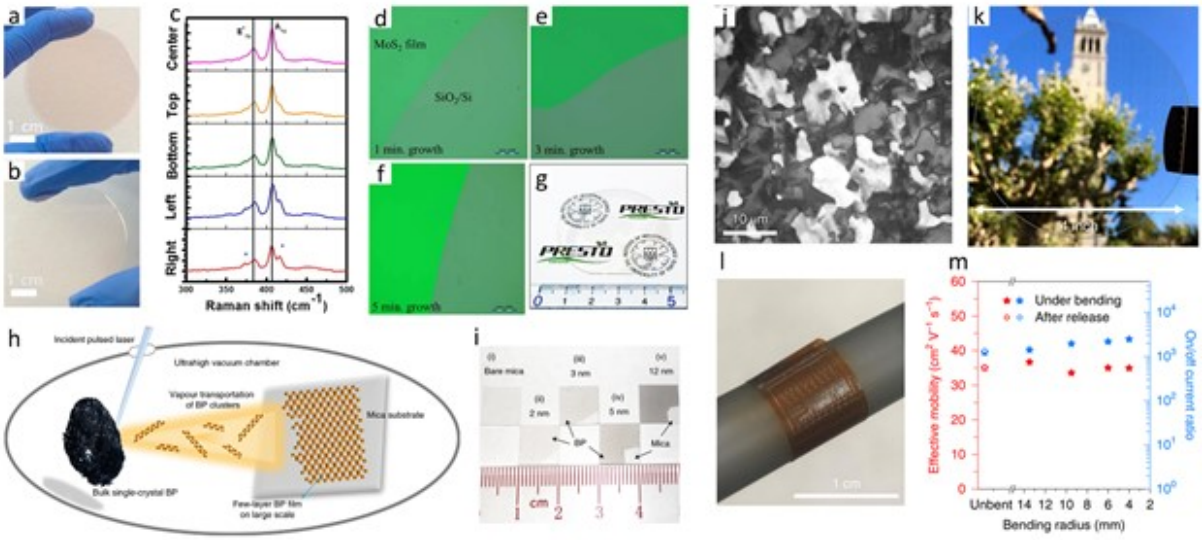

Figure 17. The growth of MoS_2, BP and Te films by PVD process. (a-c) PLD growth of MoS_2 film with different thicknesses, the uniformity was confirmed by Raman. Reproduced with permission.[133] Copyright 2016, American Chemical Society. (d-f) Sputtering growth of MoS_2 films with different thicknesses. Reproduced with permission.[134] Copyright 2016, Nature Publishing Group. (h-i) PLD growth of large-area BP film with different thicknesses. Reproduced with permission.[135] Copyright 2021, Nature Publishing Group. (j-m) Thermal evaporation of Te film with the excellent flexible electronic application. Reproduced with permission.[46] Copyright 2020, Nature Publishing Group.

Direct physical vapor deposition methods have also been explored to grow large-area 2D films using PLD[133], sputtering [134] and thermal evaporation systems. [46] PLD has been demonstrated as a powerful high-vacuum tool for high-quality oxide films.[136] PLD growth of large-area metallic graphene,[137] semiconducting TMDCs,[133, 138] BP,[139] and insulating BN films[138] has also been explored recently. Most of the graphene films using CVD were grown on metallic copper substrates, while graphene could be grown on an insulating substrate by PLD.[137] 2D semiconducting TMDCs films, especially MoS_2 have been investigated by several groups.[133, 138] The stoichiometric ratios of 2D MoS_2 films were greatly influenced by the S/MoS_2 ratio in the PLD target.[133] The 2-inch wafer MoS_2 film grown on sapphire substrate and the Raman spectra uniformity is shown in **Figure 17a-**c. Using Au (111) substrate, MoS_2 lattice orientation could be well optimized through PLD growth.[138] Growth of large-area insulating h-BN film could also be achieved on metal substrates through PLD, with the help of the dissolution of carbon into cobalt (Co) and nickel (Ni) substrates.[94] Some literature reported large-area semiconducting MoS_2 and insulating BN films using sputtering.[134, 140, 141] MoS_2 films with different thicknesses obtained through sputtering are shown in Figure 17d-f,[134] while the 2-inch wafer-scale h-BN film is shown in Figure 17g.[141] Most of the 2D semiconducting compounds obtained through the physical vapor deposition are very defective and show poor electronic properties, especially TMDCs. Chalcogen elements are much easier to evaporate in the

high-vacuum system than transition metal elements during the high-temperature growth, leaving the 2D films with a large number of chalcogen vacancies. However, PLD growth of elemental 2D BP film on ultra-flat mica substrate has been achieved recently and shows excellent film quality.[135] Also, thermal evaporation of 2D element Te films was demonstrated with high-crystalline quality (Figure 17h) and high transistor performance, when the supporting substrate was held at low temperature -80 ^{o}C during the Te deposition.[46] The 2D Te film could grow on most of the rigid and flexible substrates (Figure 17i-j) and has demonstrated excellent bendable and electrical performance (Figure 17k).

Thus, the PVD method can be used to grow 2D vdW films over large wafers, but for the compound 2D materials, the film quality is usually not as good as the two-step film conversion or chemical deposition methods. However, the PVD method can be very promising for the growth of high-quality, large-scale 2D elemental materials, such as BP and Te.

3.7. Solution growth process

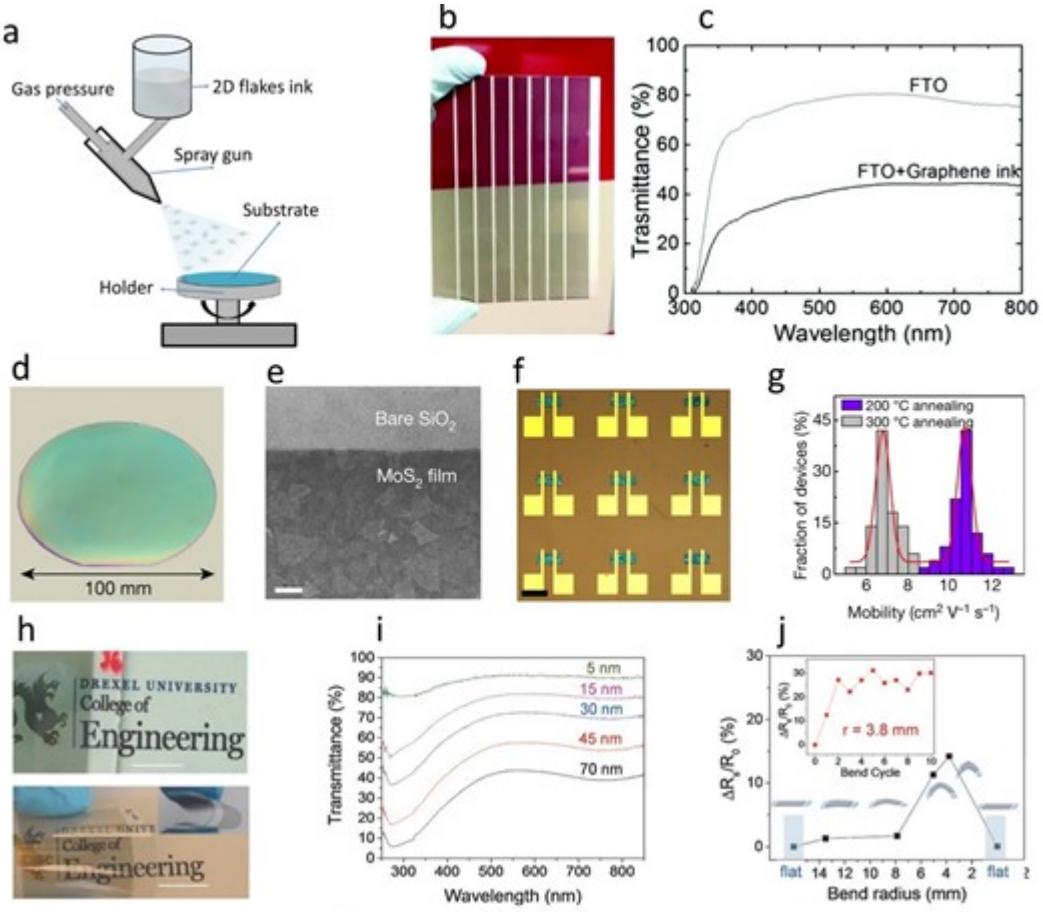

Figure 18. Growth of wafer-scale 2D films from solution process system. (a) Schematic of a spray coating system. (b) The semitransparent graphene/FTO/glass electrode sample. (c) Optical transmittance of FTO (grey curve) and graphene-coated FTO substrate (black curve). Reproduced with permission.[142] Copyright 2016, Royal Society of Chemistry. (d) MoS_2 film spin-coated on the 4-inch SiO_2/Si substrate. (e) High-magnification SEM image of the MoS_2 thin film, showing the conformal stacking of individual nanosheets along the (001) direction. Scale bar, 1 μm. (f) Transistors

array taking MoS_2 flack-stacking film as the channel, Scale bar, 100 μm. g) Field-effect mobility of MoS_2 film under different annealing temperatures. Reproduced with permission.[143] Copyright 2018, Nature Publishing Group. (h) Optical images of MXene $Ti_3C_2T_x$ films on glass and a bendable, flexible polyester substrate. Scale bar, 1 cm. (i) Optical transmittance of MXene $Ti_3C_2T_x$ films with different thicknesses. (j) Resistance changes as a function of bending. Reproduced with permission.[144] Copyright 2016, Wiley-VCH.

The solution process could be an alternative practical method to obtain wafer-scale 2D films. It is a low-cost process compared to processes that require high-vacuum systems and high-temperature reactions. One common solution process is spray coating, which is schematically displayed in **Figure 18a**. Firstly, a homo-disperse and concentration-controlled 2D flakes suspension should be prepared in an evaporable solvent (such as water or alcohol). Then using a spray gun, the 2D suspension could be dispersed uniformly on the substrate. During the stacking of 2D flakes into the wafer-scale film, the solvent undergoes evaporation so that the flake stacking occurs uniformly and continually, thus avoiding aggregation by the solvent drop residuals. Many 2D vdW materials such as graphene,[142] MoS_2, [143] MXene,[144] and h-BN[145] have been deposited at the wafer-scale by spray coating their corresponding 2D suspensions. Figure 18b shows one semi-transparent graphene film obtained by spray coating, which can be useful for large-area transparent electronics. Figure 18c illustrates the transparency of graphene spray-coated on FTO glass at a different wavelength in the visible range. Spin coating is another well-known solution process method. Wafer-scale MoS_2 films formed by 2D flake stacking through sprin-coating have shown promising electronic properties. [142] A MoS_2 film coated at the wafer-scale in Figure 18d obtained by solution processing. The film morphology shown in Figure 18e consists of uniform laterally stacked flakes on the surface of the substrate. Transistor device arrays were fabricated using standard photolithography to pattern the MoS_2 films (Figure 18f). Figure 18g confirms that solution-processed large-area 2D semiconductor films exhibit very promising electrical performance. MXenes, a new family of 2D vdW materials, have

so far been reported with large-area films only through the solution process. [144] For example, the $Ti_3C_2T_x$ MXene films formed by the spray coating process are shown in Figure 18h.[144] MXenes are promising contact materials for transparent electronics because of their high conductivity, tunable work function in a large range and easy to disperse in water without any surfactants.[146] Their transparency is inversely proportional to their thickness (Figure 18i).[144, 147] Its films formed on the flexible substrate shows stable electric conductivity after a specific bending process (Figure 18j).[144] The solution process usually forms 2D films through the lateral stacking of micro-sized 2D flakes. It means the film has randomly distributed lattice orientation of each flake, rich in flake edge defects and flake stacking-contact resistance. All these imperfect features could significantly degrade the 2D film electrical performance. Thus, it is not practical to form films through a solution process for the reliable, highly integrated electronic device. However, solution process methods provide an easy-to-operate, low-temperature, and low-cost method to form large-area 2D films. It could be very promising for fabricating devices with no requirement on high-performance, such as flexible, wearable, and display electronics.

4. Strategies of single-crystalline 2D films at the wafer-scale

To achieve reliable integrated electronics, large-area 2D vdW films with single-crystalline structures need to be grown uniformly and continuously at a wafer-scale, with minimal grain boundary and other defects.[59] The reported methods to grow single-crystalline 2D vdW films can be classified into three strategies: ① growth of an isolated domain (GID), ② growth of unidirectional domains (GUD), and ③ conversion of oriented precursors (COP). Graphene,[69] MoS_2,[74, 75, 111] and h-BN[63] have been successfully grown with a single-crystalline structure over the wafer scale. However, MXenes, TMDCs (except MoS_2, $MoSe_2$, WS_2 and WSe_2), 2D vdW elements, or oxides films

with a single-crystalline structure have not yet been reported to date at the wafer scale. Therefore, understanding these growth principles could help to develop practical strategies for preparing a high-quality wafer-scale film of many emerging 2D vdW materials.

4.1. Growth of an isolated domain (GID)

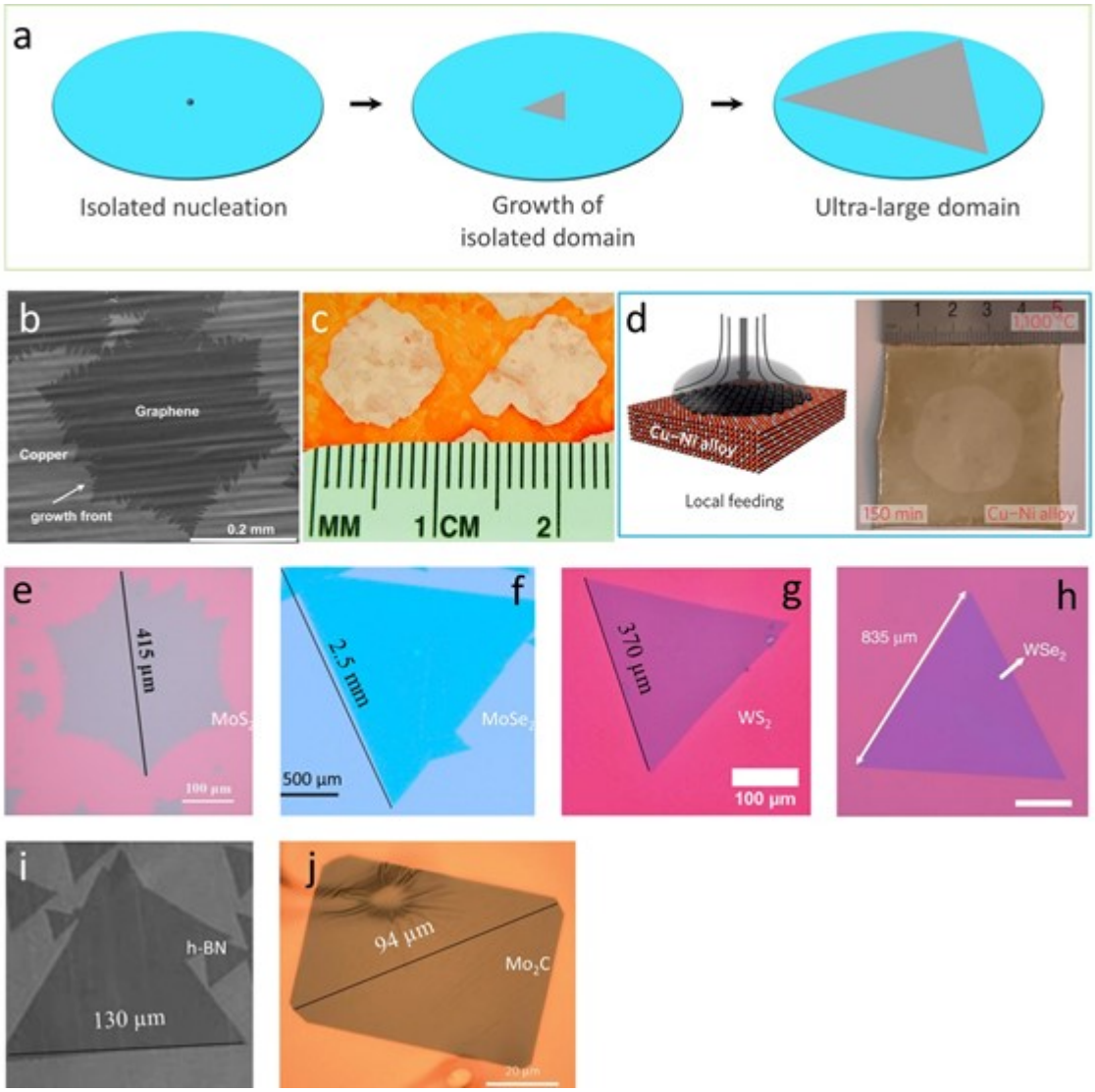

Figure 19. Growth of wafer-scale 2D single-crystalline films by GID. (a) Schematic of the enlarging process of a single 2D domain. (b) The single-crystalline graphene flake in submillimeter scale. Reproduced with permission.[148] Copyright 2011, American Chemical Society. (c) Single-crystalline Graphene flakes in centimeter scale. Reproduced with permission. [149] Copyright 2013, American Association for the Advancement of Science. (d) An inch-sized graphene film by local feeding process. Reproduced with permission.[150] Copyright 2016, Nature Publishing Group. Submillimeter-sized single-crystalline (e) MoS_2 flake. Reproduced with permission.[151] Copyright 2016, Wiley-VCH. (f) $MoSe_2$ flake. Reproduced with permission.[152] Copyright 2017, American Chemical Society. (g)WS_2 flake. Reproduced with permission [153]. Copyright 2014, Royal Society of Chemistry. (h) WSe_2 flake. Reproduced with permission.[154] Copyright 2017, Nature Publishing Group. (i) h-BN flake.

Reproduced with permission.[155] Copyright 2015, Nature Publishing Group. (j) Mo_2C flake through enlarge their single domain centers. Reproduced with permission.[156] Copyright 2015, Nature Publishing Group.

The GID route to grow large-area vdW layered 2D materials is usually operated in the tube CVD. The schematic in **Figure 19a** illustrates this process: First, a nucleation center is formed, followed by the planar growth of the 2D domain, which finally covers the whole wafer. One requirement for the successful GID process is the ultralow density of nucleation centers, ideally only one center in an inch-sized area. Another requirement is the perfect planar growth over a large area. During the CVD GID process, adatoms of precursors should always tend to be chemically adsorbed and bonded on the domain edge, nucleation and island formation of other layers on top of the 2D domain monolayer need to be eliminated. One practical strategy is to speed up the domain growth rate, thus the nucleation rate can be comparatively suppressed. Therefore, there would be more chance for achieving an isolated large domain.[157, 158]

Large-area single-crystalline growth of graphene, TMDCs, h-BN, and MXene-like Mo_2C have been investigated through the GID process. However, only the graphene domain was successfully enlarged into an inch scale, see Figure 19b-d. [69] Graphene by the GID process was first reported in 2011 by Ruoff *et al*. They successfully enlarged the lateral size of the graphene monocrystal up to 0.5 mm (Figure 19b) by using copper-foil enclosure as substrate and methane as a precursor in the low-pressure CVD system.[148] In 2013, they further enlarged the graphene single-crystalline domain size up to centimeter-scale (Figure 19c), by introducing oxygen to suppress the nucleation density and promote the diffusion-limited growth kinetics.[149] In 2015, the Xie group developed a fast growth method for the inch-sized graphene single-crystal (Figure 19d), through a localized feeding to the single nucleus on the Cu-Ni alloy substrate.[150] In 2018, the Smirnov group achieved the foot-long

single-crystal graphene film on a polycrystalline pure copper surface through the self-selection of the fastest-growing domain orientation and overwhelming the slower-growing domains.[159] Thus, the GID process could be regarded as a practical method for graphene single-crystalline film growth.

The GID process has been tried on other 2D vdW materials. Single-crystalline semiconducting TMDCs (MoS_2,[151] $MoSe_2$,[152] WS_2,[153] and WSe_2 [154]) and insulating h-BN[155] flakes were successfully enlarged into submillimeter size (Figure 19e-h). The Loh group enlarged the monolayer MoS_2 single-crystal flake up to 305 μm (Figure 19e) in an ambient-pressure CVD system, by changing the relative substrate position to the precursor and the carrier gas flow direction. [151] They also achieved a monolayer $MoSe_2$ crystal lateral size up to 2.5 mm (Figure 19f), by using the molten glass as the substrate. The glass surface isotropic feature was regarded as the reason for suppressing $MoSe_2$ nucleation events.[152] The Warner group enlarged WS_2 flake up to 370 μm (Figure 19g), by controlling the introduction time and the amount of sulfur (S) vapor relative to the WO_3 Precursor.[153] The monolayer WSe_2 flake was grown up to 835 μm (Figure 19h) by the Pan group.[154] The Xie group reported a single-crystal h-BN domain size up to 130 μm (Figure 19i) grown on uniquely designed Cu–Ni alloy foils.[155] MXene-like Mo_2C flake was just enlarged into tens of micrometer size (Figure 19j). [156] To our knowledge, there is still no report about the 2D vdW elemental (Te and BP) and oxide (MoO_3) growth by the GID process. Further efforts are needed to improve the GID process and extend it to other materials beyond graphene. Suppressing nucleation density, promoting lateral edge growth, and shortening the growth time are major concerns during the exploration of the GID process.

WILEY-VCH

4.2. Growth of unidirectional domains (GUD)

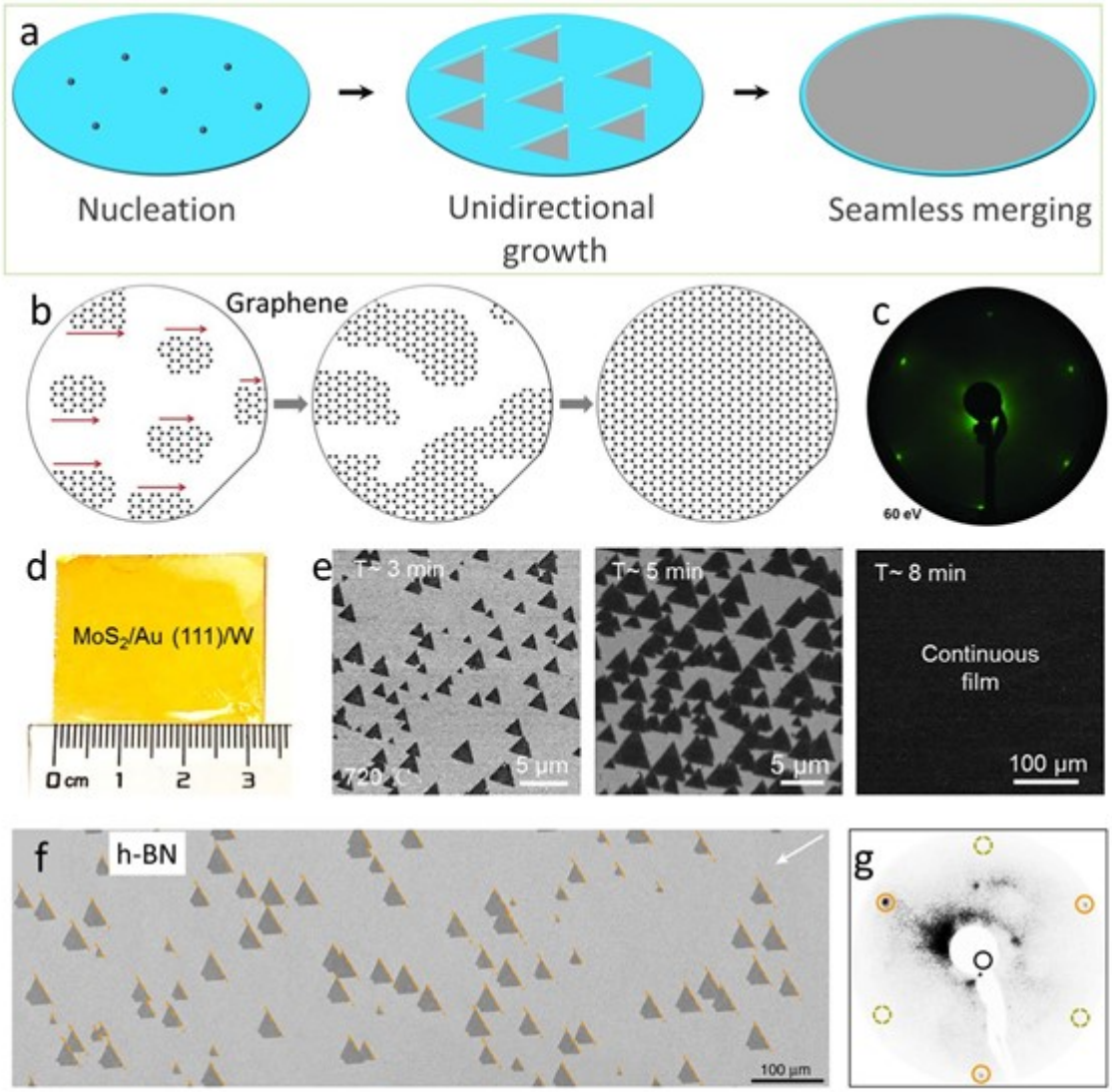

Figure 20. Growth of wafer-scale single-crystalline 2D films through the seamless GUD. (a) Schematic of the merging orientation well-aligned domains into the single-crystalline film. (b) Schematic of inch-sized single-crystalline graphene film growth. (c) Low-energy electron diffraction (LEED) pattern of single-crystal graphene grown on an (110) H-Ge substrate. Reproduced with permission.[14] Copyright 2014, American Association for the Advancement of Science. (d) Inch-sized single-crystalline MoS_2 film grown on (111) Au/W substrate. (e) SEM images showing orientation well-aligned small MoS_2 domains, extended domains, and continuous film. Reproduced with permission.[74] Copyright 2020, American Chemical Society. (f) Oriented h-BN monolayer domains in a large area on copper substrate. (g) LEED pattern of the as-grown h-BN sample. Reproduced with permission.[80] Copyright 2019, Nature Publishing Group.

Another strategy for wafer-scale 2D vdW single-crystalline film growth is through the GUD process. The schematic of this is illustrated in **Figure 20a**. In this process, numerous nuclei formed at the start of the process on a single-crystalline substrate. These 2D nuclei then grow, ideally in a single planar lattice direction, with the help of the substrate-aligned surface atomic edges. Finally, 2D domains are extended over time and then stitched together seamlessly to form a mono-oriented continuous film. The GUD strategy has been demonstrated as a very practical growth method for the single-crystalline semi-metallic graphene,[14, 66, 68] semiconducting TMDCs [74, 160], and insulating h-BN films.[79-81]

One piece of representative literature using the GUD route to prepare the single-crystalline graphene at the wafer-scale was reported in 2014 by the Whang group. They successfully grew wrinkle-free single-crystalline monolayer graphene on hydrogen-terminated (110) germanium substrate. Multiple nucleation centers were unidirectionally aligned because of the (110) surface anisotropic twofold symmetry; thus, the uniform single-crystalline graphene with a predefined orientation was successfully achieved after seamless merging of these numerous unidirectional domains, as shown in Figure 20b-c.[14] Large-area single-crystalline graphene films have been reported on many different single-crystalline metal substrates with certain lattice surfaces. More details are discussed in a very comprehensive literature review published by the Liu and Peng groups recently.[69] For the successful GUD growth of the single-crystalline MoS_2 film, the Zhang group demonstrated it on (111) Au substrate with careful control of the S/Mo ratio. The centimeter-square MoS_2 film sample grown on (111) Au/W surface is shown in Figure 20d. The mono-oriented MoS_2 domains could be seen before they merge into a continuous film, as illustrated in Figure 20e.[74] Mono-oriented MoS_2 films grown on sapphire (001) substrates were recently achieved with

excellent electrical performance by the Wang group. The miscut orientation towards the A axis (C/A) of sapphire provides excellent control over the MoS_2 domain orientation alignment.[161] Recently, several wafer-scale single-crystalline TMDCs (including WS_2, MoS_2, $MoSe_2$ and WSe_2) were successfully grown on vicinal *a*-plane sapphire by the Liu group, a dual-coupling-guided mechanism was regarded to drive their mono-orientated growth features.[160] MoS_2 domains grown with highly-oriented (two directions) feature has also been achieved on epitaxial GaN.[162, 163] However, the TMD/nitride heterostructure is yet to be achieved at the wafer scale. Several groups demonstrated the successful growth of single-crystal insulating h-BN films at the wafer-scale using the GUD method. The Shin group successfully grew single-crystalline h-BN on insulating sapphire substrate in a high-temperature and low-pressure CVD system. They could transfer h-BN film onto the targeted substrate by etching the Al layer contacting the h-BN film.[81] However, their films were multilayer, but monolayer h-BN dielectric film is preferred for nanoelectronic applications. The Kim group has successfully grown monolayer single-crystal h-BN film on a liquid Au substrate surface, which provides an opportunity for self-collimation of the BN grains with the help of the electrostatic interaction.[79] Recently, both Li[63] and Liu[80] groups achieved monolayer single-crystalline h-BN film on the cheaper copper substrate using the GUD method. Thus, the GUD method has been well demonstrated for single-crystalline graphene, MoS_2 and h-BN films grown at the wafer scale. However, TMDCs (except WS_2, MoS_2, $MoSe_2$ and WSe_2), MXenes, 2D elements, and oxide films have not yet been grown at the wafer-scale with single-crystalline structure through the GUD route.

4.3. Conversion of oriented precursors (COP)

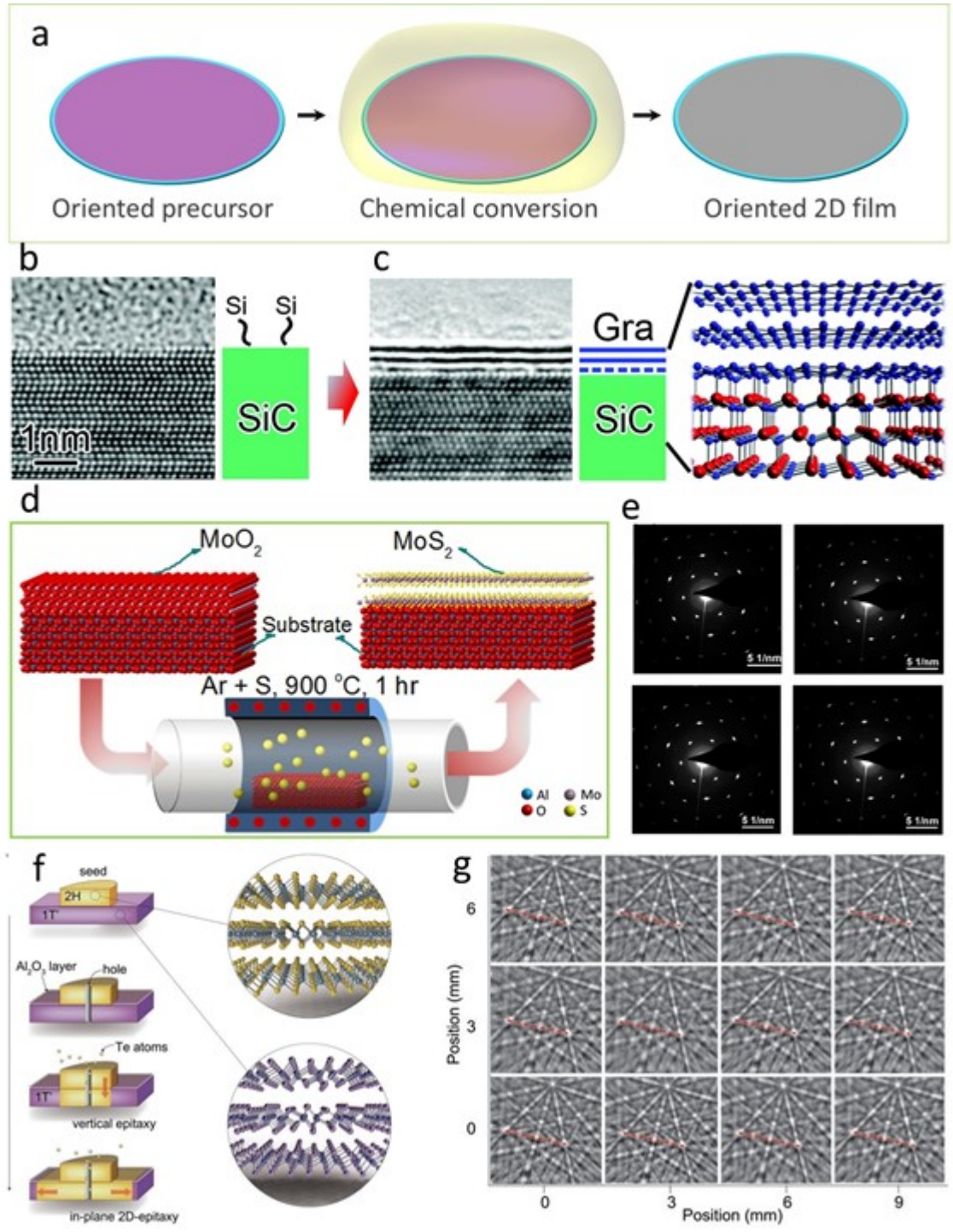

Figure 21. Growth of wafer-scale 2D mono-oriented films through the COP route. (a) Schematic of the chemical conversion of the single-crystalline precursor films. Cross-sectional TEM image and

chemical conversion schematic of (b) the (001) SiC substrate and (c) the surface graphene layer. Reproduced with permission.[164] Copyright 2011, National Academy of Sciences. (d) Schematic of epitaxial phase conversion from MoO_2 to MoS_2 film. (e) The single-crystalline feature of the MoS_2 film confirmed through selected area electronic diffraction (SAED) patterns. Reproduced with permission.[75] Copyright 2018, IOP Publishing. (f) The schematic diagrams of the wafer-scale single-crystalline 2H $MoTe_2$ thin-film converted from 1T' $MoTe_2$. (g) Electron back-scattered patterns (EBSPs) at different positions across the wafer. Reproduced with permission.[131] Copyright 2021, American Association for the Advancement of Science.

The COP process is one type of two-step conversion method that involves a chemical or physical transformation of a solid mono-oriented precursor film or wafer surface. The schematic is shown in **Figure 21a**. The first step is to obtain an oriented precursor, which could be a bulk single-crystalline wafer surface such as SiC, Pt, or an ultrathin epitaxial film such as MoO_2. This precursor should have a very high-quality single-crystalline character, which is unique to the normal two-step conversion process mentioned earlier in **section 3.5**. Once the high-quality precursor is ready, a chemical transformation is performed with well-optimized parameters, such as temperature, pressure, and atmosphere. A good transformation process results in high-quality mono-oriented 2D vdW films at the wafer scale.

To our knowledge, the COP strategy has been used to grow high-quality mono-oriented graphene,[165] 2H MoS_2 [75], 2H $MoTe_2$ [131] and $PtSe_2$ [166] films. Using the (001) SiC wafer surface as a precursor, especially when the wafer surface termination is covered with Si atoms, the mono-oriented graphene film with structure coherence over the whole wafer can be formed by thermal decomposition of the surface SiC layer. As illustrated in Figure 21b-c, the non-layered SiC surface was changed into layered graphene as can be seen by comparing the cross-sectional TEM image of the SiC sample before and after thermal transformation. This is because Si atoms are much easier to

be evaporated compared to C atoms. Thus, C atoms remain on the SiC surface to form the graphene layer, which has a mono-oriented planar lattice inherited from the single-crystalline SiC wafer. [164, 165] However, to achieve mono-oriented monolayer epitaxial graphene over the wafer, the annealing condition should be well controlled. There is a high chance that bilayer or trilayer regions are typically present at the step-edges of SiC wafer.[117] This phenomenon can have a significant impact on the electronic transport in the graphene layer.[167] Our group successfully obtained highly-oriented MoS_2 films through the COP strategy, as illustrated in a schematic in Figure 21d.[75, 111] We found that (200) MoO_2 planes have very small lattice mismatch (> 2%) to the (001) sapphire surface, and achieved epitaxial single-crystalline MoO_2 film growth on the (001) sapphire substrate using the PLD process. A well-optimized chemical conversion process was then carried out at a certain temperature, atmosphere, pressure, and minimized vapor flow fluctuation. The obtained MoS_2 films were demonstrated to have mono-orientation over the entire wafer, as indicated in Figure 21e. A 2H $MoTe_2$ single-crystalline film was also demonstrated on 1-inch wafer by the COP by the Ye group. [131]However, different from MoS_2 film, the 2H $MoTe_2$ film was achieved by physical conversion of 1T' $MoTe_2$ with the help of seed defect center. it took a much longer time for the conversion to get a 1-inch wafer-scale film. The schematic showing conversion from 1T' $MoTe_2$ to 2H $MoTe_2$ is shown in Figure 21f. The mono-orientation nature over the wafer was confirmed by Electron back-scattered patterns (EBSPs) as shown in Figure 21g. The COP growth strategy has also been performed to obtain single-crystalline $PtSe_2$ film through the selenization of a (111) Pt substrate.[166] However, single-crystalline precursor films or surfaces are not necessarily converted into single-crystalline 2D vdW films. Growth orientation, surface termination, dislocation defects of the precursors [111, 165], and transformation fluctuations [110] could be potential factors that destroy the crystal orientation, continuity, and uniformity of the 2D vdW films. The COP strategy has many advantages: growing the

film on insulating substrates, controlling the thickness and uniformity, and better reproducibility. However, research on the COP process is still in the initial stage for the other 2D vdW materials.

5. Applications of wafer-scale vdW layered 2D materials

Developing high-quality single-crystalline 2D vdW films at the wafer scale is the precondition for having scalable 2D electronics and optoelectronics. It is well known that silicon electronics are reaching Moore's law limitation. Thus, 2D semiconductors have become of great interest as a means to continue Moore's law. This effort has been called "more Moore" in the microelectronic industry technology roadmap.[168] It has two critical aspects: high-quality monolayer 2D film wafer and atomic resolution of device nanofabrication. Another significant direction is "more than Moore," which aims for multiple functions integrated onto a single chip instead of high-density integration. The 2D vdW materials have also been demonstrated to be significant parts of the "more than Moore" technology

road map.[168-170] This direction also needs a highly controllable growth method of 2D films at the wafer scale.

So far, we have discussed various growth methods of 2D films. However, it is essential to also look at the potential applications of these wafer-scale 2D materials.[171] Thus, this section will first give several representative examples for large-area vdW layered 2D films used in integrated devices, and then provide some cases for their roles in assisting 3D films epitaxial growth.

5.1. Microscale and nanoscale device integration

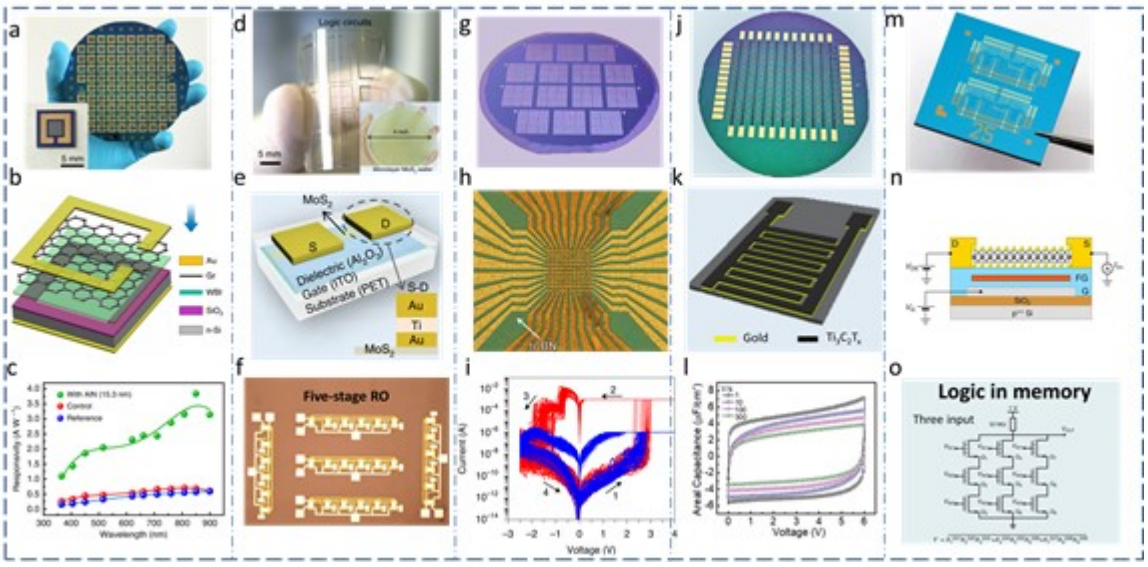

Figure 22. Microscale or nanoscale integrated devices using wafer-scale 2D vdW layered materials. (a-c)The photo-sensing array using wafer-scale 2D graphene/Si junctions, (a) the photograph of the wafer with photodetector array, Inset (lower left) is a single photodetector; (b) schematic of a single photodetector; (c) the spectra-dependent photocurrent responsivity of different photodetectors at a bias of -10 V. Reproduced with permission.[172] Copyright 2021, Springer Nature. (d-f) logic circuits using wafer-scale MoS_2 as a semiconducting layer, (d) the photograph of flexible integrated circuit sample, inset (lower right) is the photograph of the 4-inch monolayer MoS_2 wafer; (e) the architecture of the flexible MoS_2 field-effect transistor, (f) the optical image of five-stage ring oscillators (ROs). Reproduced with permission.[173] Copyright 2020, Springer Nature. (g-i) The memory array using wafer-scale 2D h-BN as the active layer, (g) the photograph fo Au/h-BN/Au memristive crossbar arrays; (h) the optical microscope image of a 10 × 10 memristor crossbar array; (i) the representative *I-V* characteristics measured during 120 cycles in one memristor using I_{CC} = 1 μA (blue lines) and I_{CC} = 1 mA (red lines). Reproduced with permission.[174] Copyright 2020, Springer Nature. (j-l) The micro supercapacitor array using wafer-scale $Ti_3C_2T_x$ MXene films, (j) the photograph; (k) a schematic of a single micro supercapacitor; (l) CV curves of 10 MXene micro-supercapacitors connected in series at various scan rates. Reproduced with permission.[175] Copyright 2019, Wiley-VCH. (m-o) logic-in-memory using the large-area MoS_2 film as a semiconducting layer, (m) the photograph the 12 × 12 mm^2 dies with logic-in-memory cell arrays; (n) schematic of a floating-gate memory device. D, drain; S, source; FG, floating gate; G, gate; (o) schematic of the three-input logic-in-memory cells. Reproduced with permission.[176] Copyright 2020, Springer Nature.

Achieving 2D vdW layered films uniformly over a wafer makes it possible for many 2D microdevices (or nanodevices) to be integrated onto a single chip. **Figure 22** shows several representative devices or circuits fabricated using large-area 2D films. They cover several functions including photo-sensing, logic computing, memory, micro-supercapacitor, and logic-in-memory. Figure 22a-c shows an example of wafer-scale graphene/AlN/Si heterojunction photodetector arrays fabricated by Li *et al*.[172] The photograph of the detector array wafer is shown in Figure 22a, with a single device displayed in the inset. Figure 22b presents the detailed structure of a typical single photodetector. It consists of a graphene/AlN/Si sandwich-like stacked junction. The AlN performs as the wide-bandgap insulating (WBI) layer in between graphene and Si, which could improve the performance of the photodetector array, as evidenced in Figure 22c. Another paper from Wu *etc.* reported high-performance photodetector arrays using wafer-scale MoS_2/graphene vdW heterojunctions.[177]

Several papers reported complicated logic circuits fabricated using large-area 2D semiconducting films such as MoS_2 and Te. Circuits using wafer-scale MoS_2 film fabricated by the Zhang group are presented in Figure 22d-f.[173] The large-scale flexible integrated circuits is shown in Figure 22d, with the inset showing the 4-inch MoS_2 monolayer film. The architecture of the top-gated MoS_2 field-effect transistor (FET) is schematically shown in Figure 22e. Transistor arrays and relevant circuits (including the five-stage ring oscillator in Figure 22f) were evidenced with high performance, high yield, excellent reliability, and good integration density. In another work, the Duan group fabricated several logic gate circuits using solution-processed wafer-scale MoS_2 film.[143] In addition, using large-area *p*-type 2D Te films as the *p*-type transistor channel, the Javey group successfully made some complicated circuits on flexible substrate.[46]

Wafer-scale memory arrays were also reported recently using 4-inch h-BN as the active layer by the Lanza group, shown in Figure 22g-i.[174] They made 10 × 10 memristor crossbar arrays using Au/h-BN/Au cells with lateral size of 5 µm × 5 µm (see Figure 22g). The wafer-scale multilayer h-BN film utilized as the resistive switching medium was grown through a CVD process. The representative *I-V* characteristics measured during 120 cycles showed excellent and very stable resistive switching performance, as shown in Figure 22i. In a recent study , this was scaled up to 100 × 100 crossbar array of Au/h-BN/Au cells with lateral size of 320 nm × 420 nm; this is the largest circuit based on 2D materials ever reported, both in terms of number of devices and integration density.[178]

Recently, our group successfully fabricated micro-supercapacitor arrays using 4-inch 2D $Ti_3C_2T_x$ MXene films prepared by spray coating.[179] The micro-supercapacitor array fabricated on a silicon wafer is presented in Figure 22j.[175] The MXene dispersions were directly sprayed onto the pre-defined current collector, followed by patterning via a lift-off process, and the device structure is given in Figure 22k. It was shown that the device consisted of 10 cells connected in series showed an ultra-high scan rate capability of up to 300 V/s with a 6 V voltage window (Figure 22l). Moreover, large-area $Ti_3C_2T_x$ MXene films were reported as the source and drain electrodes in transistor electronics. [146]

Logic in memory, unique architecture with much faster data processing and storage than the Von Neumann architecture, is a more complicated device integration. The Kis group achieved its successful fabrication and operation, using the large-area MoS_2 film as the semiconducting layer in floating-gate FETs. The circuit array they fabricated is shown in Figure 22m.[176] The cross-section diagram in Figure 22n clearly displays the single floating-gate memory structure. This large-area MoS_2 logic-in-memory circuit could achieve a multitude of memory states and thus more logic

functions. Furthermore, higher parallelism and more complex operation have also been reached via further increasing the number of logic inputs, as shown in Figure 22o.

These representative works discussed above for using wafer-scale 2D vdW films in various integrated device applications indicate their promising potential.

5.2. Assisting epitaxial growth

WILEY-VCH

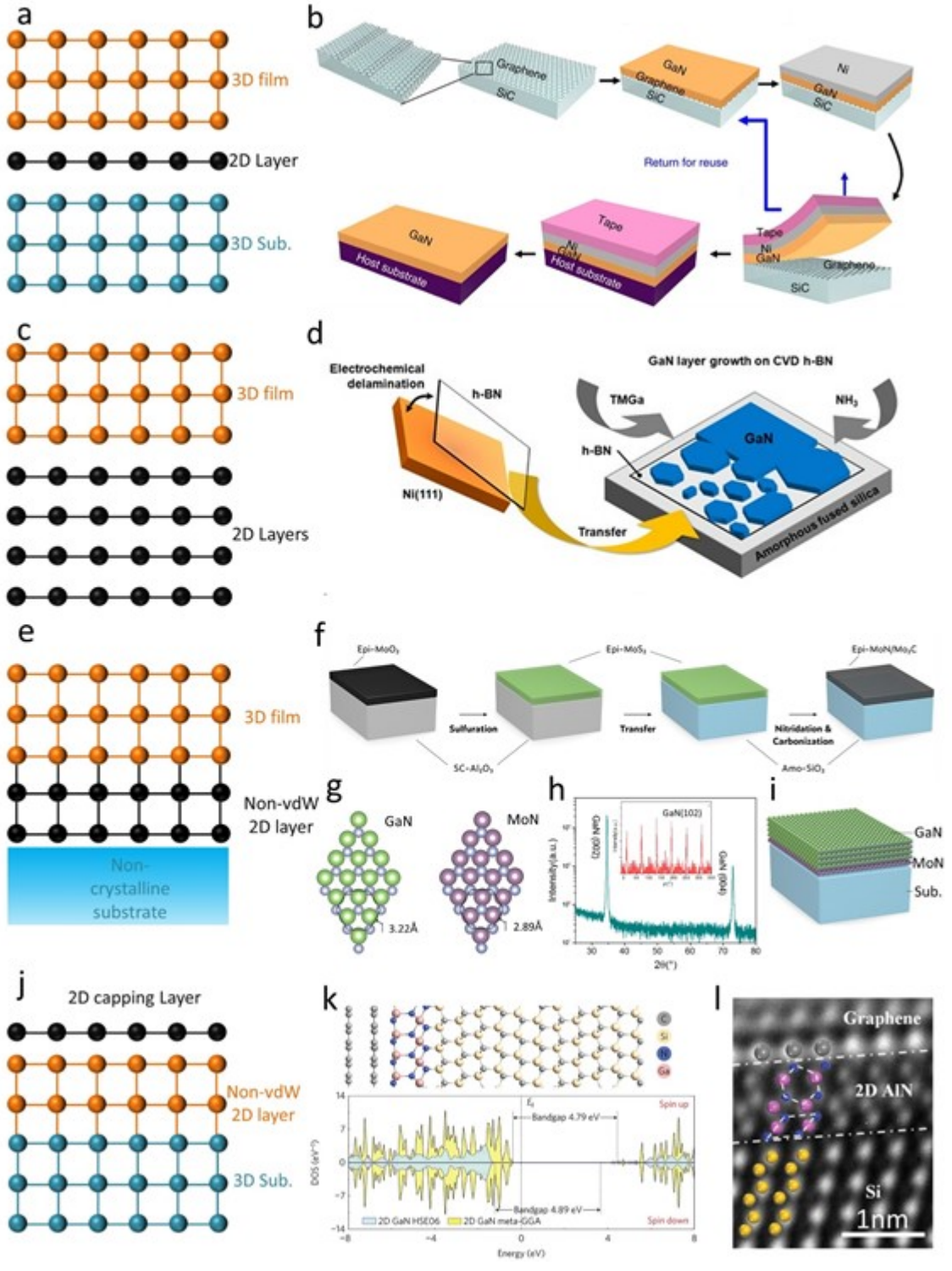

Figure 23. Assisting epitaxial growth over the wafer using vdW layered 2D films. (a-b) Remote epitaxy. (a)Schematic of the remote epitaxial growth. (b) The monolayer or bilayer graphene film as the transparent layer for GaN remote epitaxial growth on the SiC substrate. Reproduced with permission.[180] Copyright 2014, Springer Nature. (c-d) vdW epitaxy (c) Schematic of the vdW epitaxial growth. (d) The single-crystalline few-layer h-BN film as the seeding layer for GaN vdW epitaxial growth on the fused silica substrate. Reproduced with permission.[181] Copyright 2017, Springer Nature. (e-i) assisting 3D films using lattice orientation heredity (LOH): (e) Schematic of LOH-assisted epitaxial growth, (f) schematic of LOH-grown MoN films from mono-oriented MoS_2 film on a quartz substrate, (g) lattice plane model comparison between hexagonal GaN (001) and hexagonal σ-MoN (001). h) out-of-plane XRD 2ϑ-scan (inset is in-plan (102) ϕ-scan) of the mono-oriented GaN film (i) Schematic of the GaN grown on MoN/quartz substrate. Reproduced with permission.[182] Copyright 2021, Wiley-VCH. (j-l) 2D metal (Al, Ga and In) nitrides grown by graphene encapsulation: (j) Schematic of growing non-vdW 2D layer by graphene encapsulation. (k) Structure simulation with density functional theory (DFT) of the graphene/2D GaN/6H-SiC heterostructure; density of states calculation revealing the E_g of 4.79 eV (meta-generalised gradient approximation) and 4.89 eV (Heyd-Scuseria-Ernzerhof density functionals) for 2D GaN, the valence band shifts up towards the Fermi level (E_f), indicating p-type semiconducting behaviour in 2D GaN. Reproduced with permission.[183] Copyright 2016, Springer Nature. (i) The high-magnification cross-sectional TEM image for AlN layer sandwiched between graphene and Si substrate. Reproduced with permission.[184] Copyright 2019, Wiley-VCH.

Epitaxy is a method of preparing single-crystalline films on a lattice-oriented wafer, which is very important for modern solid-state electronics. There are two types of traditional 3D film epitaxial growth techniques depending on the substrate type: homoepitaxy and heteroepitaxy. Homoepitaxy is to grow single-crystalline film on a substrate of the same substance with the same lattice structure. It could achieve high-quality single-crystalline film with few defects. However, there are limited candidate substrates to select, and they are usually very expensive. Heteroepitaxy is to grow single-crystalline film on a substrate with a similar lattice structure but a different substance. However, the film has a higher density of defects, and the quality is usually not comparable to the homoepitaxial films. The reason is lattice and thermal expansion mismatch between the film and the substrate in heteroepitaxial structures. Since vdW layered 2D materials could be prepared as continuous and mono-oriented films over the wafer, they can be used to assist the 3D film epitaxial

growth and can overcome drawbacks encountered in traditional epitaxy. There are already remote epitaxy and vdW epitaxy techniques that have been developed to advance 3D film epitaxy. [185]

Remote epitaxy is one advanced epitaxial technique using the wafer-scale graphene film with only one or two layers, which is performed as a transparent layer between the epitaxial film and the single-crystalline substrate as schematically shown in **Figure 23a**. The substrate surface potential can easily penetrate through the graphene monolayer (or bilayer). It can be enough to define the film orientation because of graphene film ultrathin (less than 0.5 nm) and nonpolar features. Therefore, 3D films could still have well-defined orientations registered directly from the substrate. Also, because of the weak vdW force at the interface between the graphene layer and the 3D film, the 3D film could be readily lifted off without damaging the underneath substrate.[186] The obtained single-crystalline film could have high quality and few defects because vdW gaps could release the strain between the film and substrate. Figure 23b gives an example of using continuous monolayer or bilayer graphene film as the transparent layer for single-crystalline GaN film grown on the (0001) SiC wafer. [180] The GaN film has much fewer defects compared with the film directly grown on the substrate. It can also be easily peeled off without damaging the substrate surface so that the expensive SiC substrate could be directly reused many times.

The vdW epitaxy technique is using multilayer 2D films to assist 3D film epitaxial growth. Its schematic is shown in Figure 23c. Unlike remote epitaxy, vdW epitaxy takes the multilayer 2D film as the seeding layer to directly define the orientation of read-to-grow 3D films. Therefore, it is not necessary to use single-crystalline 3D substrate in vdW epitaxial growth. Nevertheless, it requires the multilayer 2D film to be mono-oriented and to have structure coherence over a wafer. The vdW epitaxy has similar advantages to remote epitaxy: peeling off the 3D film readily and relaxing growth

strain originates from structure mismatch. Figure 23d displays one example of vdW epitaxy, demonstrating that the wafer-scale single-crystalline h-BN film was successfully transferred onto disordered fused silica substrate and enabled the mono-oriented GaN epitaxial film growth. [181] More detailed vdW or remote epitaxy techniques have been reviewed in detail in other papers.[185, 187]

Graphene and h-BN have been reported several times to be used for remote and vdW epitaxial growth. However, their inert surfaces make the nucleation of 3D films very challenging.[187] TMDCs are not stable in the ammonia and high-temperature nitride growth atmosphere, making them challenging to perform vdW epitaxy growth. However, our group recently discovered a lattice orientation heredity (LOH) phenomenon in the chemical transformation of epitaxial MoS_2 films.[182] LOH-grown non-vdW 2D films can be used to support 3D film epitaxial growth on a disordered substrate surface, as shown in the schematic in Figure 23e. Figure 23f illustrates how we use LOH process to prepare the mono-oriented 2D MoN film on an amorphous substrate. The non-vdW MoN film with active surface N atoms makes epitaxial GaN nucleation much easier. Also, the hexagonal MoN and hexagonal GaN have small lattice mismatches, as shown in Figure 23g. We initially demonstrated the feasibility of using LOH-MoN seeding layer to grow mono-oriented GaN (confirmed by XRD 2ϑ-scan and (102) ϕ-scan in Figure 23h) on the quartz substrate, as shown schematically in Figure 23i.

Besides using 2D vdW wafer films to support 3D epitaxial growth, another promising direction is to confine metal (Al, Ga, In) nitrides as non-vdW 2D layers at the interface between the 2D vdW layer and the 3D substrate. The schematic of this approach is shown in Figure 23k. Until now, only graphene has been reported as a 2D capping layer.[183, 184, 188, 189] The strategy is to create

opportunities to allow Ga (or Al, In) and N adatoms to penetrate through the graphene defective sites, then to diffuse at the 2D/3D interface to form 2D nitride layers. The 2D feature allows these wide-bandgap nitrides to possess a bigger bandgap and even show p-type carrier distribution, according to the calculation of their density of states as illustrated in Figure 23k. All GaN,[183] AlN, [188] InN[189] 2D layers have been successfully prepared at the Graphene/SiC interface. The 2D AlN layer has also been realized at the interface between physically transferred graphene and Si substrate, which was observed by high-magnification cross-sectional TEM.[184] This may enable 2D nitride semiconductors to be compatible with the Si process technology.

The above representative examples, including remote epitaxy, vdW epitaxy, LOH process and 2D nitride growth via graphene encapsulation, indicate that the wafer-scale growth of vdW layered 2D materials can significantly advance the epitaxial growth techniques.

6. Conclusion and perspective

In summary, we have reviewed most of the vdW layered 2D materials in terms of their basic structures and properties, wafer-scale growth processes, single-crystalline film growth strategies, and applications. They include graphene, h-BN, TMDCs, MXenes, BP, Te, and layered MoO_3, which cover metallic, semimetallic, semiconducting, and insulating characteristics. Various wafer-scale growth processes have also been discussed, including tube CVD, MOCVD, MBE, ALD, two-step conversion (chemically or physically), PVD (PLD, sputtering and thermal evaporation), and solution processing. Strategies to prepare wafer-scale single-crystalline or mono-oriented films (GID, GUD,

and COP) were also discussed. The discussed 2D vdW layered materials are at different stages of development in terms of high-quality film growth at the wafer scale. Thus, future research directions in 2D materials growth will vary depending on the material in question, as discussed below.

Graphene, the first discovered 2D material, is semi-metallic with ultrahigh carrier mobility and excellent chemical stability, promising to be applied as conductive and transparent electrodes. It has the longest history in terms of wafer-scale growth among all 2D materials. The most appropriate growth process for wafer-scale graphene is the tube CVD process. Both polycrystalline and single-crystalline graphene films with large sizes have been successfully achieved on metal (copper or copper/Nickel alloy) and non-metal substrate. In the initial stages of their development, the large-scale graphene films were polycrystalline with random lattice orientations. Years later, three growth strategies have achieved highly oriented or even single-crystalline graphene films: GID, GUD, and COP. The growth of single-crystalline graphene film through GID has few requirements in terms of substrate lattice orientation. The size of the GID-grown graphene film has already reached more than several inches, but the process is relatively time-consuming.[150, 159] GUD and COP strategies could grow single-crystalline or mono-oriented monolayer graphene films faster and at a larger scale but require mono-oriented substrates.[14, 190] So far, graphene has experienced sufficient research on large-area growth and lattice mono-orientation engineering,[69] which could provide very beneficial experiences to the development of other 2D vdW materials at the wafer scale. Commercialized graphene films are already available, especially for the research community. However, there is still a gap in bringing large-scale graphene films into the electronic industry.[191] The current challenge for large-area graphene film growth is how to achieve defect-free films with an ultraclean surface with minimal contamination.[192] Except for grain boundaries resulting from lattice misorientation, other

defects such as wrinkles,[193] vacancies, carbon clusters [194], or metal residues[195] should also be minimized.

h-BN, another 2D material with a relatively long history in research, is an insulator with a bandgap of about 6 eV, one of the highest among all 2D layered materials known.[196] It is an excellent 2D material that can be used as a dielectric layer or passivation layer with no dangling bonds in integrated electronics. CVD is the major method used for large-area growth of h-BN. Both polycrystalline and single-crystalline h-BN films have been achieved on metal alloy (Copper/Nickel) substrates. Wafer-scale single-crystalline h-BN films were successfully grown only through the GUD method.[80] GID method was reported to produce h-BN flakes no more than 130 μm large.[155] To our knowledge, there is still no report using the COP method to grow highly oriented h-BN films. However, single-crystalline h-BN films grown at the wafer-scale by the GUD method could be promising for scalable applications. Similar to graphene, defects (beside grain boundaries) and metal residues are main concerns in h-BN films that should be addressed to improve its quality.[197, 198] Still, it is important to emphasize that the leakage current across defect-free single-crystalline monolayer h-BN is still too high and impedes its use as dielectric in most electronic devices (i.e., transistors, memristors). Therefore, the growth of single-crystalline multilayer h-BN is one of the main challenges to face in the field of 2D materials-based devices in the next years.

TMDCs, a big family of 2D binary compounds, are rich in many physical properties. Representative 2H MoS_2 ($MoSe_2$, WS_2, WSe_2, and $MoTe_2$) are very promising semiconducting channel layers for the next generation low-energy circuits. Therefore, most of the wafer-scale growth developments were focused on these semiconducting 2D TMDCs. Wafer-scale films of several TMDCs with the polycrystalline feature have already been reported by tube CVD, MOCVD, MBE, and

two-step conversion processes many times. However, TMDC wafer-scale films with a single-crystalline structure have only been reported a few times. MoS_2 single-crystalline films have been obtained using the GUD method in a tube CVD process on Au substrate.[74] It was also achieved by the chemical COP method on sapphire substrates.[75] WS_2 epitaxial films were reported using the GUD method using an MOCVD process.[92] $MoTe_2$ films with mono-orientation were reported through a physical COP method.[131] However, there are few reports on using the GID method for the successful growth of wafer-scale single-crystalline TMDCs films. Largest monolayer TMDC crystals (MoS_2,[151] $MoSe_2$,[152] WS_2,[153] WSe_2[154]) by GID route are only in submillimeter scale. The challenge in achieving industrial-quality TMDCs films still remains: single-crystalline MoS_2 film by GUD needs an expensive gold substrate and a process to transfer the film from the metal substrate without metal residues contaminations. The growth of single-crystalline MoS_2 film through the COP method is very promising and scalable, but defects other than lattice misorientation need to be further minimized.[199] The single-crystalline $MoTe_2$ film grown by the COP method requires too a long growth time, so more time-efficient growth methods are needed for practical applications.[131] The common challenge for all these TMDC films is their electronic properties are still inferior to their corresponding exfoliated flakes. Defects such as chalcogen vacancies, antisite metal or chalcogen defects, and elemental impurities could be another significant reason for degrading the single-crystalline TMDC film quality, which need more attention.[199]

MXenes are another emerging family of more complex 2D compounds. Many MXenes are metallic and highly conductive. Besides, their surface work-function could be engineered over a wide range, which makes them very promising as ohmic contacts for 2D electronics.[200, 201] Large-area $Ti_3C_2T_x$ MXene films were obtained through a solution process, which has been initially

demonstrated as excellent contact in microelectronics.[202] The large MXene-like 2D Mo_2C single crystal grown by the GID method in the CVD process is still less than one hundred micrometers in the lateral dimension.[156] So far, there is still no report on growing MXenes at the wafer scale through the vacuum deposition.

Elemental 2D Te and BP are very promising p-type semiconductors. The semiconducting property of BP attracted broad attention in 2014.[11] Also, 2D Te p-type transistor was demonstrated with very attractive performance since 2018.[8] They have been initially deposited as large-area films through direct physical deposition. Electronic-grade Te films have been reported on both rigid and flexible substrates by a low-temperature EBE process.[46] BP films with excellent electrical performance have also been achieved by PLD .[135] In addition, BP film could be obtained through a physical two-step conversion process if using large-area h-BN film as the capping layer on the RP film.[121] However, it will be significant development if Te and BP film with a single-crystalline structure could be grown over the whole wafer.

The vdW oxide family, such as MoO_3, is still very new but is already showing some promising physical properties.[10, 13] Its exploration in electronic and optoelectronic devices is much less common compared with other materials. Therefore, more effort is needed to understand the potential physical properties of vdW oxides and their role in electronics. Also, developing the growth processes of 2D oxides at a wafer scale is less mature and could be a key topic in the near future.

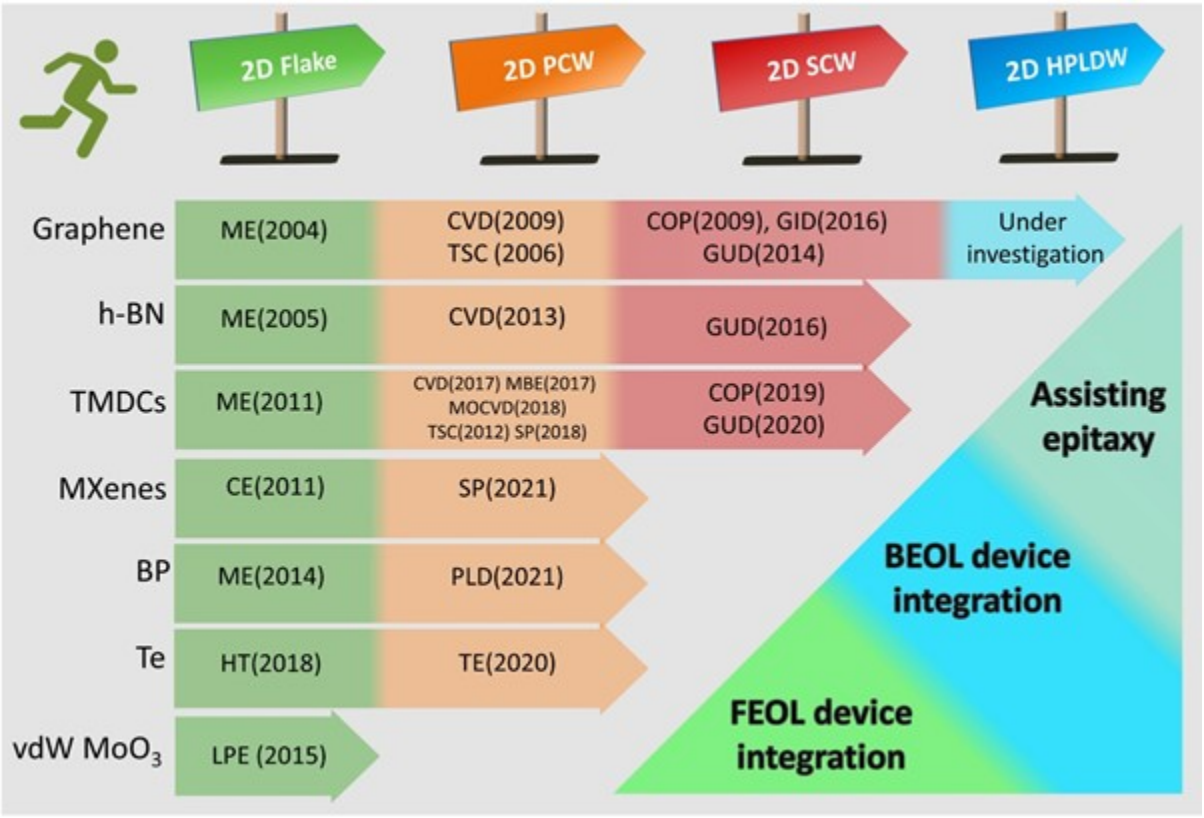

Figure 24. Progress of growth processes for 2D vdW layered materials: from flakes to wafer-scale. Note for references: graphene: ME(2004); [1] CVD(2009);[203] TSC(2006),[204] COP(2009),[117] GID(2016),[150] GUD (2014);[14] ultraclean graphene under investigation.[192] h-BN: ME(2005),[205] CVD(2013),[62] GUD(2016).[81] TMDCs: ME(2011),[2] CVD(2017), [16] MBE(2017),[93] MOCVD(2015),[85] TSC(2012),[108] SP(2018);[143] COP(2019),[75] GUD(2020).[74] MXenes: CE(011);[5] SP(2021).[206] BP: ME(2014),[11] TE(2021).[135] Te: HT(2018); [47] TE(2020).[46] vdW MoO_3: LPE(2015).[13] (Note: PCW: polycrystalline wafer; SCW: single-crystalline wafer; HPLDW: high-purified and low-defect wafer; ME: mechanical exfoliation; CE: chemical etching; HT: hydrothermal reaction; LPE: liquid phase exfoliation; CVD: chemical vapor deposition; MOCVD: metal-organic chemical vapor deposition; MBE: molecular beam epitaxy; TSC: two-step conversion; SP: solution process; PLD: pulsed laser deposition; TE: thermal evaporation; GID: growth of an isolated domain; GUD: growth of unidirectional domains; COP**:** conversion of oriented precursors; BEOL: back-end-of-line; FEOL: front-end-of-line)

In conclusion, we have discussed processes and strategies for the growth of van der Waal layered 2D materials at the wafer scale. The progression of these materials from the growth of single

flakes to wafer-scale has proceeded at different rates, as illustrated in **Figure 24**. Significant progress has been made in graphene, where many groups can now grow large-area single-crystalline graphene films. Efforts are currently focused on improving graphene quality by minimizing defects through clean growth methods.[192] The h-BN and TMDCs (especially MoS_2) are at the stage of developing mono-oriented growth methods. Only several groups achieved their single-crystalline wafer-scale films, and many other TMDCs have not yet been achieved as high-quality films. MXenes could be prepared as large-area films only through the solution process. High-quality large-area growth of Mxenes by vacuum methods still needs to be explored, probably based on high-temperature vacuum deposition. Elemental BP and Te p-type semiconductors have also reached the stage of large-area growth. Only one or two groups obtained their films over a large area. The Te film is grown by EBE and BP film by PLD. The vdW MoO_3 is still at the stage of basic physical property exploration. The discovery of its unique role in integrated circuits still needs time.

Developing growth methods of high-quality 2D films at a wafer scale is the shared goal for these various vdW layered materials. The existing strategies for well-developed 2D material growth at wafer scale could provide precious experiences to grow other 2D materials, and this is one of the key objectives of this review. By assembling these well-developed wafer-scale 2D vdW films, wafer-scale vdW heterojunctions can be obtained. This is very promising in building up new devices. Also, experiences of 2D vdW film growth can be beneficial to grow wafer-scale vdW heterojunctions. Detailed progress of wafer-scale vdW heterostructures has been reported elsewhere.[207] Besides, the future exploration of growth methods should consider potential applications. The reason is that different terminal devices and applications may have additional requirements on 2D films in terms of lattice orientation, continuity, uniformity, defects, thickness, and even growth conditions. We

present three potential representative applications in the bottom-right corner area of Figure 24. They include front-end-of-line (FEOL) device integration, back-end-of-line (BEOL) device integration, and assisting epitaxy. Usually, the FEOL logic device integration requires 2D materials with high-quality and few defects. Developing strategies for single-crystalline 2D film growth with few defects is needed to meet the FEOL device requirement. Moreover, two directions need to be considered: one is to directly grow the high-quality 2D monolayer films on the silicon wafer, which is chip fabrication compatible. The other is to develop damage-free transfer techniques to move the single-crystalline 2D film from the growth substrate onto the silicon wafer without any additional contaminations. However, to integrate 2D materials in the BEOL applications, high crystal quality with mono-oriented lattice and fewer defects are usually not necessary. BEOL integration requires low-temperature growth (less than 500 ^{o}C) so that direct grow 2D film would not damage the devices on the chip.[208] In addition, large-area uniformity and continuity are also necessary for process stability. Recently, low-temperature TMDCs growth by ALD and MOCVD processes were reported.[208, 209] To support epitaxial film growth, requirements on 2D film wafer should heavily consider structure coherence in terms of thickness and lattice orientation. For vdW epitaxial growth, multilayer layer graphene and h-BN films have been verified to enable GaN epitaxial growth.[181, 187] This process requires the film to be multilayer and lattice monoriented, but less requirement on line and point defects. Mono-oriented multilayer TMDCs films have not yet been confirmed to support vdW epitaxial GaN growth at the wafer scale. One reason is TMDCs are not stable in the GaN growth environment. However, lattice orientation heredity in the transformation of TMDC films can help to synthesis mono-oriented stable metal nitride and carbide films, which can then support GaN epitaxial growth.[182] For remote epitaxial growth, only monolayer or bilayer graphene has been verified as the transparent layer in remote compound epitaxial growth.[186] It has no requirement on

the graphene lattice orientation since 3D film growth is only confined by the 3D substrate. But it requires graphene to have no more than 2 layers, and the film should be large-area uniform and continuous without wrinkles and pinholes.[185] To synthesis 2D wide-bandgap semiconducting nitride (AlN, GaN, InN), the capping layer graphene should have defective sites to allow the adatoms to penetrate through and to diffuse at the graphene/3D substrate interface. [183]

Finally, we believe that the field of vdW 2D film growth at the wafer scale will continue to grow in importance in foreseeable future. Current techniques must be optimized to improve film quality, new growth techniques need to be developed for single-crystal 2D wafers and for emerging 2D materials. All along the nature of the intended application should always be kept in mind as film properties vary depending on the target application.

References

[1] K. S. Novoselov, A. K. Geim, S. V. Morozov, D.-e. Jiang, Y. Zhang, S. V. Dubonos, I. V. Grigorieva, A. A. Firsov, *science* **2004**, *306*, 666.

[2] B. Radisavljevic, A. Radenovic, J. Brivio, V. Giacometti, A. Kis, *Nat. Nanotechnol.* **2011**, *6*, 147.

[3] A. Laturia, M. L. Van de Put, W. G. Vandenberghe, *npj 2D Materials and Applications* **2018**, *2*, 1.

[4] S. B. Desai, S. R. Madhvapathy, A. B. Sachid, J. P. Llinas, Q. X. Wang, G. H. Ahn, G. Pitner, M. J. Kim, J. Bokor, C. M. Hu, H. S. P. Wong, A. Javey, *Science* **2016**, *354*, 99.

[5] M. Naguib, M. Kurtoglu, V. Presser, J. Lu, J. Niu, M. Heon, L. Hultman, Y. Gogotsi, M. W. Barsoum, *Adv. Mater.* **2011**, *23*, 4248.

[6] Q. Tang, D.-e. Jiang, *Chem. Mater.* **2015**, *27*, 3743.

[7] X. Ling, H. Wang, S. Huang, F. Xia, M. S. Dresselhaus, *Proceedings of the National Academy of Sciences* **2015**, *112*, 4523.

[8] Y. Wang, G. Qiu, R. Wang, S. Huang, Q. Wang, Y. Liu, Y. Du, W. A. Goddard, M. J. Kim, X. Xu, P. D. Ye, W. Wu, *Nat. Electron.* **2018**, *1*, 228.
[9] D. Wickramaratne, L. Weston, C. G. Van de Walle, *The Journal of Physical Chemistry C* **2018**, *122*, 25524.
[10] G. Hu, Q. Ou, G. Si, Y. Wu, J. Wu, Z. Dai, A. Krasnok, Y. Mazor, Q. Zhang, Q. Bao, C.-W. Qiu, A. Alù, *Nature* **2020**, *582*, 209.
[11] L. Li, Y. Yu, G. J. Ye, Q. Ge, X. Ou, H. Wu, D. Feng, X. H. Chen, Y. Zhang, *Nat. Nanotechnol.* **2014**, *9*, 372.
[12] R. V. Gorbachev, I. Riaz, R. R. Nair, R. Jalil, L. Britnell, B. D. Belle, E. W. Hill, K. S. Novoselov, K. Watanabe, T. Taniguchi, A. K. Geim, P. Blake, *Small* **2011**, *7*, 465.
[13] M. M. Y. A. Alsaif, A. F. Chrimes, T. Daeneke, S. Balendhran, D. O. Bellisario, Y. Son, M. R. Field, W. Zhang, H. Nili, E. P. Nguyen, K. Latham, J. van Embden, M. S. Strano, J. Z. Ou, K. Kalantar-zadeh, *Adv. Funct. Mater.* **2016**, *26*, 91.
[14] J.-H. Lee, E. K. Lee, W.-J. Joo, Y. Jang, B.-S. Kim, J. Y. Lim, S.-H. Choi, S. J. Ahn, J. R. Ahn, M.-H. Park, C.-W. Yang, B. L. Choi, S.-W. Hwang, D. Whang, *Science* **2014**, *344*, 286.
[15] M. S. Bresnehan, M. J. Hollander, M. Wetherington, M. LaBella, K. A. Trumbull, R. Cavalero, D. W. Snyder, J. A. Robinson, *ACS Nano* **2012**, *6*, 5234.
[16] H. Yu, M. Liao, W. Zhao, G. Liu, X. Zhou, Z. Wei, X. Xu, K. Liu, Z. Hu, K. Deng, *ACS nano* **2017**, *11*, 12001.
[17] J. Borysiuk, J. Sołtys, R. Bożek, J. Piechota, S. Krukowski, W. Strupiński, J. M. Baranowski, R. Stępniewski, *Phys. Rev. B.* **2012**, *85*, 045426.
[18] A. W. Robertson, J. H. Warner, *Nanoscale* **2013**, *5*, 4079.
[19] A. H. Castro Neto, F. Guinea, N. M. R. Peres, K. S. Novoselov, A. K. Geim, *Reviews of Modern Physics* **2009**, *81*, 109.
[20] R. S. Shishir, D. K. Ferry, *Journal of Physics: Condensed Matter* **2009**, *21*, 232204.
[21] A. Di Bartolomeo, F. Giubileo, F. Romeo, P. Sabatino, G. Carapella, L. Iemmo, T. Schroeder, G. Lupina, *Nanotechnology* **2015**, *26*, 475202.
[22] K. F. Mak, J. Shan, T. F. Heinz, *Phys. Rev. Lett.* **2011**, *106*, 046401.
[23] Y. Cao, V. Fatemi, S. Fang, K. Watanabe, T. Taniguchi, E. Kaxiras, P. Jarillo-Herrero, *Nature* **2018**, *556*, 43.
[24] S. Akhtar, Acta Universitatis Upsaliensis, **2012**.
[25] S. M. Kim, A. Hsu, M. H. Park, S. H. Chae, S. J. Yun, J. S. Lee, D.-H. Cho, W. Fang, C. Lee, T. Palacios, M. Dresselhaus, K. K. Kim, Y. H. Lee, J. Kong, *Nat. Commun* **2015**, *6*, 8662.
[26] K. Watanabe, T. Taniguchi, H. Kanda, *Nat. Mater.* **2004**, *3*, 404.
[27] A. Laturia, M. L. Van de Put, W. G. Vandenberghe, *npj 2D Materials and Applications* **2018**, *2*, 6.

[28] G. Grosso, H. Moon, B. Lienhard, S. Ali, D. K. Efetov, M. M. Furchi, P. Jarillo-Herrero, M. J. Ford, I. Aharonovich, D. Englund, *Nat. Commun* **2017**, *8*, 705.
[29] J. D. Caldwell, A. V. Kretinin, Y. Chen, V. Giannini, M. M. Fogler, Y. Francescato, C. T. Ellis, J. G. Tischler, C. R. Woods, A. J. Giles, M. Hong, K. Watanabe, T. Taniguchi, S. A. Maier, K. S. Novoselov, *Nat. Commun* **2014**, *5*, 5221.
[30] I. Jo, M. T. Pettes, J. Kim, K. Watanabe, T. Taniguchi, Z. Yao, L. Shi, *Nano Lett.* **2013**, *13*, 550.
[31] A. Kumar, P. K. Ahluwalia, in *MoS2: Materials, Physics, and Devices*, DOI: 10.1007/978-3-319-02850-7_3 (Ed: Z. M. Wang), Springer International Publishing, Cham **2014**, p. 53.
[32] J. Y. Zheng, X. X. Yan, Z. X. Lu, H. L. Qiu, G. C. Xu, Z. Xu, W. Peng, X. Q. Pan, K. H. Liu, L. Y. Jiao, *Adv. Mater.* **2017**, *29*.
[33] T. Cao, G. Wang, W. Han, H. Ye, C. Zhu, J. Shi, Q. Niu, P. Tan, E. Wang, B. Liu, J. Feng, *Nat. Commun* **2012**, *3*, 887.
[34] K. F. Mak, K. He, C. Lee, G. H. Lee, J. Hone, T. F. Heinz, J. Shan, *Nat. Mater.* **2013**, *12*, 207.
[35] S. Manzeli, D. Ovchinnikov, D. Pasquier, O. V. Yazyev, A. Kis, *Nat. Rev. Mater.* **2017**, *2*, 17033.
[36] M. Calandra, *Phys. Rev. B.* **2013**, *88*, 245428.
[37] P. R. Pudasaini, M. G. Stanford, A. Oyedele, A. T. Wong, A. N. Hoffman, D. P. Briggs, K. Xiao, D. G. Mandrus, T. Z. Ward, P. D. Rack, *Nanotechnology* **2017**, *28*, 475202.
[38] Q. He, P. Li, Z. Wu, B. Yuan, Z. Luo, W. Yang, J. Liu, G. Cao, W. Zhang, Y. Shen, *Adv. Mater.* **2019**, *31*, 1901578.
[39] X. Wang, X. Shen, Y. Gao, Z. Wang, R. Yu, L. Chen, *J. Am. Chem. Soc.* **2015**, *137*, 2715.
[40] C. Zhang, B. Anasori, A. Seral-Ascaso, S.-H. Park, N. McEvoy, A. Shmeliov, G. S. Duesberg, J. N. Coleman, Y. Gogotsi, V. Nicolosi, *Adv. Mater.* **2017**, *29*, 1702678.
[41] M. Ghidiu, J. Halim, S. Kota, D. Bish, Y. Gogotsi, M. W. Barsoum, *Chem. Mater.* **2016**, *28*, 3507.
[42] Y. Liu, H. Xiao, W. A. Goddard, *J. Am. Chem. Soc.* **2016**, *138*, 15853.
[43] J. K. El-Demellawi, S. Lopatin, J. Yin, O. F. Mohammed, H. N. Alshareef, *ACS Nano* **2018**, *12*, 8485.
[44] M. Khazaei, M. Arai, T. Sasaki, A. Ranjbar, Y. Liang, S. Yunoki, *Phys. Rev. B.* **2015**, *92*, 075411.
[45] L. Zhang, B. Wang, Y. Zhou, C. Wang, X. Chen, H. Zhang, *Adv. Opt. Mater. n/a*, 2000045.

[46] C. Zhao, C. Tan, D.-H. Lien, X. Song, M. Amani, M. Hettick, H. Y. Y. Nyein, Z. Yuan, L. Li, M. C. Scott, A. Javey, *Nat. Nanotechnol.* **2020**, *15*, 53.
[47] Y. Wang, G. Qiu, R. Wang, S. Huang, Q. Wang, Y. Liu, Y. Du, W. A. Goddard, M. J. Kim, X. Xu, *Nature Electronics* **2018**, *1*, 228.
[48] Z.-X. Guo, Y.-Y. Zhang, H. Xiang, X.-G. Gong, A. Oshiyama, *Phys. Rev. B.* **2015**, *92*, 201413.
[49] H. Zhong, K. Huang, G. Yu, S. Yuan, *Phys. Rev. B.* **2018**, *98*, 054104.
[50] Q. Qu, W.-B. Zhang, K. Huang, H.-M. Chen, *Comp Mater Sci* **2017**, *130*, 242.
[51] Y. Guo, J. Robertson, *Appl. Phys. Lett.* **2014**, *105*, 222110.
[52] S. Balendhran, J. Deng, J. Z. Ou, S. Walia, J. Scott, J. Tang, K. L. Wang, M. R. Field, S. Russo, S. Zhuiykov, M. S. Strano, N. Medhekar, S. Sriram, M. Bhaskaran, K. Kalantar-zadeh, *Adv. Mater.* **2013**, *25*, 109.
[53] R. Kumar, G. Kumar, A. Umar, *J. Nanosci. Nanotechnol.* **2014**, *14*, 1911.
[54] S. N. Ogugua, O. M. Ntwaeaborwa, H. C. Swart, *Coatings* **2020**, *10*, 1078.
[55] K. S. Kim, Y. Zhao, H. Jang, S. Y. Lee, J. M. Kim, K. S. Kim, J.-H. Ahn, P. Kim, J.-Y. Choi, B. H. Hong, *Nature* **2009**, *457*, 706.
[56] D. H. Jung, C. Kang, J. E. Nam, H. Jeong, J. S. Lee, *Sci. Rep.* **2016**, *6*, 21136.
[57] H. Tian, Y. He, P. Das, Z. Cui, W. Shi, A. Khanaki, R. K. Lake, J. Liu, *Adv. Mater. Interfaces* **2019**, *6*, 1901198.
[58] N. Briggs, S. Subramanian, Z. Lin, X. Li, X. Zhang, K. Zhang, K. Xiao, D. Geohegan, R. Wallace, L.-Q. Chen, *2D. Mater.* **2019**, *6*, 022001.
[59] P. Y. Huang, C. S. Ruiz-Vargas, A. M. van der Zande, W. S. Whitney, M. P. Levendorf, J. W. Kevek, S. Garg, J. S. Alden, C. J. Hustedt, Y. Zhu, J. Park, P. L. McEuen, D. A. Muller, *Nature* **2011**, *469*, 389.
[60] S. Bae, H. Kim, Y. Lee, X. Xu, J.-S. Park, Y. Zheng, J. Balakrishnan, T. Lei, H. Ri Kim, Y. I. Song, Y.-J. Kim, K. S. Kim, B. Özyilmaz, J.-H. Ahn, B. H. Hong, S. Iijima, *Nat. Nanotechnol.* **2010**, *5*, 574.
[61] P. Yang, X. Zou, Z. Zhang, M. Hong, J. Shi, S. Chen, J. Shu, L. Zhao, S. Jiang, X. Zhou, Y. Huan, C. Xie, P. Gao, Q. Chen, Q. Zhang, Z. Liu, Y. Zhang, *Nat. Commun* **2018**, *9*, 979.
[62] X. Song, J. Gao, Y. Nie, T. Gao, J. Sun, D. Ma, Q. Li, Y. Chen, C. Jin, A. Bachmatiuk, M. H. Rümmeli, F. Ding, Y. Zhang, Z. Liu, *Nano Res* **2015**, *8*, 3164.
[63] T.-A. Chen, C.-P. Chuu, C.-C. Tseng, C.-K. Wen, H. S. P. Wong, S. Pan, R. Li, T.-A. Chao, W.-C. Chueh, Y. Zhang, Q. Fu, B. I. Yakobson, W.-H. Chang, L.-J. Li, *Nature* **2020**, *579*, 219.
[64] X. Li, W. Cai, L. Colombo, R. S. Ruoff, *Nano Lett.* **2009**, *9*, 4268.
[65] Y. Lee, S. Bae, H. Jang, S. Jang, S.-E. Zhu, S. H. Sim, Y. I. Song, B. H. Hong, J.-H. Ahn, *Nano Lett.* **2010**, *10*, 490.

[66] V. L. Nguyen, D. J. Perello, S. Lee, C. T. Nai, B. G. Shin, J.-G. Kim, H. Y. Park, H. Y. Jeong, J. Zhao, Q. A. Vu, S. H. Lee, K. P. Loh, S.-Y. Jeong, Y. H. Lee, *Adv. Mater.* **2016**, *28*, 8177.

[67] W. Ma, M.-L. Chen, L. Yin, Z. Liu, H. Li, C. Xu, X. Xin, D.-M. Sun, H.-M. Cheng, W. Ren, *Nat. Commun* **2019**, *10*, 2809.

[68] H.-S. Jang, J.-Y. Lim, S.-G. Kang, Y.-M. Seo, J.-Y. Moon, J.-H. Lee, D. Whang, *ACS Nano* **2020**, *14*, 3141.

[69] J. Zhang, L. Lin, K. Jia, L. Sun, H. Peng, Z. Liu, *Adv. Mater.* **2020**, *32*, 1903266.

[70] Q. Wang, N. Li, J. Tang, J. Zhu, Q. Zhang, Q. Jia, Y. Lu, Z. Wei, H. Yu, Y. Zhao, Y. Guo, L. Gu, G. Sun, W. Yang, R. Yang, D. Shi, G. Zhang, *Nano Lett.* **2020**, *20*, 7193.

[71] M. Kim, J. Seo, J. Kim, J. S. Moon, J. Lee, J.-H. Kim, J. Kang, H. Park, *ACS Nano* **2021**, *15*, 3038.

[72] C. Lan, Z. Zhou, Z. Zhou, C. Li, L. Shu, L. Shen, D. Li, R. Dong, S. Yip, J. C. Ho, *Nano Res* **2018**, *11*, 3371.

[73] J. Shi, X. Chen, L. Zhao, Y. Gong, M. Hong, Y. Huan, Z. Zhang, P. Yang, Y. Li, Q. Zhang, Q. Zhang, L. Gu, H. Chen, J. Wang, S. Deng, N. Xu, Y. Zhang, *Adv. Mater.* **2018**, *30*, 1804616.

[74] P. Yang, S. Zhang, S. Pan, B. Tang, Y. Liang, X. Zhao, Z. Zhang, J. Shi, Y. Huan, Y. Shi, S. J. Pennycook, Z. Ren, G. Zhang, Q. Chen, X. Zou, Z. Liu, Y. Zhang, *ACS Nano* **2020**, *14*, 5036.

[75] X. Xu, Z. Wang, S. Lopatin, M. A. Quevedo-Lopez, H. N. Alshareef, *2D. Mater.* **2018**, *6*, 015030.

[76] J. Han, J.-Y. Lee, H. Kwon, J.-S. Yeo, *Nanotechnology* **2014**, *25*, 145604.

[77] W.-H. Lin, V. W. Brar, D. Jariwala, M. C. Sherrott, W.-S. Tseng, C.-I. Wu, N.-C. Yeh, H. A. Atwater, *Chem. Mater.* **2017**, *29*, 4700.

[78] C. Zhang, L. Fu, S. Zhao, Y. Zhou, H. Peng, Z. Liu, *Adv. Mater.* **2014**, *26*, 1776.

[79] J. S. Lee, S. H. Choi, S. J. Yun, Y. I. Kim, S. Boandoh, J.-H. Park, B. G. Shin, H. Ko, S. H. Lee, Y.-M. Kim, Y. H. Lee, K. K. Kim, S. M. Kim, *Science* **2018**, *362*, 817.

[80] L. Wang, X. Xu, L. Zhang, R. Qiao, M. Wu, Z. Wang, S. Zhang, J. Liang, Z. Zhang, Z. Zhang, W. Chen, X. Xie, J. Zong, Y. Shan, Y. Guo, M. Willinger, H. Wu, Q. Li, W. Wang, P. Gao, S. Wu, Y. Zhang, Y. Jiang, D. Yu, E. Wang, X. Bai, Z.-J. Wang, F. Ding, K. Liu, *Nature* **2019**, *570*, 91.

[81] A. R. Jang, S. Hong, C. Hyun, S. I. Yoon, G. Kim, H. Y. Jeong, T. J. Shin, S. O. Park, K. Wong, S. K. Kwak, N. Park, K. Yu, E. Choi, A. Mishchenko, F. Withers, K. S. Novoselov, H. Lim, H. S. Shin, *Nano Lett.* **2016**, *16*, 3360.

[82] C. Wen, X. Li, T. Zanotti, F. M. Puglisi, Y. Shi, F. Saiz, A. Antidormi, S. Roche, W. Zheng, X. Liang, J. Hu, S. Duhm, J. B. Roldan, T. Wu, V. Chen, E. Pop, B. Garrido, K. Zhu, F. Hui, M. Lanza, *Adv. Mater.* **2021**, *33*, 2100185.

[83] Y. Shi, X. Liang, B. Yuan, V. Chen, H. Li, F. Hui, Z. Yu, F. Yuan, E. Pop, H. S. P. Wong, M. Lanza, *Nat. Electron.* **2018**, *1*, 458.

[84] T. Knobloch, Y. Y. Illarionov, F. Ducry, C. Schleich, S. Wachter, K. Watanabe, T. Taniguchi, T. Mueller, M. Waltl, M. Lanza, M. I. Vexler, M. Luisier, T. Grasser, *Nat. Electron.* **2021**, *4*, 98.

[85] K. Kang, S. Xie, L. Huang, Y. Han, P. Y. Huang, K. F. Mak, C.-J. Kim, D. Muller, J. Park, *Nature* **2015**, *520*, 656.

[86] Y.-C. Lin, B. Jariwala, B. M. Bersch, K. Xu, Y. Nie, B. Wang, S. M. Eichfeld, X. Zhang, T. H. Choudhury, Y. Pan, *ACS nano* **2018**, *12*, 965.

[87] T. H. Choudhury, X. Zhang, Z. Y. A. Balushi, M. Chubarov, J. M. Redwing, *Annual Review of Materials Research* **2020**, *50*, 155.

[88] C. Zhang, J. Huang, R. Tu, S. Zhang, M. Yang, Q. Li, J. Shi, H. Li, L. Zhang, T. Goto, H. Ohmori, *Carbon* **2018**, *131*, 10.

[89] G. Siegel, G. Gryzbowcki, A. Hilton, C. Muratore, M. Snure, *Crystals* **2019**, *9*, 339.

[90] D. Y. Kim, N. Han, H. Jeong, J. Kim, S. Hwang, K. Song, S.-Y. Choi, J. K. Kim, *Cryst Growth Des* **2017**, *17*, 2569.

[91] T. Kim, J. Mun, H. Park, D. Joung, M. Diware, C. Won, J. Park, S. H. Jeong, S. W. Kang, *Nanotechnology* **2017**, *28*.

[92] M. Chubarov, T. H. Choudhury, D. R. Hickey, S. Bachu, T. Zhang, A. Sebastian, A. Bansal, H. Zhu, N. Trainor, S. Das, M. Terrones, N. Alem, J. M. Redwing, *ACS Nano* **2021**, *15*, 2532.

[93] D. Fu, X. Zhao, Y.-Y. Zhang, L. Li, H. Xu, A. R. Jang, S. I. Yoon, P. Song, S. M. Poh, T. Ren, Z. Ding, W. Fu, T. J. Shin, H. S. Shin, S. T. Pantelides, W. Zhou, K. P. Loh, *J. Am. Chem. Soc.* **2017**, *139*, 9392.

[94] H. Tian, A. Khanaki, P. Das, R. Zheng, Z. Cui, Y. He, W. Shi, Z. Xu, R. Lake, J. Liu, *Nano Lett.* **2018**, *18*, 3352.

[95] L. A. Walsh, C. L. Hinkle, *Applied Materials Today* **2017**, *9*, 504.

[96] S. M. Poh, S. J. R. Tan, H. Wang, P. Song, I. H. Abidi, X. Zhao, J. Dan, J. Chen, Z. Luo, S. J. Pennycook, A. H. Castro Neto, K. P. Loh, *Nano Lett.* **2018**, *18*, 6340.

[97] S. Liu, X. Yuan, Y. Zou, Y. Sheng, C. Huang, E. Zhang, J. Ling, Y. Liu, W. Wang, C. Zhang, J. Zou, K. Wang, F. Xiu, *npj 2D Materials and Applications* **2017**, *1*, 30.

[98] L. K. Tan, B. Liu, J. H. Teng, S. Guo, H. Y. Low, K. P. Loh, *Nanoscale* **2014**, *6*, 10584.

[99] B. Groven, A. Nalin Mehta, H. Bender, J. Meersschaut, T. Nuytten, P. Verdonck, T. Conard, Q. Smets, T. Schram, B. Schoenaers, A. Stesmans, V. Afanas'ev, W. Vandervorst, M. Heyns, M. Caymax, I. Radu, A. Delabie, *Chem. Mater.* **2018**, *30*, 7648.

[100] J. Yang, L. Liu, *ACS Appl. Mater. Inter.* **2019**, *11*, 36270.

[101] W. Hao, C. Marichy, C. Journet, *2D. Mater.* **2018**, *6*, 012001.
[102] J. Cai, X. Han, X. Wang, X. Meng, *Matter* **2020**, *2*, 587.
[103] J. Jenny, S. G. Müller, A. Powell, V. Tsvetkov, H. Hobgood, R. Glass, C. Carter, *J Electron Mater* **2002**, *31*, 366.
[104] C. Ahn, J. Lee, H. U. Kim, H. Bark, M. Jeon, G. H. Ryu, Z. Lee, G. Y. Yeom, K. Kim, J. Jung, *Adv. Mater.* **2015**, *27*, 5223.
[105] Y. Lee, J. Lee, H. Bark, I.-K. Oh, G. H. Ryu, Z. Lee, H. Kim, J. H. Cho, J.-H. Ahn, C. Lee, *Nanoscale* **2014**, *6*, 2821.
[106] J. Robertson, X. Liu, C. Yue, M. Escarra, J. Wei, *2D. Mater.* **2017**, *4*, 045007.
[107] H. U. Kim, V. Kanade, M. Kim, K. S. Kim, B. S. An, H. Seok, H. Yoo, L. E. Chaney, S. I. Kim, C. W. Yang, *Small* **2020**, 1905000.
[108] Y. C. Lin, W. J. Zhang, J. K. Huang, K. K. Liu, Y. H. Lee, C. T. Liang, C. W. Chu, L. J. Li, *Nanoscale* **2012**, *4*, 6637.
[109] Y. Kim, A. R. Kim, G. Zhao, S. Y. Choi, S. C. Kang, S. K. Lim, K. E. Lee, J. Park, B. H. Lee, M. G. Hahm, *ACS Appl. Mater. Inter.* **2017**, *9*, 37146.
[110] X. Xu, G. Das, X. He, M. N. Hedhili, E. D. Fabrizio, X. Zhang, H. N. Alshareef, *Adv. Funct. Mater.* **2019**, 1901070.
[111] X. Xu, C. Zhang, M. K. Hota, Z. Liu, X. Zhang, H. N. Alshareef, *Adv. Funct. Mater.* **2020**, *30*, 1908040.
[112] Y. R. Lim, W. Song, J. K. Han, Y. B. Lee, S. J. Kim, S. Myung, S. S. Lee, K. S. An, C. J. Choi, J. Lim, *Adv. Mater.* **2016**, *28*, 5025.
[113] H. Yang, A. Giri, S. Moon, S. Shin, J.-M. Myoung, U. Jeong, *Chem. Mater.* **2017**, *29*, 5772.
[114] R. Ionescu, B. Campbell, R. Wu, E. Aytan, A. Patalano, I. Ruiz, S. W. Howell, A. E. McDonald, T. E. Beechem, K. A. Mkhoyan, M. Ozkan, C. S. Ozkan, *Sci. Rep.* **2017**, *7*, 6419.
[115] Y. R. Lim, J. K. Han, S. K. Kim, Y. B. Lee, Y. Yoon, S. J. Kim, B. K. Min, Y. Kim, C. Jeon, S. Won, *Adv. Mater.* **2018**, *30*, 1705270.
[116] K. V. Emtsev, F. Speck, T. Seyller, L. Ley, J. D. Riley, *Phys. Rev. B.* **2008**, *77*, 155303.
[117] K. V. Emtsev, A. Bostwick, K. Horn, J. Jobst, G. L. Kellogg, L. Ley, J. L. McChesney, T. Ohta, S. A. Reshanov, J. Röhrl, E. Rotenberg, A. K. Schmid, D. Waldmann, H. B. Weber, T. Seyller, *Nat. Mater.* **2009**, *8*, 203.
[118] A. Jannat, Q. Yao, A. Zavabeti, N. Syed, B. Y. Zhang, T. Ahmed, S. Kuriakose, M. Mohiuddin, N. Pillai, F. Haque, *Mater Horiz* **2020**.
[119] M. Wang, T.-J. Ko, M. S. Shawkat, S. S. Han, E. Okogbue, H.-S. Chung, T.-S. Bae, S. Sattar, J. Gil, C. Noh, K. H. Oh, Y. Jung, J. A. Larsson, Y. Jung, *ACS Appl. Mater. Inter.* **2020**, *12*, 10839.

[120] X. Xu, S. Chen, S. Liu, X. Cheng, W. Xu, P. Li, Y. Wan, S. Yang, W. Gong, K. Yuan, P. Gao, Y. Ye, L. Dai, *J. Am. Chem. Soc.* **2019**, *141*, 2128.

[121] C. Li, Y. Wu, B. Deng, Y. Xie, Q. Guo, S. Yuan, X. Chen, M. Bhuiyan, Z. Wu, K. Watanabe, T. Taniguchi, H. Wang, J. J. Cha, M. Snure, Y. Fei, F. Xia, *Adv. Mater.* **2018**, *30*, 1703748.

[122] I.-H. Baek, J. J. Pyeon, G.-Y. Lee, Y. G. Song, H. Lee, S. O. Won, J. H. Han, C.-Y. Kang, T.-M. Chung, C. S. Hwang, S. K. Kim, *Chem. Mater.* **2020**, *32*, 2313.

[123] M. S. Shawkat, J. Gil, S. S. Han, T.-J. Ko, M. Wang, D. Dev, J. Kwon, G.-H. Lee, K. H. Oh, H.-S. Chung, T. Roy, Y. Jung, Y. Jung, *ACS Appl. Mater. Inter.* **2020**, *12*, 14341.

[124] M. L. Shi, L. Chen, T. B. Zhang, J. Xu, H. Zhu, Q. Q. Sun, D. W. Zhang, *Small* **2017**, *13*, 1603157.

[125] S. Hussain, M. F. Khan, M. A. Shehzad, D. Vikraman, M. Z. Iqbal, D.-C. Choi, W. Song, K.-S. An, Y. Seo, J. Eom, W.-G. Lee, J. Jung, *J Mater Chem C* **2016**, *4*, 7846.

[126] J. J. Pyeon, I.-H. Baek, W. C. Lim, K. H. Chae, S. H. Han, G. Y. Lee, S.-H. Baek, J.-S. Kim, J.-W. Choi, T.-M. Chung, *Nanoscale* **2018**, *10*, 17712.

[127] W.-S. Lin, H. Medina, T.-Y. Su, S.-H. Lee, C.-W. Chen, Y.-Z. Chen, A. Manikandan, Y.-C. Shih, J.-H. Yang, J.-H. Chen, *ACS Appl. Mater. Inter.* **2018**, *10*, 9645.

[128] T.-J. Dai, Y.-C. Liu, X.-D. Fan, X.-Z. Liu, D. Xie, Y.-R. Li, *Nanophotonics-Berlin* **2018**, *7*, 1959.

[129] S. Song, Y. Sim, S.-Y. Kim, J. H. Kim, I. Oh, W. Na, D. H. Lee, J. Wang, S. Yan, Y. Liu, J. Kwak, J.-H. Chen, H. Cheong, J.-W. Yoo, Z. Lee, S.-Y. Kwon, *Nat. Electron.* **2020**, *3*, 207.

[130] E. Okogbue, T.-J. Ko, S. S. Han, M. S. Shawkat, M. Wang, H.-S. Chung, K. H. Oh, Y. Jung, *Nanoscale* **2020**, *12*, 10647.

[131] X. Xu, Y. Pan, S. Liu, B. Han, P. Gu, S. Li, W. Xu, Y. Peng, Z. Han, J. Chen, *Science* **2021**, *372*, 195.

[132] X. Li, B. Deng, X. Wang, S. Chen, M. Vaisman, S.-i. Karato, G. Pan, M. Larry Lee, J. Cha, H. Wang, F. Xia, *2D. Mater.* **2015**, *2*, 031002.

[133] M. I. Serna, S. H. Yoo, S. Moreno, Y. Xi, J. P. Oviedo, H. Choi, H. N. Alshareef, M. J. Kim, M. Minary-Jolandan, M. A. Quevedo-Lopez, *ACS Nano* **2016**, *10*, 6054.

[134] S. Hussain, J. Singh, D. Vikraman, A. K. Singh, M. Z. Iqbal, M. F. Khan, P. Kumar, D.-C. Choi, W. Song, K.-S. An, J. Eom, W.-G. Lee, J. Jung, *Sci. Rep.* **2016**, *6*, 30791.

[135] Z. Wu, Y. Lyu, Y. Zhang, R. Ding, B. Zheng, Z. Yang, S. P. Lau, X. H. Chen, J. Hao, *Nat. Mater.* **2021**, DOI: 10.1038/s41563-021-01001-7.

[136] H. M. Christen, G. Eres, *Journal of Physics: Condensed Matter* **2008**, *20*, 264005.

[137] S. C. Xu, B. Y. Man, S. Z. Jiang, A. H. Liu, G. D. Hu, C. S. Chen, M. Liu, C. Yang, D. J. Feng, C. Zhang, *Laser Phys Lett* **2014**, *11*, 096001.

[138] F. Tumino, C. S. Casari, M. Passoni, V. Russo, A. Li Bassi, *Nanoscale Advances* **2019**, *1*, 643.
[139] Z. Yang, J. Hao, S. Yuan, S. Lin, H. M. Yau, J. Dai, S. P. Lau, *Adv. Mater.* **2015**, *27*, 3748.
[140] J. Tao, J. Chai, X. Lu, L. M. Wong, T. I. Wong, J. Pan, Q. Xiong, D. Chi, S. Wang, *Nanoscale* **2015**, *7*, 2497.
[141] J. Ohta, H. Fujioka, *APL Mater.* **2017**, *5*, 5.
[142] S. Casaluci, M. Gemmi, V. Pellegrini, A. Di Carlo, F. Bonaccorso, *Nanoscale* **2016**, *8*, 5368.
[143] Z. Lin, Y. Liu, U. Halim, M. Ding, Y. Liu, Y. Wang, C. Jia, P. Chen, X. Duan, C. Wang, *Nature* **2018**, *562*, 254.
[144] K. Hantanasirisakul, M.-Q. Zhao, P. Urbankowski, J. Halim, B. Anasori, S. Kota, C. E. Ren, M. W. Barsoum, Y. Gogotsi, *Adv. Electron. Mater.* **2016**, *2*, 1600050.
[145] X. Zhu, L. W. T. Ng, G. Hu, T.-C. Wu, D.-S. Um, N. Macadam, T. Hasan, *Adv. Funct. Mater.* **2020**, *30*, 2002339.
[146] Z. Wang, H. Kim, H. N. Alshareef, *Adv. Mater.* **2018**, *30*, 1706656.
[147] H. Kim, Z. Wang, H. N. Alshareef, *Nano Energy* **2019**, *60*, 179.
[148] X. Li, C. W. Magnuson, A. Venugopal, R. M. Tromp, J. B. Hannon, E. M. Vogel, L. Colombo, R. S. Ruoff, *J. Am. Chem. Soc.* **2011**, *133*, 2816.
[149] Y. Hao, M. S. Bharathi, L. Wang, Y. Liu, H. Chen, S. Nie, X. Wang, H. Chou, C. Tan, B. Fallahazad, H. Ramanarayan, C. W. Magnuson, E. Tutuc, B. I. Yakobson, K. F. McCarty, Y.-W. Zhang, P. Kim, J. Hone, L. Colombo, R. S. Ruoff, *Science* **2013**, *342*, 720.
[150] T. Wu, X. Zhang, Q. Yuan, J. Xue, G. Lu, Z. Liu, H. Wang, H. Wang, F. Ding, Q. Yu, X. Xie, M. Jiang, *Nat. Mater.* **2016**, *15*, 43.
[151] J. Chen, W. Tang, B. Tian, B. Liu, X. Zhao, Y. Liu, T. Ren, W. Liu, D. Geng, H. Y. Jeong, H. S. Shin, W. Zhou, K. P. Loh, *Adv. Sci.* **2016**, *3*, 1500033.
[152] J. Chen, X. Zhao, S. J. R. Tan, H. Xu, B. Wu, B. Liu, D. Fu, W. Fu, D. Geng, Y. Liu, W. Liu, W. Tang, L. Li, W. Zhou, T. C. Sum, K. P. Loh, *J. Am. Chem. Soc.* **2017**, *139*, 1073.
[153] Y. Rong, Y. Fan, A. Leen Koh, A. W. Robertson, K. He, S. Wang, H. Tan, R. Sinclair, J. H. Warner, *Nanoscale* **2014**, *6*, 12096.
[154] T. Yang, B. Zheng, Z. Wang, T. Xu, C. Pan, J. Zou, X. Zhang, Z. Qi, H. Liu, Y. Feng, W. Hu, F. Miao, L. Sun, X. Duan, A. Pan, *Nat. Commun* **2017**, *8*, 1906.
[155] G. Lu, T. Wu, Q. Yuan, H. Wang, H. Wang, F. Ding, X. Xie, M. Jiang, *Nat. Commun* **2015**, *6*, 6160.
[156] C. Xu, L. Wang, Z. Liu, L. Chen, J. Guo, N. Kang, X.-L. Ma, H.-M. Cheng, W. Ren, *Nat. Mater.* **2015**, *14*, 1135.

[157] Y. Gao, Y.-L. Hong, L.-C. Yin, Z. Wu, Z. Yang, M.-L. Chen, Z. Liu, T. Ma, D.-M. Sun, Z. Ni, X.-L. Ma, H.-M. Cheng, W. Ren, *Adv. Mater.* **2017**, *29*, 1700990.

[158] C. Liu, X. Xu, L. Qiu, M. Wu, R. Qiao, L. Wang, J. Wang, J. Niu, J. Liang, X. Zhou, Z. Zhang, M. Peng, P. Gao, W. Wang, X. Bai, D. Ma, Y. Jiang, X. Wu, D. Yu, E. Wang, J. Xiong, F. Ding, K. Liu, *Nat. Chem.* **2019**, *11*, 730.

[159] I. V. Vlassiouk, Y. Stehle, P. R. Pudasaini, R. R. Unocic, P. D. Rack, A. P. Baddorf, I. N. Ivanov, N. V. Lavrik, F. List, N. Gupta, K. V. Bets, B. I. Yakobson, S. N. Smirnov, *Nat. Mater.* **2018**, *17*, 318.

[160] J. Wang, X. Xu, T. Cheng, L. Gu, R. Qiao, Z. Liang, D. Ding, H. Hong, P. Zheng, Z. Zhang, Z. Zhang, S. Zhang, G. Cui, C. Chang, C. Huang, J. Qi, J. Liang, C. Liu, Y. Zuo, G. Xue, X. Fang, J. Tian, M. Wu, Y. Guo, Z. Yao, Q. Jiao, L. Liu, P. Gao, Q. Li, R. Yang, G. Zhang, Z. Tang, D. Yu, E. Wang, J. Lu, Y. Zhao, S. Wu, F. Ding, K. Liu, *Nat. Nanotechnol.* **2021**, DOI: 10.1038/s41565-021-01004-0.

[161] T. Li, W. Guo, L. Ma, W. Li, Z. Yu, Z. Han, S. Gao, L. Liu, D. Fan, Z. Wang, Y. Yang, W. Lin, Z. Luo, X. Chen, N. Dai, X. Tu, D. Pan, Y. Yao, P. Wang, Y. Nie, J. Wang, Y. Shi, X. Wang, *Nat. Nanotechnol.* **2021**, DOI: 10.1038/s41565-021-00963-8.

[162] D. Ruzmetov, K. Zhang, G. Stan, B. Kalanyan, G. R. Bhimanapati, S. M. Eichfeld, R. A. Burke, P. B. Shah, T. P. O'Regan, F. J. Crowne, A. G. Birdwell, J. A. Robinson, A. V. Davydov, T. G. Ivanov, *ACS Nano* **2016**, *10*, 3580.

[163] F. Giannazzo, E. Schilirò, R. Lo Nigro, P. Prystawko, Y. Cordier, in *Nitride Semiconductor Technology*, DOI: https://doi.org/10.1002/9783527825264.ch11 **2020**, p. 397.

[164] W. A. de Heer, C. Berger, M. Ruan, M. Sprinkle, X. Li, Y. Hu, B. Zhang, J. Hankinson, E. Conrad, *Proceedings of the National Academy of Sciences* **2011**, *108*, 16900.

[165] W. Norimatsu, M. Kusunoki, *Physical Chemistry Chemical Physics* **2014**, *16*, 3501.

[166] Y. Wang, L. Li, W. Yao, S. Song, J. T. Sun, J. Pan, X. Ren, C. Li, E. Okunishi, Y.-Q. Wang, E. Wang, Y. Shao, Y. Y. Zhang, H.-t. Yang, E. F. Schwier, H. Iwasawa, K. Shimada, M. Taniguchi, Z. Cheng, S. Zhou, S. Du, S. J. Pennycook, S. T. Pantelides, H.-J. Gao, *Nano Lett.* **2015**, *15*, 4013.

[167] F. Giannazzo, I. Deretzis, A. La Magna, F. Roccaforte, R. Yakimova, *Phys. Rev. B.* **2012**, *86*, 235422.

[168] I. R. Committee, 2010.

[169] in *Beyond-CMOS Nanodevices 2*, DOI: https://doi.org/10.1002/9781118985137.ch3 **2014**, p. 97.

[170] N. Collaert, A. Alian, H. Arimura, G. Boccardi, G. Eneman, J. Franco, T. Ivanov, D. Lin, J. Mitard, S. Ramesh, R. Rooyackers, M. Schaekers, A. Sibaya-Hernandez, S. Sioncke, Q. Smets, A. Vais, A. Vandooren, A. Veloso, A. Verhulst, D. Verreck, N.

Waldron, A. Walke, L. Witters, H. Yu, X. Zhou, A. V. Thean, presented at 2016 International Conference on IC Design and Technology (ICICDT), 27-29 June 2016, **2016**.

[171] M. Díaz, C. Martín, B. Rubio, *Journal of Network and Computer Applications* **2016**, *67*, 99.

[172] J. Yin, L. Liu, Y. Zang, A. Ying, W. Hui, S. Jiang, C. Zhang, T. Yang, Y.-L. Chueh, J. Li, *Light: Science & Applications* **2021**, *10*, 1.

[173] N. Li, Q. Wang, C. Shen, Z. Wei, H. Yu, J. Zhao, X. Lu, G. Wang, C. He, L. Xie, *Nature Electronics* **2020**, *3*, 711.

[174] S. Chen, M. R. Mahmoodi, Y. Shi, C. Mahata, B. Yuan, X. Liang, C. Wen, F. Hui, D. Akinwande, D. B. Strukov, *Nature Electronics* **2020**, *3*, 638.

[175] Q. Jiang, N. Kurra, K. Maleski, Y. Lei, H. Liang, Y. Zhang, Y. Gogotsi, H. N. Alshareef, *Advanced Energy Materials* **2019**, *9*, 1901061.

[176] G. M. Marega, Y. Zhao, A. Avsar, Z. Wang, M. Tripathi, A. Radenovic, A. Kis, *Nature* **2020**, *587*, 72.

[177] Q. Liu, B. Cook, M. Gong, Y. Gong, D. Ewing, M. Casper, A. Stramel, J. Wu, *ACS Appl. Mater. Inter.* **2017**, *9*, 12728.

[178] Y. Shen, W. Zheng, K. Zhu, Y. Xiao, C. Wen, Y. Liu, X. Jing, M. Lanza, *Adv. Mater.* **2021**, *33*, 2103656.

[179] A. VahidMohammadi, J. Rosen, Y. Gogotsi, *Science* **2021**, *372*.

[180] J. Kim, C. Bayram, H. Park, C.-W. Cheng, C. Dimitrakopoulos, J. A. Ott, K. B. Reuter, S. W. Bedell, D. K. Sadana, *Nat. Commun* **2014**, *5*, 4836.

[181] K. Chung, H. Oh, J. Jo, K. Lee, M. Kim, G.-C. Yi, *NPG Asia Materials* **2017**, *9*, e410.

[182] X. Xu, J. Smajic, K.-h. Li, J.-W. Min, Y. Lei, B. Davaasuren, X. He, X. Zhang, B. S. Ooi, P. M. Da Costa, H. N. Alshareef, *Adv. Mater. n/a*, 2105190.

[183] Z. Y. Al Balushi, K. Wang, R. K. Ghosh, R. A. Vilá, S. M. Eichfeld, J. D. Caldwell, X. Qin, Y.-C. Lin, P. A. DeSario, G. Stone, S. Subramanian, D. F. Paul, R. M. Wallace, S. Datta, Joan M. Redwing, J. A. Robinson, *Nat. Mater.* **2016**, *15*, 1166.

[184] W. Wang, Y. Zheng, X. Li, Y. Li, H. Zhao, L. Huang, Z. Yang, X. Zhang, G. Li, *Adv. Mater.* **2019**, *31*, 1803448.

[185] H. Kum, D. Lee, W. Kong, H. Kim, Y. Park, Y. Kim, Y. Baek, S.-H. Bae, K. Lee, J. Kim, *Nat. Electron.* **2019**, *2*, 439.

[186] W. Kong, H. Li, K. Qiao, Y. Kim, K. Lee, Y. Nie, D. Lee, T. Osadchy, R. J. Molnar, D. K. Gaskill, R. L. Myers-Ward, K. M. Daniels, Y. Zhang, S. Sundram, Y. Yu, S.-h. Bae, S. Rajan, Y. Shao-Horn, K. Cho, A. Ougazzaden, J. C. Grossman, J. Kim, *Nat. Mater.* **2018**, *17*, 999.

[187] J. Yu, L. Wang, Z. Hao, Y. Luo, C. Sun, J. Wang, Y. Han, B. Xiong, H. Li, *Adv. Mater.* **2020**, *32*, 1903407.

[188] A. Kakanakova-Georgieva, G. K. Gueorguiev, D. G. Sangiovanni, N. Suwannaharn, I. G. Ivanov, I. Cora, B. Pécz, G. Nicotra, F. Giannazzo, *Nanoscale* **2020**, *12*, 19470.
[189] B. Pécz, G. Nicotra, F. Giannazzo, R. Yakimova, A. Koos, A. Kakanakova-Georgieva, *Adv. Mater.* **2021**, *33*, 2006660.
[190] P. Avouris, C. Dimitrakopoulos, *Mater. Today* **2012**, *15*, 86.
[191] L. Lin, H. Peng, Z. Liu, *Nat. Mater.* **2019**, *18*, 520.
[192] J. Zhang, L. Sun, K. Jia, X. Liu, T. Cheng, H. Peng, L. Lin, Z. Liu, *ACS Nano* **2020**, *14*, 10796.
[193] B. Deng, Z. Pang, S. Chen, X. Li, C. Meng, J. Li, M. Liu, J. Wu, Y. Qi, W. Dang, H. Yang, Y. Zhang, J. Zhang, N. Kang, H. Xu, Q. Fu, X. Qiu, P. Gao, Y. Wei, Z. Liu, H. Peng, *ACS Nano* **2017**, *11*, 12337.
[194] T. Niu, M. Zhou, J. Zhang, Y. Feng, W. Chen, *J. Am. Chem. Soc.* **2013**, *135*, 8409.
[195] L. Zheng, Y. Chen, N. Li, J. Zhang, N. Liu, J. Liu, W. Dang, B. Deng, Y. Li, X. Gao, C. Tan, Z. Yang, S. Xu, M. Wang, H. Yang, L. Sun, Y. Cui, X. Wei, P. Gao, H.-W. Wang, H. Peng, *Nat. Commun* **2020**, *11*, 541.
[196] J. Sun, C. Lu, Y. Song, Q. Ji, X. Song, Q. Li, Y. Zhang, L. Zhang, J. Kong, Z. Liu, *Chem. Soc. Rev.* **2018**, *47*, 4242.
[197] J. Zhang, R. Sun, D. Ruan, M. Zhang, Y. Li, K. Zhang, F. Cheng, Z. Wang, Z.-M. Wang, *J. Appl. Phys.* **2020**, *128*, 100902.
[198] R. Wang, D. G. Purdie, Y. Fan, F. C. P. Massabuau, P. Braeuninger-Weimer, O. J. Burton, R. Blume, R. Schloegl, A. Lombardo, R. S. Weatherup, S. Hofmann, *ACS Nano* **2019**, *13*, 2114.
[199] J. Hong, Z. Hu, M. Probert, K. Li, D. Lv, X. Yang, L. Gu, N. Mao, Q. Feng, L. Xie, J. Zhang, D. Wu, Z. Zhang, C. Jin, W. Ji, X. Zhang, J. Yuan, Z. Zhang, *Nat. Commun* **2015**, *6*, 6293.
[200] H. Kim, H. N. Alshareef, *ACS Mater. Lett.* **2020**, *2*, 55.
[201] H. Kim, M. I. Nugraha, X. Guan, Z. Wang, M. K. Hota, X. Xu, T. Wu, D. Baran, T. D. Anthopoulos, H. N. Alshareef, *ACS Nano* **2021**, *15*, 5221.
[202] B. Lyu, M. Kim, H. Jing, J. Kang, C. Qian, S. Lee, J. H. Cho, *ACS Nano* **2019**, *13*, 11392.
[203] X. Li, W. Cai, J. An, S. Kim, J. Nah, D. Yang, R. Piner, A. Velamakanni, I. Jung, E. Tutuc, *Science* **2009**, *324*, 1312.
[204] C. Berger, Z. Song, X. Li, X. Wu, N. Brown, C. Naud, D. Mayou, T. Li, J. Hass, A. N. Marchenkov, E. H. Conrad, P. N. First, W. A. d. Heer, *Science* **2006**, *312*, 1191.
[205] K. S. Novoselov, D. Jiang, F. Schedin, T. J. Booth, V. V. Khotkevich, S. V. Morozov, A. K. Geim, *P Natl Acad Sci USA* **2005**, *102*, 10451.
[206] M. Mojtabavi, A. VahidMohammadi, K. Ganeshan, D. Hejazi, S. Shahbazmohamadi, S. Kar, A. C. T. van Duin, M. Wanunu, *ACS Nano* **2021**, *15*, 625.

[207] L. Liu, T. Zhai, *InfoMat* **2021**, *3*, 3.
[208] J. Lin, S. Monaghan, N. Sakhuja, F. Gity, R. K. Jha, E. M. Coleman, J. Connolly, C. P. Cullen, L. A. Walsh, T. Mannarino, M. Schmidt, B. Sheehan, G. S. Duesberg, N. McEvoy, N. Bhat, P. K. Hurley, I. M. Povey, S. Bhattacharjee, *2D. Mater.* **2020**, *8*, 025008.
[209] A. Kozhakhmetov, J. R. Nasr, F. Zhang, K. Xu, N. C. Briggs, R. Addou, R. Wallace, S. K. Fullerton-Shirey, M. Terrones, S. Das, J. A. Robinson, *2D. Mater.* **2019**, *7*, 015029.

Xiangming Xu *received his Ph.D. degree in 2020 in Materials Science & Engineering from King Abdullah University of Science and Technology (KAUST) under the guidance of Professor Husam N. Alshareef. He is currently a Postdoctoral Fellow with Prof. Husam N. Alshareef as his advisor in King Abdullah University of Science and Technology (KAUST). His research interests focus on the growth of large-area high-quality 2D films (MXenes, TMDs, MOFs) and their electronic device applications.*

Tianchao Guo *received his MS degree in Physics in 2020 from China University of Petroleum (UPC). He is currently a PhD student in Material Science and Engineering at King Abdullah University of Science and Technology under the supervision of Prof. Husam N. Alshareef. His research interests mainly focus on low dimensional material synthesis and the applications of MXene in various types of electronic devices.*

Hyunho Kim *obtained both his M.S. (2015) and Ph.D. (2020) degrees in Materials Science and Engineering at King Abdullah University of Science and Technology (KAUST) under the guidance of Professor Husam N. Alshareef. He currently works as a postdoctoral research associate in chemistry department at Imperial College London. His research interest includes electronic applications of MXenes and other solution processed 2D materials.*

Mrinal Kanti Hota *received his Ph.D. degree in Engineering in May 2013 under the joint supervision of Prof. Chinmay Kumar Maiti of Indian Institute of Technology, Kharagpur, and Prof. Chandan Kumar Sarkar of Jadavpur University, India. He is currently working as a Research Scientist at King Abdullah University of Science and Technology (KAUST), Saudi Arabia. His current research interests include electrochemical electronics devices, thin-film transistors, transparent oxide thin films, and resistive switching memory devices.*

Rajeh S. Alsaadi *received his BS degree, with honors, in Materials Science and Engineering from the Pennsylvania State University in 2020. He is currently pursuing his MS degree in Materials Science and Engineering at King Abdullah University of Science and Technology. His research interests include the epitaxy of thin films, two-dimensional materials, and emerging electronics.*

Prof. ***Mario Lanza*** *got the PhD in Electronic Engineering in 2010 at Universitat Autonoma de Barcelona, and did two postdocs, one at Peking University and another at Stanford University. Between 2013 and 2020 he was Young 1000 Talent Professor at Soochow University, where he conosolidated as a world-leading scientist in the field of 2D materials based electronic devices. In 2020 he joined KAUST as Associate Professor of Materials Science and Engineering. He is a Distinguished Lecturer of the IEEE-Electron Devices Socitey and won the 2017 Microelectronic Engineering Young Investigator Award (Elsevier). He is editor in chief of Microelectronic Engineering (Elsevier) and member of the board of multiple journals and international conferences, including IEEE-IEDM, IEEE-IRPS and APS meetings.*

Prof. ***Xi-Xiang Zhang*** *obtained his PhD degree from the University of Barcelona, Spain, in 1992. After working as a research scientist at Department de Fisica Fonamental, University de Barcelona for five years (1992–1997), he joined Hong Kong University of Science and Technology as an assistant professor, and then became a full-time professor in July 2008. In September 2008, he joined KAUST as the manager/director of the core lab and became a full-time professor in January 2014. His research interests include magnetism, spintronics, nanomaterials, multiferroic materials, two-dimensional (2D) materials and graphene. He is a fellow of the American Physical Society.*

WILEY-VCH

Prof. ***Husam N. Alshareef*** *is a Professor of Materials Science & Engineering at KAUST. After nearly ten years in the semiconductor industry, he joined KAUST in 2009 where he initiated an active research group working on inorganic nanomaterial development for energy storage and emerging electronics. Prof. Alshareef is a Fellow of the American Physical Society, Fellow of the Royal Society of Chemistry, IEEE Distinguished Speaker in Nanotechnology, Senior Member of IEEE, and Clarivate Analytics Highly Cited Researcher in Materials Science (2019, 2020 and 2021).*

This review introduces various two-dimentional van der Waals layered materials and summarizes their wafer-scale growth processes, including strategies for mono-orientated film growth. Applications of these materials in integrated devices and new epitaxial technologies are discussed, as well as the required future research directions in this very important field.

X. Xu, T. Guo, H. Kim, M. K. Hota, R. S. Alsaadi, M. Lanza, X. Zhang, H. N. Alshareef*

Growth of Two-Dimensional Materials at the Wafer Scale